MARINET

Marine Renewables Infrastructure Network

Work Package 2: Ocean Energy System Testing – Standardisation and Best Practice

D2.6: Report on Offshore Wind System Monitoring Practice and Normalisation Procedures

Author(s):

Prof. P. Schaumann	LUH
Prof. M. Achmus	LUH
Prof. T. Schlurmann	LUH
R. Eichstädt	LUH
K. Abdel - Rahman	LUH
M. Wilms	LUH
A. Rettenmeier	USTUTT
A. Brandt	ECNeth
E. Marino	UNIFI-CRIACIV
M. Courtney	DTU WIND
L. Sætran	NTNU

SEVENTH FRAMEWORK PROGRAMME

Revision: 02

Date: 06-Dec-2013

ABOUT MARINET

MARINET (Marine Renewables Infrastructure Network for Emerging Energy Technologies) is an EC-funded consortium of 29 partners bringing together a network of 42 specialist marine renewable energy testing facilities. MARINET offers periods of free access to these facilities at no cost to research groups and companies. The network also conducts coordinated research to improve testing capabilities, implements common testing standards and provides training and networking opportunities in order to enhance expertise in the industry. The aim of the MARINET initiative is to accelerate the development of marine renewable energy technology.

Companies and research groups who are interested in availing of access to test facilities free of charge can avail of a range of infrastructures to test devices at any scale in areas such as wave energy, tidal energy and offshore-wind energy or to conduct specific tests on cross-cutting areas such as power take-off systems, grid integration, moorings and environmental data. In total, over 700 weeks of access is available to an estimated 300 projects and 800 external users.

MARINET is consists of five main areas of focus or 'Work Packages': Management & Administration, Standardisation & Best Practice, Transnational Access & Networking, Research and Training & Dissemination. The initiative runs for four years until 2015.

Partners

Ireland
University College Cork, HMRC (UCC_HMRC) *Coordinator*
Sustainable Energy Authority of Ireland (SEAI_OEDU)

Denmark
Aalborg Universitet (AAU)
Danmarks Tekniske Universitet (RISOE)

France
Ecole Centrale de Nantes (ECN)
Institut Français de Recherche Pour l'Exploitation de la Mer (IFREMER)

United Kingdom
National Renewable Energy Centre Ltd. (NAREC)
The University of Exeter (UNEXE)
European Marine Energy Centre Ltd. (EMEC)
University of Strathclyde (UNI_STRATH)
The University of Edinburgh (UEDIN)
Queen's University Belfast (QUB)
Plymouth University(PU)

Spain
Ente Vasco de la Energía (EVE)
Tecnalia Research & Innovation Foundation (TECNALIA)

Belgium
1-Tech (1_TECH)

Netherlands
Stichting Tidal Testing Centre (TTC)
Stichting Energieonderzoek Centrum Nederland (ECNeth)

Germany
Fraunhofer-Gesellschaft Zur Foerderung Der Angewandten Forschung E.V (Fh_IWES)
Gottfried Wilhelm Leibniz Universität Hannover (LUH)
Universitaet Stuttgart (USTUTT)

Portugal
Wave Energy Centre – Centro de Energia das Ondas (WavEC)

Italy
Università degli Studi di Firenze (UNIFI-CRIACIV)
Università degli Studi di Firenze (UNIFI-PIN)
Università degli Studi della Tuscia (UNI_TUS)
Consiglio Nazionale delle Ricerche (CNR-INSEAN)

Brazil
Instituto de Pesquisas Tecnológicas do Estado de São Paulo S.A. (IPT)

Norway
Sintef Energi AS (SINTEF)
Norges Teknisk-Naturvitenskapelige Universitet (NTNU)

Acknowledgements

The research leading to these results has received funding from the European Union Seventh Framework Programme (FP7) under grant agreement no. 262552.

Legal Disclaimer

REVISION HISTORY

Rev.	Date	Description	Author	Checked by
00	31-10-2013	1st DRAFT	LUH/USTUTT	Self checked
01	29-11-2013	Rev 1 (for discussion)	LUH,USTUTT,ECNeth, UNIFI-CRIACIV,DTU, NTNU	Cross checked
02	06-12-2013	Rev 2 (final)	LUH,USTUTT,ECNeth, UNIFI-CRIACIV,DTU, NTNU	LUH,USTUTT,ECNeth, UNIFI-CRIACIV,DTU, NTNU

EXECUTIVE SUMMARY

In the present report elaborated testing practices are presented which are applied at MaRINET research facilities in different fields of offshore wind system experimental testing. The results aim for the development of references for harmonisation of testing practices between different facilities. To this end specific methodologies, adoptable instrumentation as well as data processing methods are identified.

To cover a wide field of research activities the report includes respective elaborations of testing practices from all partners in the MaRINET consortium which are involved in the offshore wind system standardisation and normalization task. References for testing practices where collated in cases where common fields of research are covered by different institutions of the consortium.

In chapters 2 to 4 experimental assessment methodologies for three significant technical issues regarding support structures of offshore wind turbines are covered. Firstly, tests on material fatigue of steel components are covered on the example of large sized bolts, as they are commonly used in ring flange connections. Secondly, assessment procedures for pile foundations under cyclic loading are given, which consider structure-soil interactions. Finally, for investigations on scour phenomena of the soil at the foundation piles as well as protection systems against scour exemplary testing procedures on small as well as large scale models are presented.

Additionally to experimental investigations on support structures in chapter 5 reviews are given about further research activities on offshore wind system components, which are conducted at MaRINET research institutions. Focus is directed to research objectives, applicable instrumentations and test facilities as well as data presentation. Research topics treated are the analysis of wind field behaviour and wake interactions, aerodynamic aerofoils design as well as validation of loading conditions in full model tests.

CONTENTS

1 INTRODUCTION

Due to remote site locations offshore wind turbines need to be designed to endure harsh offshore environmental conditions for a service life of 20 years and more with a minimum of maintenance. Detailed laboratory investigations with the purpose of analyzing the performance of structural components of offshore wind turbines are thus essential for design purposes. Regarding the support structure material fatigue caused by cyclic wind and wave loading with very large numbers of load cycles is a very important issue to be investigated. The cyclic loading conditions further lead to challenges in the design of the pile foundations systems of offshore wind turbines which may be pre-analyzed by soil explorations and laboratory test. Furthermore, the investigation of scour phenomena at the boundary level between water and soil around the pile foundations requires demanding experimental analysis procedures. Analysis of wind field behaviour both before and after interaction with the rotor, aerodynamic aerofoils design and validation of loading conditions in full model tests are further important subjects which are experimentally investigated.

Within the framework of the MARINET project procedures for experimental testing activities were elaborated which are employed at the participating research facilities in the specific fields of research regarding offshore wind turbines. The elaborated results are presented in this report. Specific methodologies, adoptable instrumentation as well as data processing methods are identified. The results can be used as reference for harmonisation of testing practices between different facilities.

2 PROCEDURES FOR FATIGUE ASSESSMENT OF STRUCTURAL DETAILS IN SUPPORT STRUCTURES FOR OFFSHORE WIND TURBINES

2.1 GENERAL

Support structures of offshore wind turbines are exposed to a combination of arbitrary wind and wave loads. Within the desired service life of 20 to 30 years the structures have to endure considerable amounts of dynamic load cycles which cause material fatigue. In the majority of cases the structures bearing capacity is limited by fatigue. It is the task of the structural engineer to assess the sensitivity of the structure in regard to fatigue and to design reliable an economic support structures which endure the desired lifetime. For a reliable fatigue assessment secured data from experimental analyses is required. Thereby it must be considered, that the fatigue behaviour does not only depend on characteristics of the material but also on the specific configuration of the structural component.

2.2 SUPPORT STRUCTURES FOR OFFSHORE WIND TURBINES

Within the last decades several types of support structures have been investigated. Generally, the support structure of an Offshore Wind Turbine consists of the tower and the substructure, which includes all structural components below the tower including the foundation, cf. Figure 2-1. An appropriate substructure must be designed in dependence of water depth, turbine size and the local site conditions. Most offshore wind parks in Europe are supported by Monopile foundations. This type of foundation is suitable for low to intermediate water depths. Bottom fixed foundations, which can be used for higher water depths, are Jackets, Tripiles and Tripods. For very high water depths floating structures come into play. In the following sections different types of foundations for offshore wind turbines are briefly described.

Monopile

Monopiles are simple constructions which extent effectively the turbine tower under water and into the seabed. The Monopile consists of a steel pile with a diameter usually between 3.5 and 5.5 meters driven or drilled 10 to 40 meters into the seabed. This cylindrical tube is connected to the steel tower by a so-called transition piece. This transition piece unifies the tower pile with the foundation pile. Within this unit, the foundation tube overlaps the tower tube and the annulus between the tubes is filled with high performance grout. This type of connection is also called grouted joint. Monopiles are used extensively in the near- and offshore environment up to water depths of 25 m. For the installation of Monopiles only small preparations of the seabed are necessary. Heavy piling equipment drills the foundation into the seabed. Monopiles are not suitable for locations with many large boulders.

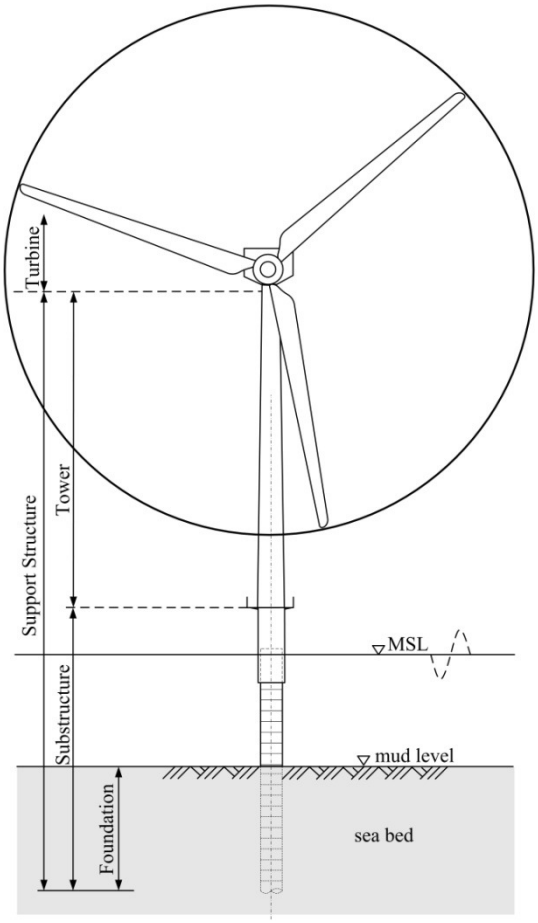

Figure 2-1: Components of an offshore wind turbine with Monopile foundation; Schaumann et al. (2013)

Jacket

The Jacket resembles with a lattice tower (Figure 2-2, left). Its skeleton alike design favours an efficient material consumption. Thus, compared to other offshore foundations the required steel amount and consequently material costs are reduced. At the top of the Jacket construction, the tower including turbine is mounted. The anchorage of the foundation is formed by piles at the structure's feet. The specific structural details are of comparatively small dimensions affording a standardized largely production. Jackets can be used in water depths up to 50 m.

Tripod

The three legged Tripod foundation consists of a central steel cylinder connected with a steel lattice to three foundation piles symmetrically arranged around the central pile (Figure 2-2, middle). The three legs transfer the forces from the tower into the foundation piles. Depending on soil conditions, the three piles are driven 10 to 20 meters into the seabed. The installation needs marginal seabed prearrangement what leads to a rapid assembling. However, the seabed needs to be free of boulders. Compared to the dimensions of the Monopile, the pile diameter of the three legs is significantly reduced. Tripods can be used for water depths up to 50 m.

Tripile

The Tripile foundation is a development by BARD Engineering (Figure 2-2, right). The Tripile is suitable for water depths of 25 to around 40 meters and is more compact, lighter and cheaper than other offshore support structures. The supporting crosspiece and struts are welded from flat steel elements. However, compared to other offshore structure the torsional stiffness is smaller. This influence has to be considered thoroughly.
The three piles are driven into the seabed. For different soil conditions the lengths of the three piles can be varied. After driving of the three piles the crosspiece is attached on top of the three piles with an overlapping grouted connection.

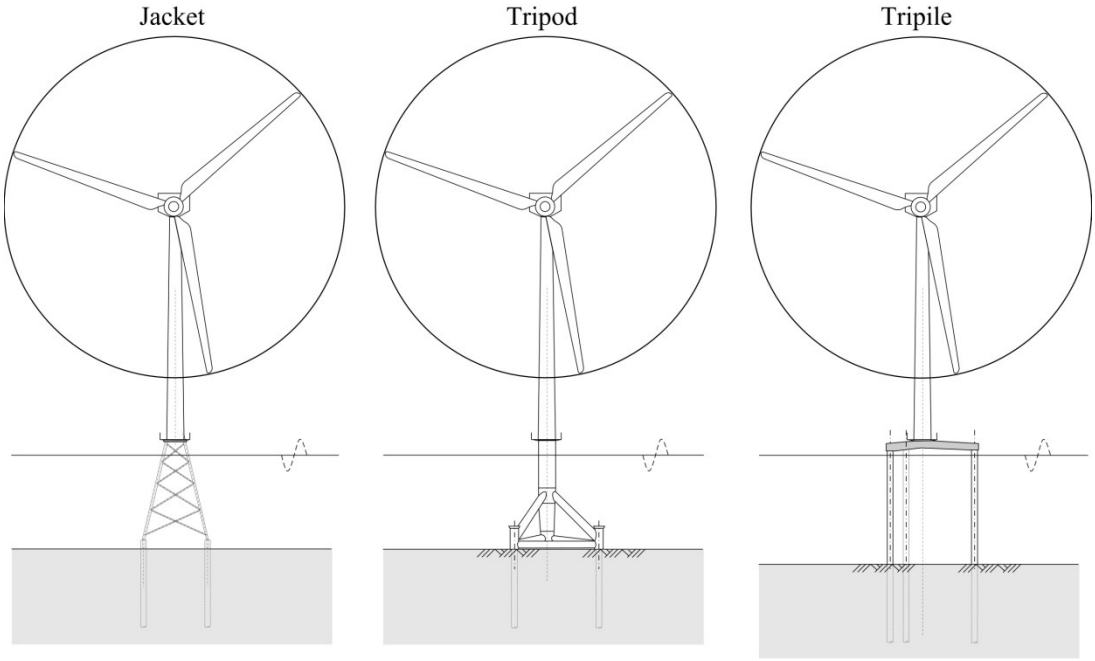

Figure 2-2: Support structures of offshore wind energy converters (Jacket, Tripod, Tripile); Schaumann et al. (2013)

Suction Bucket

Suction Buckets are tubular steel foundations that consist of an upside down cylinder. They are installed by sealing the top and applying suction inside the bucket. The hydrostatic pressure difference of the outer and the inner side and the deadweight cause the bucket to penetrate the soil.
This benign installation procedure allows the bucket to be connected to the rest of the structure before installation, enabling a reduction in steps of the installation procedure. The bucket technology has been widely used in the construction of offshore oil and gas platforms. Concerning the application for offshore wind turbines there is still considerable demand of scientific investigations. Compared to other support structures advantage is given by the installation without drilling procedures, low noise emissions and the small demand of costly steel material.

Floating Structures

Floating structures are one of the latest developments for Offshore Wind Turbine support structures. Theoretically suitable for very large water depths up to several hundreds of meters, these types of substructures are kept in position by mooring chains and anchors. Additionally, the chains have the advantage that they contribute to dampen the motions of the floater. The installation is simple because the structure can be towed to the site with tower and turbines already attached to the foundations. After the anchors have been installed, the chains can be attached and tightened and hook-up cables can be assembled.
To date only a few demonstrator projects are realized with Offshore Wind Turbine supported by a floating substructure.

2.3 FATIGUE ASSESSMENT METHODS

2.3.1 General

Temporally fluctuating and frequently repeating loadings lead to material damage due to material fatigue phenomena. Preferable on defects, notches and cross-sectional variations incipient cracks arise due to fluctuating loads. First an initial crack is the trigger which starts the crack propagation in a cross section under amplitude loadings. The damage process starts with the crack initiation phase followed by the crack propagation process. Figure 2-3 shows different stages of fatigue. The crack propagation starts with an initial crack on the tension side. The stage of 'initial crack' is followed by the 'crack propagation'. Under cyclic loads the stress concentrations at the crack tip leads to a local exceedance of yield strength, so that the crack tip opening displacement (CTOD) is increased. Every single stress cycle exceeding a particular stress level leads to crack propaga-

tion can be seen in the number of grid lines. The more stress cycles are loading the component and the more the crack is opened, the faster is the crack propagation.
The forced rupture occurs when the remaining area is smaller than the area which is necessary for the stress transfer.

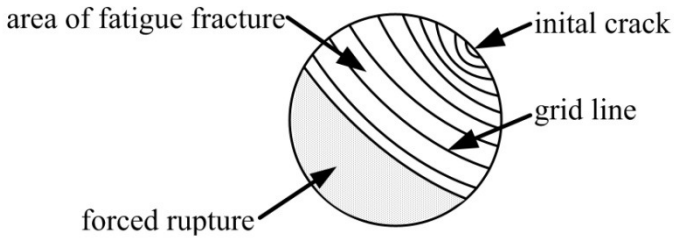

Figure 2-3: Fracture areas; Schaumann et al. (2013)

The fatigue damage-causing load has a smaller value than the static strength. Consequently, the verification of fatigue strength is an important design part especially for highly dynamic loaded structures and structural components as can be found on support structures for offshore wind turbines. This procedure evaluates the endurance of the construction. In order to define the fatigue strength, different approaches can be used.

Commonly, the fatigue design procedure is based on a global concept which depends on nominal stress S-N curves, which are established on published test results. Limitation is given to this global concept due to the failure criterion of total damage. The service life results from the nominal stress S-N curve and the nominal stress spectrum according to damage accumulation hypotheses. Several hypotheses exist whereas the Miner`s rule is used most frequently, e.g. cf. Haibach (1989).
The evaluation of the durability generally results from the linear damage accumulation hypothesis. The literature recommends different hypotheses based on the nominal stress and in accordance with the basic Miner`s rule. The linear damage accumulation encompasses the damage ratio proceeding from the number of load cycles at one level compared to the number of cycles to failure on the corresponding level, cf. Eq. (1).

$$D = \sum_{i=1}^{I} \frac{n_i}{N_i} \leq 1 \qquad (1)$$

With the damage rate D, the number of stress cycles n_i in block i and N_i as the number of endured stress cycles in block i.

Proof to the service life is given by the damage ratio not exceeding a value of 1.0. The introduced Palmgren/Miner equation displays the original one published 1945 by Miner. Several researches established further damage accumulation rules as the elementary and the modified Palmgren/Miner rule. The elementary Palmgren/Miner rule developed by Cortan and Dolan additionally regards the damage beneath the endurance strength. Refinement of this method combines the modified Palmgren/Miner rule by Haibach (1989).

For fatigue assessment a prediction of load cycles is required. The number of load cycles can be derived by counting the load cycles between the cusp points of calculated load time functions. This load time functions have to be characteristic for the specific structure and its specific site. Possible counting methods are the Rainflow cycle counting or the Reservoir counting method, which are schematically illustrated in Figure 2-4.

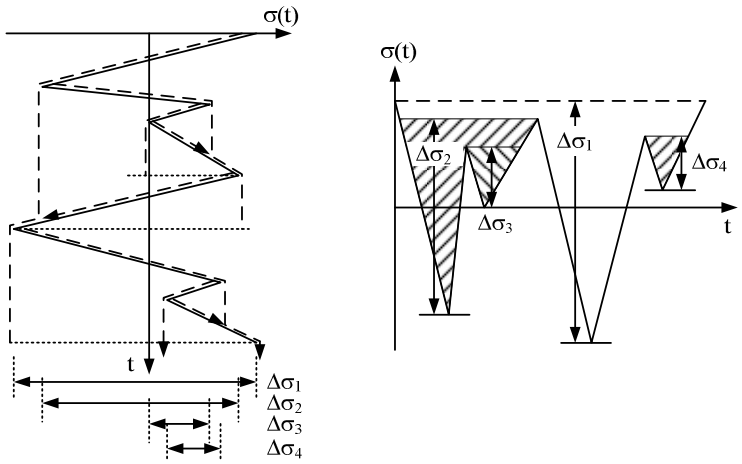

Figure 2-4: Counting methods (left: Rainflow, right: Reservoir); Schaumann et al. (2013)

The fatigue assessment of structural components can be performed with different assessment approaches with different degrees of complexity. Theses assessment methods are described in the following sections.

2.3.2 Nominal Stress Approach

The fatigue strength evaluation of less complex structural steel components is usually performed by the nominal stress approach if a nominal cross section is defined and nominal stress S-N curves are available for the particular construction detail, e.g. EN 1993-1-9 (2005). Occurring fatigue load series have to be described by load functions. Statistical evaluation of the loading function results in the stress spectrum. Generally, the nominal stress approach proceeds from these nominal stress amplitudes, i.e. the stresses as load per nominal cross-section, compared with the S-N curve of the permissible nominal stress amplitudes. The nominal stress S-N curve for welded constructions comprises the influence of material, notch class and weld quality.

Because the nominal stress approach is limited to the availability of nominal S-N curves, its applicability for main load carrying parts of offshore foundations is limited. Furthermore, defining a reasonable nominal cross-section is not always possible.

2.3.3 Structural stress approach

The structural stress approach, also known as geometric or hot-spot approach, considers the local stress peaks within the stress calculations and not within the S-N-curve. The stress calculations is based on an extrapolation of stresses from specific relevant sections, cf. Figure 2-5.

The structural stress includes the local structural details, which are defined by geometric parameters. But welds, notch effects and surface properties are included in the S-N-curves, similar to the nominal stress approach. To reduce the effort of calculating the stress increase, Stress Concentration Factors (SFC) can be defined to describe the ratio between the nominal and the structural stress, cf. eq.3-2.

$$SCF = \frac{\sigma_s}{\sigma_n} \qquad (2)$$

Where

σ_s structural stress

σ_s nominal stress

SCFs can be calculated either by parametric equations or by finite element analysis. Parametric equations have been published by Efthymiou (1988) and are included in the offshore standard DNV-OS-J101 (2013). For finite element analysis guidance is given regarding the modelling and the extrapolation path e.g. by Hobbacher (2007). In Figure 2-5 distance definitions are exemplary shown for tubular joints, as they are found e.g. on Jacket foundations. The structural stress approach is state-of-the-art for offshore foundations.

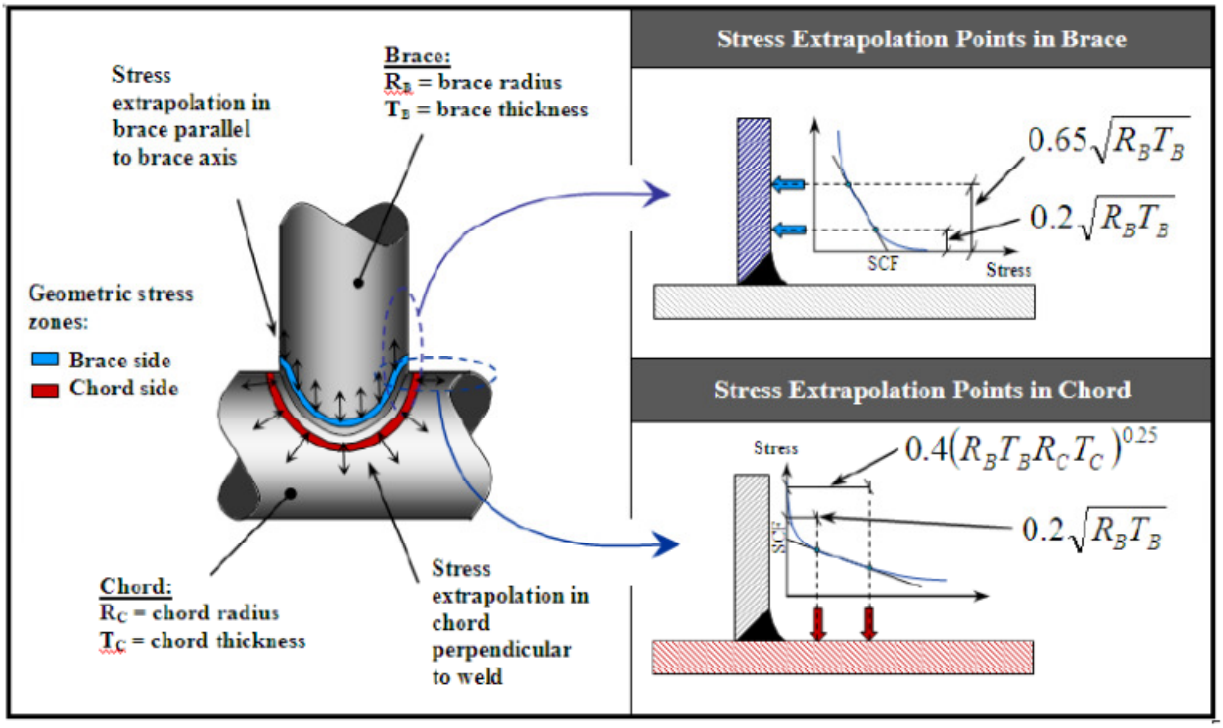

Figure 2-5: Definition of structural stress zone in tubular joints. The structural stress is calculated by linear extrapolation of the stresses in the structural stress zone to the weld toes; DNV-OS-J101 (2013)

2.3.4 Notch stress approach

The notch stress approach considers notch effects within the stress calculation, cf. e.g. Radaj et al. (2006). By modelling the exact structural detail including e.g. welds and a fictitious notch, by means of a rounding, the stress peak at the notch surface can be calculated. The accuracy of the numerical results is much more sensitive to the finite element model than in the structural stress approach.

The notch stress approach requires substantial information about the investigated detail and an elaborated modelling. Thus, its benefit lies more in investigating existing structures than in designing structures. Consequently, the notch stress approach is not yet standardised but it is mentioned in DNV-OS-J101 (2013) as an additional tool.

2.3.5 Notch strain approach and fracture mechanics

The strain at the notch root, which is in the centre of the fatigue process, is investigated within the notch strain approach, cf. e.g. Radaj et al. (2006) or Haibach (2006). On the one hand, this allows the most precise description of the fatigue process. On the other hand, similar to the notch stress approach, the accuracy of the results is highly dependent on the information available for the structural details.

Basic assumption of the notch strain approach is equality between stresses and strains at the notch root and at the unnotched specimen cf. Figure 2-6. Thereby, the specimen has a diameter of the size of the initial technical crack. Therefore, the unnotched specimen fails at the point of crack initiation at the notch root. Due to the strain based description, the notch strain approach allows the inclusion of plastifications.

The previously described approaches define damage as rupture of the structural detail. According to the notch strain approach damage is defined by crack initiation. Therefore a full fatigue assessment, comparable to previously introduced methods, is only possible using fracture mechanics subsequent to the notch stress approach.

Similar to the notch stress approach, the notch strain approach is more appropriate for assessment of existing structures than for the design process.

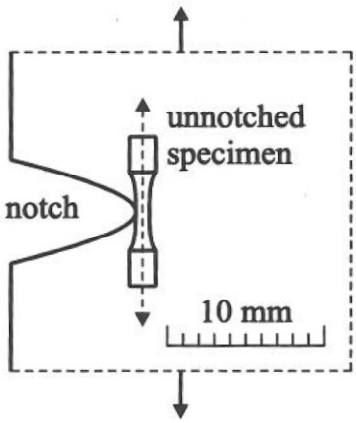

Figure 2-6: Unnotched specimen at notch root; Radaj & Vormwald (2007)

2.3.6 Practical approach

It is possible and common practice as well, to assess the fatigue performance of structures and structural details on the basis of experimental tests. These tests are conducted with true-scale or full-scale specimens. Due to their time and monetary expenditure, real tests are usually the last step in the design process. However, for certain details such as large sized bolted connections, they become necessary because of the limited knowledge on the actual fatigue strength and the lack of applicable S-N-curves. Experimentally secured data is also required to evaluate the results of local fatigue assessment approaches, i.e. notch stress and notch strain approach.

2.4 FATIGUE TESTING OF LARGE SIZE BOLTS FOR BOLTED CONNECTIONS

2.4.1 General

Ring flange connections with preloaded high strength bolts (HV) are the state-of-the-art design solution for the conjunction between tubular steel tower sections in offshore wind turbines. They are also used for connecting the lower end of steel towers to any type of substructure, cf. chapter 2.2. Furthermore, the application of ring flange connections is also under discussion as alternative design solution for grouted joints for the conjunction between transition piece and monopile foundations.

Ring flange connections are commonly executed with about 70 to 120 hot-dip galvanized bolts with diameters between M30 and M48. However, with progressing technical development of turbines and structures the application of larger bolt diameters up to M64 and in some cases M72 becomes reasonable, especially at lower connection levels. Bolt diameters of more than M36 exceed the recommended application limits of conventional construction standards.

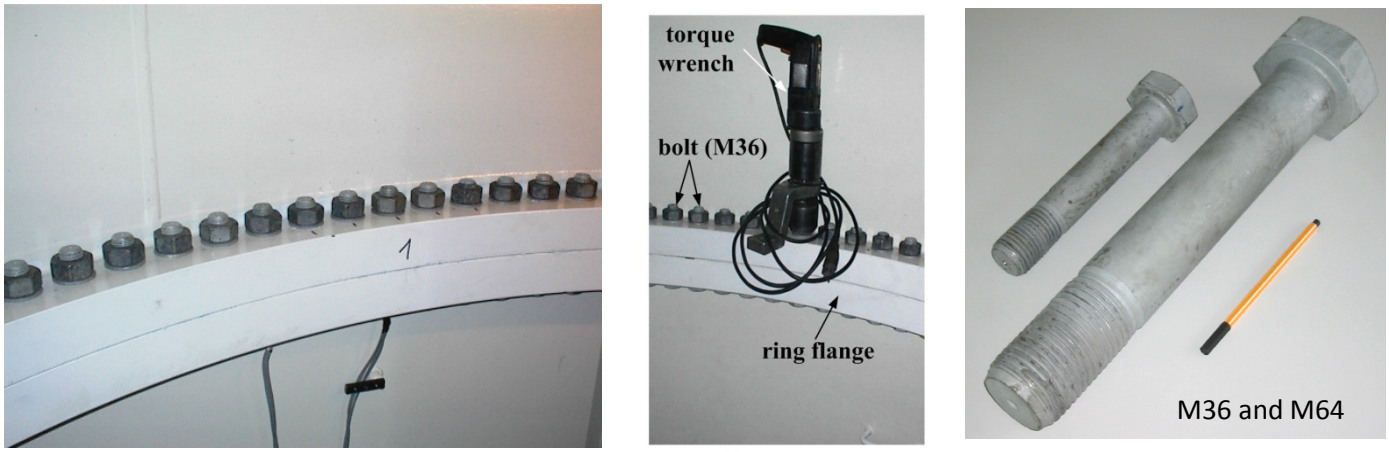

Figure 2-7: left: ring flange connection in wind turbine tower, centre: hydraulic torque wrench for tightening: right: comparison of M36 and M64 bolts; Marten (2009)

For design and assessment purposes the whole connection is usually reduced to the maximum loaded segment, cf. Figure 2-8. This simplification leads to manageable and more economic calculation efforts. However, some important factors such as the supporting effect of the tubular structure or the effect of shell imperfections are neglected. Therefore the segment approach is not appropriate for all assessment purposes.

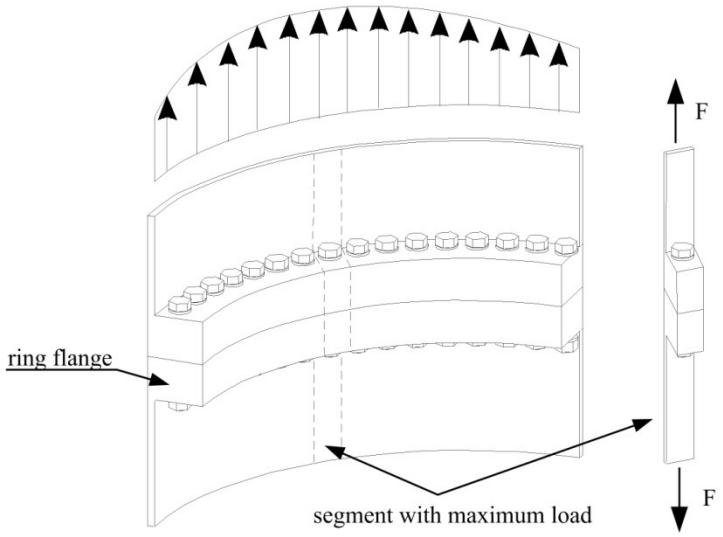

Figure 2-8: Segment approach for design of ring flange connection; Seidel (2001)

According to applicable standards and guidelines for wind turbine structures (e.g. EN 1993-1-8 (2005), Germanischer Lloyd (2012)) ring flange connections in wind turbine structures have to be preloaded. The nominal preloading force F_v for bolts in ring flange connections is calculated to:

$$F_v = 0.7 \cdot A_s \cdot f_{y,b,k} \qquad (3)$$

Where

A_S	tensile stress area
$f_{y,b,k}$	yield strength of the bolt material

Since the connection is loaded highly dynamically, fatigue design becomes essential. Due to the pronounced geometric notch of the bolt thread fatigue damage of the bolt is the critical aspect when analyzing the connection. Applicable SN-curves from construction standards such as EN 1993-1-9 (2005) are not verified for bolt diameters larger than M36. Furthermore, several influence effects on bolt fatigue are not yet fully investigated. To increase knowledge about large size bolt fatigue experimental tests become essential. In the subsequent sections several aspects for conducting experimental tests to investigate fatigue of bolts with large diameters are elaborated.

2.4.2 Test specimens

High strength bolt HV-Sets with strength class 10.9 consist of the bolt with bolt head, plain shaft and notched thread, a nut with inside thread and two washers. As in practical application experimental tests always have to be performed using the full HV-Set with the same material for every component from one single manufacturer.

HV-Sets up to a diameter of 36 mm are regulated in European standard EN 14399 (2005). Among others the standard gives values and acceptable tolerances for all relevant geometric parameters, including the notch geometry of the thread. The application of larger diameters is regulated on national basis. In Germany HV-Sets between M39 and M64 are standardized in DASt-Guideline 021 (2006). The guideline is about to be extended to bolt diameters M72.

Unlike conventional steel the stress-strain characteristic of high strength bolt material does not show a pronounced yield plateau, cf. Figure 2-10. Therefore the yield strength which may be applied in the design is defined by the 0.2 %-strain limit $R_{p0,2}$.

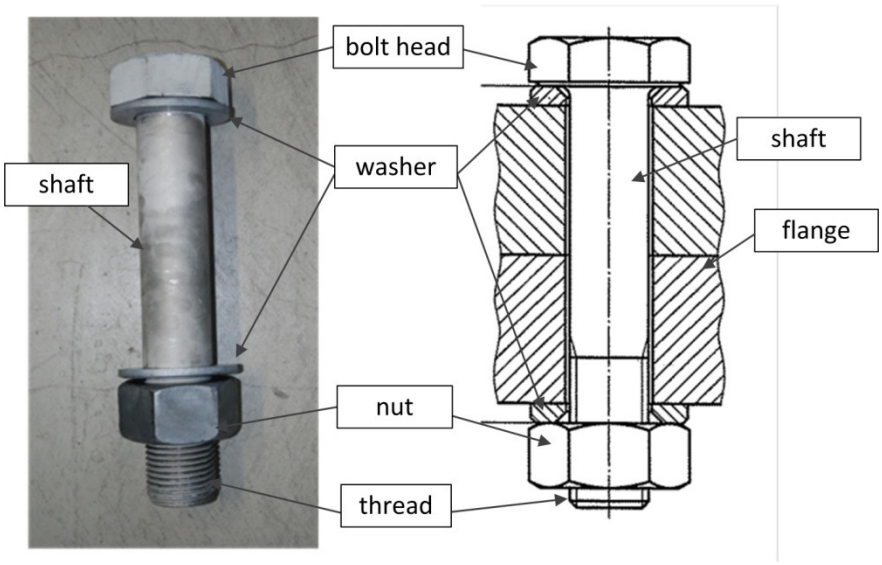

Figure 2-9: Components of HV-Sets

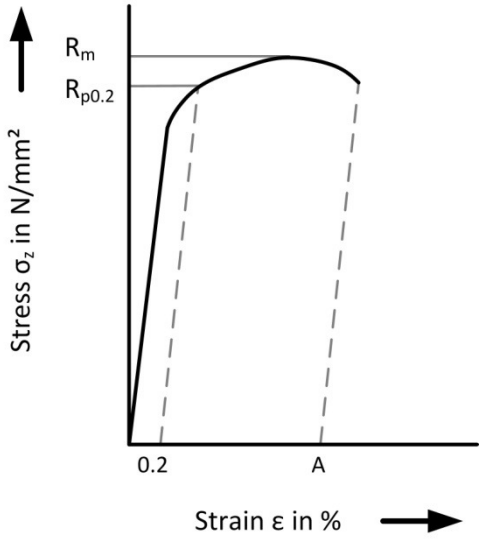

Characteristic tensiel strength: f_{ubk}/ R_p = 1000 N/mm²

Characteristic yield strength: f_{ybk}/ $R_{p0,2}$ = 900 N/mm²

Figure 2-10: Stress-Strain characteristic of high strength bolt material strength class 10.9

2.4.3 Influences on fatigue strength

2.4.3.1 Size effects

Generally, the fatigue strength of components decreases with increasing dimensions. According to Kloos (1976) it may be distinguished between the following size effects:

- geometric size effect
- technological size effect
- statistical size effect
- surface-technological size effect

Geometric size effect

The stress gradient inside the thread depends on the bolt diameters, cf. Figure 2-11. This is described by the geometric size effect. Consequently, under identical nominal stress the region of high stresses is larger for large diameters than for smaller ones. Furthermore, the ratio between thread pitch and bolt diameter decreases with increasing diameter and geometric affinity of the threads of different bolt diameters is not secured. This additionally influences the stress gradient inside the bolt. This has to be kept in mind when analyzing the geometrical size effect.

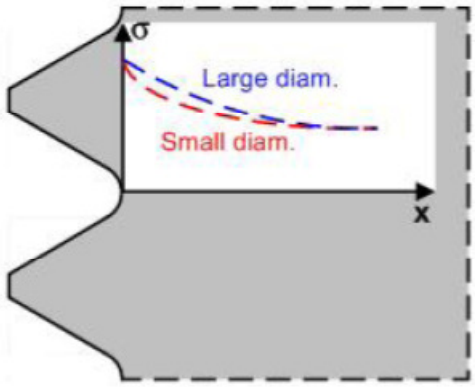

Figure 2-11: Stress distribution for different bolt diameters; Schaumann & Marten (2009)

Technological size effect

Fatigue relevant aspects of the manufacturing process are considered in the technological size effect. The crystalline structure of the material depends on specific aspects of the manufacturing process, such as mechanical forming process and head treatment. Since material and manufacturing process vary in dependence of the bolt diameter the technological size effect can hardly be investigated for bolts.

Statistical size effect

Damage relevant defects at micro-structural level are statistically more likely to occur on larger components. Consequently, the probability of crack initiation increases with large diameters. This is considered in the statistical size effect. In order to quantify the influence of the statistical size effect an identical material and manufacturing process for different diameters would be required. Therefore, as for the technological size effect investigations on the statistical size effect are not possible for bolts.

Surface-technological size effect

Hardening procedures of the bolt surface can influence its fatigue strength because of occurring residual stresses in the boundary layer. The surface-technological size effect considers dependencies between boundary layer with residual stresses, component thickness and fatigue strength.

2.4.3.2 Influence of load frequency

According to Yotobori (1976) high loading frequencies in experimental tests lead to higher fatigue strength, i.e. a higher number of load cycles before rupture. For the high cycle fatigue range ($N = 5 \cdot 10^4$ to $2 \cdot 10^6$) Dünkel (1999) determined an increase of load cycles until rupture under the same load amplitude by a factor of 1.5 for an increase of loading frequency of one decade from 1,3 Hz to 13 Hz. In the same regime a decrease of fatigue resistance for lower testing frequencies was also observed by Berger & Schaumann (2008) However, these findings could not be confirmed by Alt (2005) for the very high cycle fatigue range ($N > 2 \cdot 10^6$). Until now the influence of loading frequency on the fatigue strength of bolts is still subject of scientific research.

2.4.3.3 Influence of mean stress

Cyclically loaded bolted connections have to be pre-loaded, cf. section 2.4.1. Under cyclic loading the pre-load leads to a constant mean stress of the occurring stress cycles. Consequently, bolts in ring flange connections are usually subjected to tensile loads only.

The influence of the mean stress on the fatigue resistance depends on the applied manufacturing process and on the magnitude of the load amplitude.
According to Schneider (1991) the fatigue resistance in the very high cycle fatigue regime of bolts with threads rolled before head treatment is approximately unaffected by the mean stress, provided the mean stress lies within a range between 25 % and 70 % of the nominal yield strength. For higher mean stresses a reduction of fatigue strength was observed. Lower mean stress could lead to a larger scatter of test results, cf. Schaumann & Marten (2008).

On the contrary, the fatigue strength of bolts with threads rolled after heat treatment decrease significantly with increasing mean stress, cf. Schneider (1991). However, even for high mean stresses the fatigue strength of bolts with threads rolled after head treatment lie above the fatigue strength of bolts with threads rolled before head treatment. This can be explained with favourably acting residual stresses in the area of the thread notch.
According to Dünkel (1999) and Schaumann & Marten (2008) in the low and high cycle fatigue range the number of load cycles may be reduced when increasing the mean stress because the higher maximum stress accelerates the crack propagation.

For tests on bolts for the application in ring flange connections of wind turbine towers it is recommended to apply a pre-tension which corresponds to the magnitude of the nominal preloading force, cf. section 2.4.1.

2.4.3.4 Influence of loading conditions

Ring flange connections in wind turbine towers are usually executed in L-shape. Therefore, the bolt axis lies eccentric to the line of force of the connection. Consequently, bolts in ring flange connections are loaded by combined axial force and bending moment.
Investigations in the literature mostly refer to the fatigue tests under axial loading only. Seidel & Schaumann (2001) evaluated collected testing results of high strength bolts 10.9 with diameters M20 and M30 under pure axial loading. The results confirm the corresponding detail category 50 as defined in EN 1993-1-9 (2005) (following: EC3). Under consideration of the "size effect" reduction given in EC3, detail category 50* was also confirmed for bolts M48 by Schaumann & Marten (2009).
Experimental data from tests under pure bending or combined axial and bending loading are significantly less than from test under pure axial loads. However, it is acknowledged that the fatigue strength of bolts under bending loading is higher than under axial loading. Tests under pure bending loading from Schaumann & Marten (2009) on bolts M48 have confirmed EC3 detail category 80* under consideration of "size effect" reduction. Consequently, the fatigue resistance of bolts under combined axial and bending loading can be assumed to be higher than under pure axial loading.
Since the realization of tests under combined axial and bending loading is very challenging, the favourable effect of eccentric loading on the fatigue strength of bolts in ring flange connections has not yet been sufficiently quantified. Test results from Berger & Schaumann (2008) indicate a fatigue resistance between EC3 detail category 70 and 80.
In conclusion the application of detail category 50* for bolts up to M48 may be assumed as conservative for bolts in ring flange connections, cf. also Marten (2009).
However, it is noted that this implies that the approach of load determination has to consider the load contribution from the eccentric bending moment, e.g. according to Seidel (2001) or by use of the finite element method. If only axial forces are considered, the applied detail category has to be reduced.

2.4.4 Instrumentation

2.4.4.1 Test facilities

Due to the high pre-tension of 70% of the materials nominal yield strength, bolt fatigue test require the application of high tensile mean loads. Consequently, the maximum values of the applied stress cycles are rather high. Since testing facilities are limited by the cyclic load capabilities, appropriate facilities must be available in dependence of the tested bolt diameter. Table 2-1 shows nominal preloading forces for bolt diameters M36 to M72.

Bolt diameter	Pre load
M 36	510 kN
M 42	710 kN
M 48	930 kN
M 56	1280 kN
M 64	1680 kN
M 72	2200 kN

Table 2-1: Nominal tensile pre- loads for different bolt diameters

Besides load capabilities fatigue tests are often limited by achievable testing frequency. A statistically significant determination of fatigue strength in the very high cycle fatigue range requires cyclic tests with load cycle numbers up to $N = 5 \cdot 10^6$ and more on a multitude of specimens. Consequently, time and monetary expenses are directly affected by frequency of cyclic loading. Table 2-2 shows the time demand for the application of $N = 5 \cdot 10^6$ load cycles to one specimen for different testing frequencies.

Frequency	Test duration
1 Hz	56 days
5 Hz	11 days
10 Hz	6 days
25 Hz	2.5 days
50 Hz	1.2 days
250 Hz	0.25 days

Table 2-2: Test duration for application of $N = 5 \cdot 10^6$ load cycles

Unfortunately, high dynamic load capabilities of test machinery go hand in hand with a reduction of test frequency. The limitations of technically realisable and affordable test facilities significantly complicate the performance of fatigue tests on bolts with large diameters.

For fatigue tests two different technical mechanisms of cyclic load generation can be used. Servo-hydraulic load application systems enable testing with high forces. Depending on the size of the testing facility loads up to 10 MN and more are possible. Therefore, servo-hydraulic test facilities are widely used for testing large structural components. However, the hydraulic load application leads to low testing frequencies. Depending on amplitude and mean value of the dynamic load cycle achievable frequencies may decrease to 5 Hz and lower.

Magnetic resonance test facilities are especially developed for the performance of cyclic load tests with high numbers of load cycles. The systems uses the resonance amplification of two oscillating masses which are excited by powerful magnets. However, compared to servo-hydraulic systems the magnitudes of testable loads are significantly reduced. To enable an economic fatigue testing of bolts with large diameters with magnetic resonance testing machines, usually the mean stress needs to be reduced significantly under the nominal pre- load. This however may influence the fatigue strength of the bolts, cf. section 2.4.3.3.

Figure 2-12: Test facilities at LUH, left: "SincoTec©" Magnetic resonance max. force 400 kN, right: "Instron©" Servo-hydraulic, max. force 10 MN

2.4.4.2 Test set-up

In the majority of cases bolt fatigue is tested under pure axial loading, i.e. under simplification of the real loading condition in ring flange connections. Requirements for axial load fatigue tests of threatened fasteners are defined in DIN 969 (1997) and ISO 3800 (1993).
The load adaption of the specimens to the test facilities is achived by so called “tractive-torpedos”. The load adaption system has to transfer the axial load to the specimen, cf. Figure 2-13.

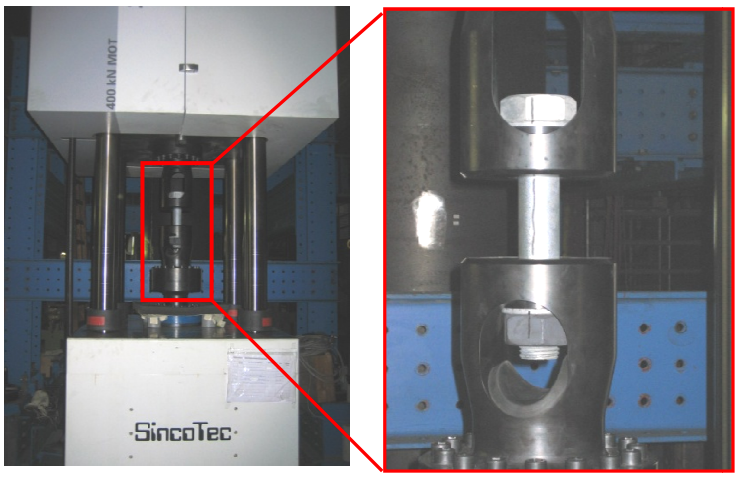

Figure 2-13: Load adaption for bolt M 48; Berger & Schaumann (2008)

To avoid torsional stresses inside the bolt, the nut is attached without any mechanical or hydraulic tool by hand only to fixate the specimen inside the load adaption. Mean stress and the load amplitude are introduced by the testing machine.
The inside threat of the nut must be fully attached to the bolt threat. A minimum of 4 turns of the bolt threat (P) must be located in the loaded area outside the nut. At least two turns of the bolt thread must protrude beyond the nut, cf. Figure 2-14.
Considering the stress distribution inside the specimen rapture should occur in the first loaded turn of the bolt threat. The temperature of the specimen must not exceed 50 °C. Thus, temperature should be monitored when testing with high frequencies.

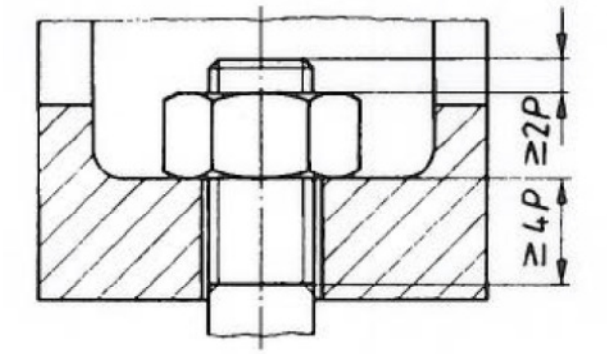

Figure 2-14: Assembly of the testing nut; DIN 969 (1997)

In order to investigate the influence of bending, modifications in test set up and/or test machinery are required. By Berger & Schaumann (2008) pure bending tests on M48 bolts were performed in an specifically designed magnetic resonance testing machine developed by Dr. Attila Alt (Patent-No. 102 04 258), cf. Figure 2-15, left.

For combined loading conditions pre-stressed high strength bolts M48 were tested inside a ring flange segment with representative dimensions, cf. Figure 2-15, right. The flange segments were attached by hydraulic clamps to a servo-hydraulic testing machine. Due to a nonlinear load transfer function between tensile forces introduced to the flange segment and resulting bolt loading (cf. e.g. Seidel (2001)), in this testing set-up the bolts need to be pre-loaded as in real application by use of a hydraulic tightening tool, cf. Figure 2-7.

Figure 2-15: left: testing machine for fatigue test under pure bending (Pat.-No. 10 04 258), right: flange segment connection for fatigue test und combined loading; Berger & Schaumann (2008)

2.4.5 Test procedures

Based on the dominating stress level in wind turbines, fatigue tests are commonly performed in the high cycle fatigue (HCF) regime or in the transition region to the long life fatigue strength (LLF), denoted as endurance limit, cf. Figure 2-16. The determination of the long life fatigue strength requires long lasting tests with very large number of load cycles. For tests in the Low Cycle Fatigue (LCF) regime, powerful test facilities are required. Additionally, frequency effects may influence the test result in LCF significantly. Furthermore, the static strength is more important than the LCF performance of steel materials.

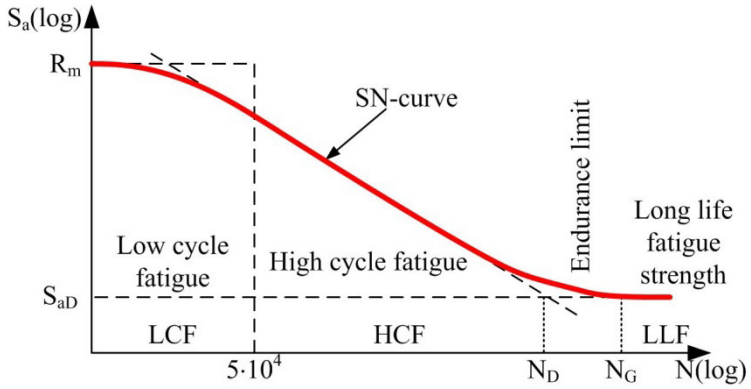

Figure 2-16: Schematic SN-curve for steel and metallic materials; Schaumann et al. (2013)

For an outright description of SN-curves of high strength bolt sets, the pathway in the high cycle fatigue range as well as the location of the transition region to the long life fatigue strength need to be known. For determination of the respective regions of the SN-curve different testing procedures are applied. The results are evaluated by use of statistical methods in order to determine the statistical probability of failure. Within the following sections common procedures for fatigue tests in different fatigue regimes are presented.

For determination of SN-curves individual bolt fatigue tests are performed with different load amplitudes. During the individual tests the load amplitude as well as the mean load is kept constant. This does not represent the actual load conditions in practical application. Fatigue tests with variable amplitude during the individual test are very demanding and need to be planed thoroughly. They are not elaborated in this report.

2.4.5.1 Transition region to endurance limit

The scatter range of the transition region to the endurance limit can be statistically determined by us of the “staircase-method”. The procedure has been originally developed by Dixon & Mood (1948) and is included in standards DIN 969 (1997) and ISO 3800 (1993). Different modifications have been published in the literature, which differ in

the way of statistical evaluation of results, cf. Dünkel (1999). However, the planning and conduction of the test series remains identical.

For conduction of fatigue tests with the "staircase-method" a test series is performed where the load amplitude is changed by a defined load increment after every individual bolt test. The end of the individual bolt tests are defined either by bolt failure (rupture or initial crack) or by exceeding a defined limit number of load cycles (run-out). It is assumed that after exceeding the run-out limit no bolt damage occurs for an infinite number of further cycles. Run-out limits for bolt tests are commonly defined to $N = 5 \cdot 10^6$ or $N = 1 \cdot 10^7$.

After end of an individual test by bolt failure the load amplitude for the following test is reduced by the defined increment whereas after a run-out it is increased, cf. Figure 2-17. The "staircase-method" enables an automated calibration of results around the mean value of the endurance limit. However, for a sufficiently accurate determination of the standard deviation a large number of tests (>25) is required.

For the conduction the initial load amplitude as well as the load increment needs to be reasonably estimated. It is preferable to choose an initial amplitude which lies above the endurance limit in order to enable approaching the endurance limit from the high cycle fatigue regime. The load increment should approximate the statistical variant of the mean value of the endurance limit. In case during the test series the chosen load increment proves to be inappropriate (e.g. when the results constantly alternate between rupture and run-out) the increment can be modified after about half of the test series.

Recommendations for the estimation of initial amplitude and load increment in dependence of the bolt diameter are given by Dünkel (1999). The formulae for determination of the statistical mean value and standard deviation of endurance limit based on the test results according to Dixon & Mood can be found in DIN 969 (1997) and ISO 3800 (1993).

F_A [N]	x failure o run out														
4700													×		
4300						×		×				○		×	
3900	×		×		○		○		×		○				×
3500		○		○						○					
No.	1	2	3	4	5	6	7	8	9	10	11	12	13	14	15

Figure 2-17: Schematic illustration of test procedure with the "staircase-method"; DIN 969 (1997)

Alternatively to the "staircase-method" the endurance limit can be determined by the "boundary-method" introduced by Maening (1977). The method enables a more effective determination of the statistical margins of the endurance limit. During the test series a defined number of individual tests is performed with constant amplitudes at the estimated upper and lower margin of the endurance limit. Documented failures and run-out at the two levels are statistically evaluated, cf. DIN 969 (1997) and ISO 3800 (1993). As for the "staircase-method" proper estimation of the test levels is crucial for the significance of the obtained results. A discussion can be found in Dünkel (1999).

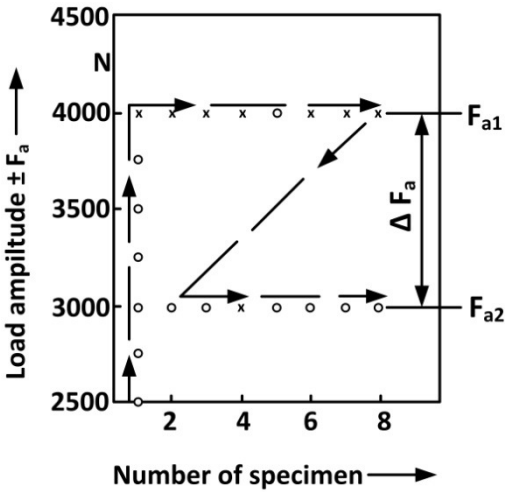

Figure 2-18: Schematic illustration of test procedure with the "boundary-method", acc. to DIN 969 (1997)

2.4.5.2 High cycle fatigue regime

For reliable assessment of SN-curves in the high cycle fatigue range it is recommended practice to test a series of individual bolts at least at two load levels ("horizons") under identical amplitude and mean stress. The number of specimens for each horizon significantly influences the accuracy of the results. Thus, in order to achive statistically meaningful results 8 bolts should be tested for each horizon. In any case the bolt number should not be lower than 5.
In DIN 969 (1997) it is recommended to choose the load levels in dependence of the previously determined mean value of the endurance limit to $1.6 \cdot \sigma_D$ and $2.4 \cdot \sigma_D$. With the achieved number of load cycles until bolt failure the results are commonly evaluated based on a Gaussian distribution; cf. DIN 969 (1997). Under consideration of both load levels, pathway and scatter of the SN-curve in the high cycle fatigue range can be determined.

In case only a limited number of individual bolt tests are possible, fatigue tests can also be statistically evaluated based on a series of individual tests with different load amplitudes. The SN-curves with different probabilities of failure can then be determined by use of a log-normal distribution. The conduction of this procedure requires a distinct relation between load amplitude and load cycles until failure for the obtained results. Not all of the individual tests do necessarily need to be run with different load amplitudes. However, for evaluation no less then 3 load levels should be considered.

2.4.6 Data analysis and presentation formats

Results of fatigue tests are commonly presented and evaluated in Quantile-SN-curves which express the relation between stress cycles and failures with distinct probabilities of survival. Quantile-SN-curves can be determined based on a log-normal distribution and are illustrated in double logarithmic scale. Figure 2-19 exemplary shows the result presentation of bolts M48 with probabilities of survival p_s = 10 %, 50 %, 90 %. In addition to the regression functions the actual test results are displayed. For better evaluation the illustration distinguishes between results in the high cycle fatigue regime (black triangles for two load levels) and results in the transition region to the endurance limit (red and blank cycles). The blank cycles correspond to the bolts which have reached the defined run-out limit of load cycles without failure.

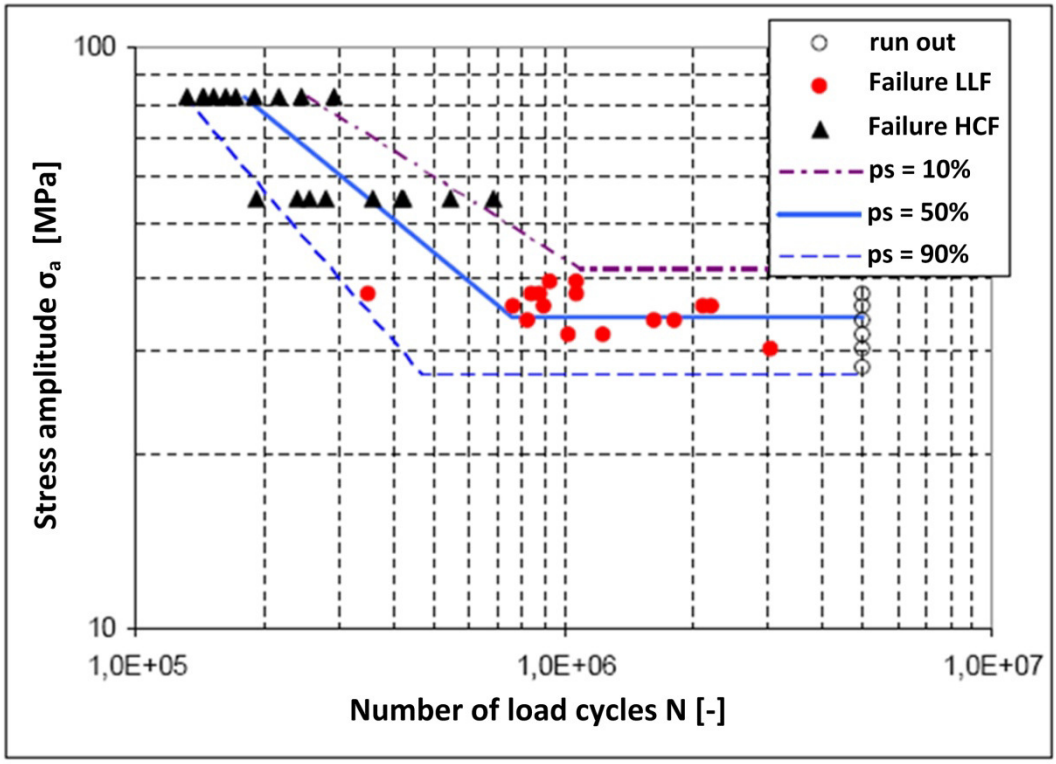

Figure 2-19: Result presentation of fatigue test on bolt M48; Berger & Schaumann (2009)

Additionally to the graphical illustration, information about crucial characteristic values of the respective Quantile-SN-curves is required to compare results. The most relevant parameters are given in Table 2-3.

Parameter	Entity
Probability of survival	%
Endurance limit	MPa
Transition to long life fatigue strength	Number of load cycles [-]
Slope of SN-curve in HCF range	-

Table 2-3: Characteristic values of Quantile-SN-Curves

The characteristics of the Quantile-SN-curves depend on the applied static evaluation procedure of mean values and standard deviation, cf. chapter 2.4.5. Therefore the specific procedure always needs to be stated in order to enable clear interpretation of results.

2.5 Conclusion

Due to cyclic loading accurate fatigue assessment is crucial for design of structural components in support structures for offshore wind turbines.

Experimental fatigue assessment of large components is often limited by available test facilities as well as timely and monetary expenditures. For statistical significance large numbers of tests have to be performed with high mean loads and considerable numbers of load cycles. These requirements often exceed the capabilities of test facilities. However, for certain details in support structures for offshore wind turbines common fatigue assessment approaches need to be complimented by experimental tests. In this way an economic design can be improved.

As an example for experimental fatigue assessment of characteristic structural details of offshore wind turbine support structures, testing procedures for large sized bolts have been elaborated. For large sized bolts only a small number of fatigue test data exists. First investigations indicate that the thickness effect acc. to EN 1993-1-9 (2009) and GL-Guideline (2012) leads to conservative design results. Especially for application of diameters larger than M48 further investigations are necessary for an appropriate fatigue design. Especially the reduction of fatigue strength due to large dimensions, but also of other influencing factors, has not yet been sufficiently investigated.

3 ASSESSMENT PROCEDURES FOR FOUNDATION SYSTEMS OF OFFSHORE WIND TURBINES UNDER CYCLIC LOADING

3.1 GENERAL

Piled structures, gravity foundations and bucket foundations could be used as foundation structures for offshore wind energy converters in the German offshore regions. Soil exploration and assessment as well as the geotechnical design of the foundation elements are extremely difficult tasks for the geotechnical engineer. In particular, the behaviour of the structures under the intensively cyclic effects from wind and waves is not in all details fully understood, and calculation methods are just under development.

In the North Sea and the Baltic Sea in Europe a vast number of offshore wind farms are being planned and several have already been installed in recent years. In Germany it is planned to erect about 8,000 turbines with a total rated power of 27 GW within the next few decades. This is a very challenging task.

Figure 3-1 shows the components of an offshore wind energy structure and possible foundation structures. It consists of the turbine with the rotor, the tower and the substructure with the foundation elements.

In the German parts of North Sea and Baltic Sea water depths of up to 50m exist. For water depths up to about 30m a monopile can be used as foundation structure. A monopile consists of a single large diameter open steel pipe pile, which is driven into the seabed. Diameters of 5m and more have been realized recently. For water depths greater than 30m steel frame structures (jackets with four legs or tripods with three legs) can be used, which are supported by three or four piles located in the edges of the construction. Alternatives are the gravity and the bucket foundation. The latter is of particular interest, because the installation needs no heavy vessels and almost no noise is emitted, which is of great importance with regard to Environmental issues. Here the bucket, which is a large steel cylinder, is pushed into the ground by suction applied inside the cavity between the bucket lid and the sea-bottom.

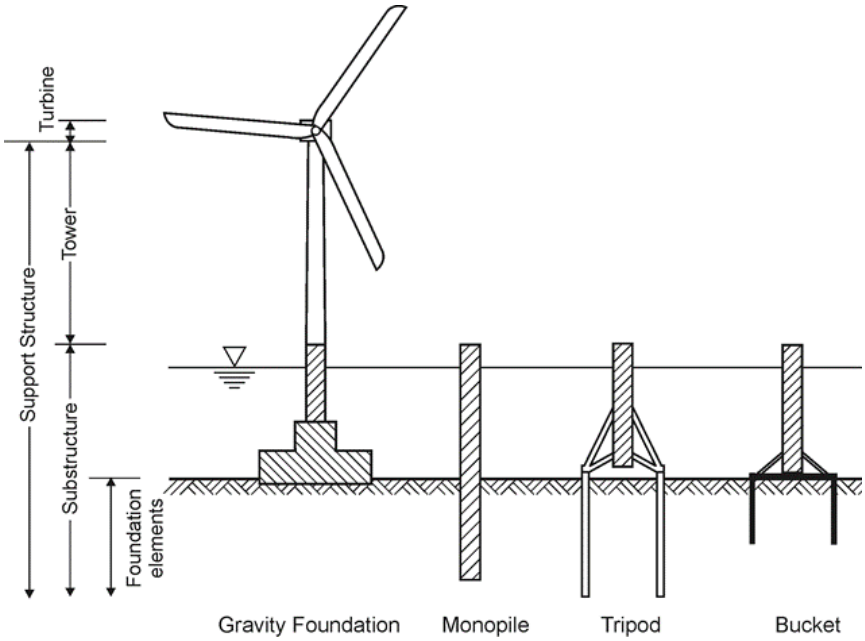

Figure 3-1 Foundation structures for offshore wind farms

Design methods and experience with offshore piles exist mainly from structures built by the oil and gas industry. However, the loading conditions for offshore wind farm foundations are different. The vertical loads are much smaller than for oil or gas platforms, and thus the horizontal loads are of similar magnitude compared to the vertical loads. This means that the extremely cyclic nature of wind and wave forces is much more important than for very heavy structures. Due to that, consideration of cyclic load effects is crucial.

The authority responsible for the approval of offshore wind farms in German sea regions is the BSH (Federal Maritime and Hydrographic Agency of Germany). The BSH has developed special regulations which must be kept to achieve approval of wind farms.
An important issue is that the explicit consideration of cyclic load effects in the design is required. Due to impact of wind and waves, the foundations of a WEA are exposed to heavy cyclic loading. Over the expected lifespan of about 25 to 30 years the structure has to endure approx. 10^9 stress cycles. The influence of the cyclic loading on the deformation (SLS) and the structural safety (ULS) have to be taken into account when calculating the dimensions of a structure.
These rules are adopted in the guidelines for the design of offshore constructions (e.g. (DNV, 2007), (API, 2000)). The BSH-standard for soil exploration (BSH, 2008) suggests cyclic triaxial-, shear- and compression tests for soil investigation. These tests could help us to predict the deformation of the offshore structure and the soil behaviour under cyclic loading. Ready-to-use methods do not yet exist, which makes the geotechnical design a very difficult task.
In the ultimate limit state (ULS) proof, sufficient capacity of the foundation to withstand the extreme load during a storm event has to be proven. Herein, the effect of the cyclic loads on the soil strength must be taken into account.
In the serviceability limit state (SLS) the stiffness of the foundation elements and the deformations due to the cyclic loads must be predicted and compared with admissible deflections or rotations of the different foundation types.
Up to now, the details of the behaviour of foundations under the intensively cyclic effects of wind and waves are not fully understood. Calculation methods are currently under development.

3.2 SOIL EXPLORATION

Minimum requirements regarding soil explorations for offshore wind farms in German sea regions are given in the BSH-Standard Soil Investigation (BSH, 2008). The geological exploration (with geophysical methods) and the geotechnical exploration are distinguished. The sequence of soil explorations for an offshore wind farm is shown in Figure 3-2.
In the first phase, existing data regarding the subsoil of a wind farm (for instance, knowledge of the geological genesis, exploration results from adjacent wind farms) are gathered and evaluated. A geophysical survey of the wind farm area is then carried out, and the results are presented in a preliminary geological report. In the subsequent preliminary geotechnical investigation, borings and soundings (cone penetration tests, CPT) are carried out. At least five borings and CPTs have to be executed at the edges and in the centre of the wind farm area. For wind farms with more than 50 converters, a boring and an adjacent CPT is required in at least 10% of the converter locations. The results of these explorations and the related soil tests in the laboratory are presented in the preliminary soil investigation report.

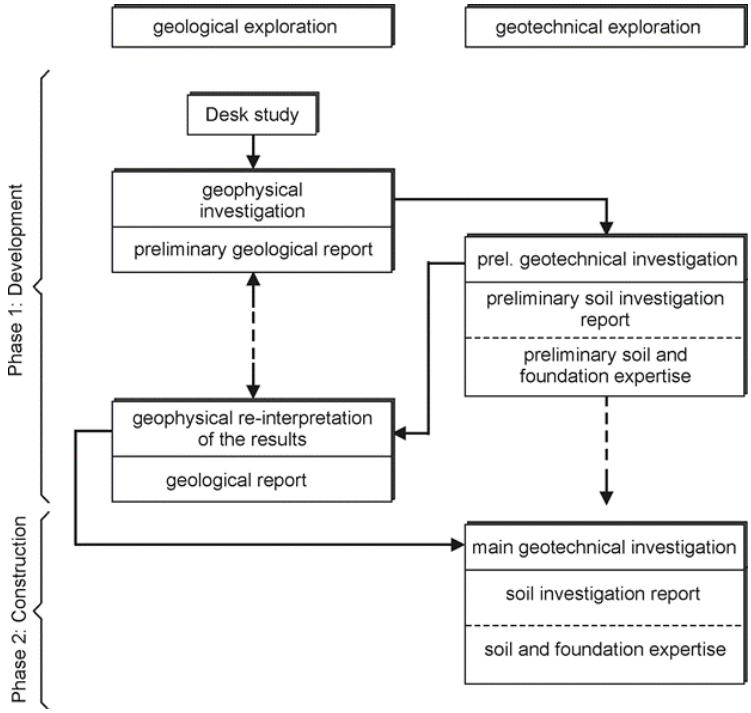

Figure 3-2 Sequence of soil explorations for an offshore wind farm to BSH-standard soil investigation (Lesny, 2008)

The results of the geotechnical investigations shall be used for a reinterpretation of the geophysical survey. The final result of the geological exploration is then the geological report.
At the end of the first exploration phase, the geological report, the preliminary soil investigation report and the preliminary soil and foundation expertise are presented. In the latter, the conclusions regarding engineering purposes are drawn, and the feasibility of the wind farm project and of different foundation variants is assessed in cooperation with the designing engineer. The reports mentioned have to be submitted with the application for the first approval from BSH.
In the second exploration phase (main geotechnical exploration) additional borings and CPTs are carried out. According to the BSH-Standard Soil Exploration, at least one exploration (boring or CPT) at each wind energy converter location has to be carried out. The results of all investigations and soil mechanical laboratory tests are presented in the final soil investigation report. Based on this report, the final soil and foundation expertise is worked out, which presents the soil stratification and the magnitude of the soil parameters of the different layers necessary for design calculations for each location. The final soil investigation report and the soil and foundation expertise have to be submitted with the application documents for the second BSH approval.
In the instructions for use of the BSH-standard construction (BSH, 2011) requirements for the verification for exposure to cyclic loadings are given. For the first release of a design, a concept for the consideration of cyclic loading is required. EAP (EAP, 2011) defines at the beginning, what should be understood under cyclic loading (meant here are not dynamic or shock pulse loads):

„Zyklische Einwirkungen: Darunter werden sich wiederholende Einwirkungen auf die Pfähle verstanden, bei denen Trägheitskräfte des Pfahl-Boden-Systems nicht berücksichtigt werden müssen.“

“Cyclic loads are repeating forces on piles, whereby it is not necessary to consider inertial forces of the pile-soil system”.

In the second release of the design, a detailed report with the required concept for the proposed foundation system should be prepared.

3.3 EFFECTS OF CYCLIC LOADING

3.3.1 Laterally loaded piles

The usual design procedure for foundations of offshore wind energy converters in Germany is given in the Germanische Lloyd (GL) rules and regulations (GL, 2005). In these regulations, concerning the behaviour of piles under horizontal loading (monotonic & cyclic) reference is made to the regulation code of the American Petroleum Institute (API, 2000). In the API code the p-y method is recommended for the design of horizontally loaded piles. Also the Scandinavian guideline (DNV, 2007)proposes the p-y method for the design of horizontally loaded piles. In principle, the p-y method is a subgrade modulus method with non-linear and depth-dependent load-deformation (p-y) characteristics of the soil springs.

One of the limitations of the p-y method regards the consideration of cyclic load effects. The explicit number of load cycles is not considered. In the pile tests used for the calibration of the p-y approaches only a limited number of cycles was applied. In the tests of (Reese, 1974) for piles in sand at maximum 200 and in most tests much less cycles were applied. Due to that, the p-y method is usually assumed to be valid for up to 100 cycles.

For piles supporting offshore wind towers, up to 10^9 load cycles have to be considered over the structure's lifetime of usually 20 or 25 years. Although the load amplitudes vary and the largest part of the cycles have small amplitudes, the question has to be answered how the actual number of cyclic loads can be considered in the design.

Figure 3-3 shows the results of a model test with a monopile embedded in dry sand under one-way cyclic loading. The horizontal displacement of the pile head under cyclic loading increases nearly with logarithmic function. According to the safety guidelines the horizontal shift of the Monopile are not allowed to be large and the accumulation under cyclic loading has to be taken into account.

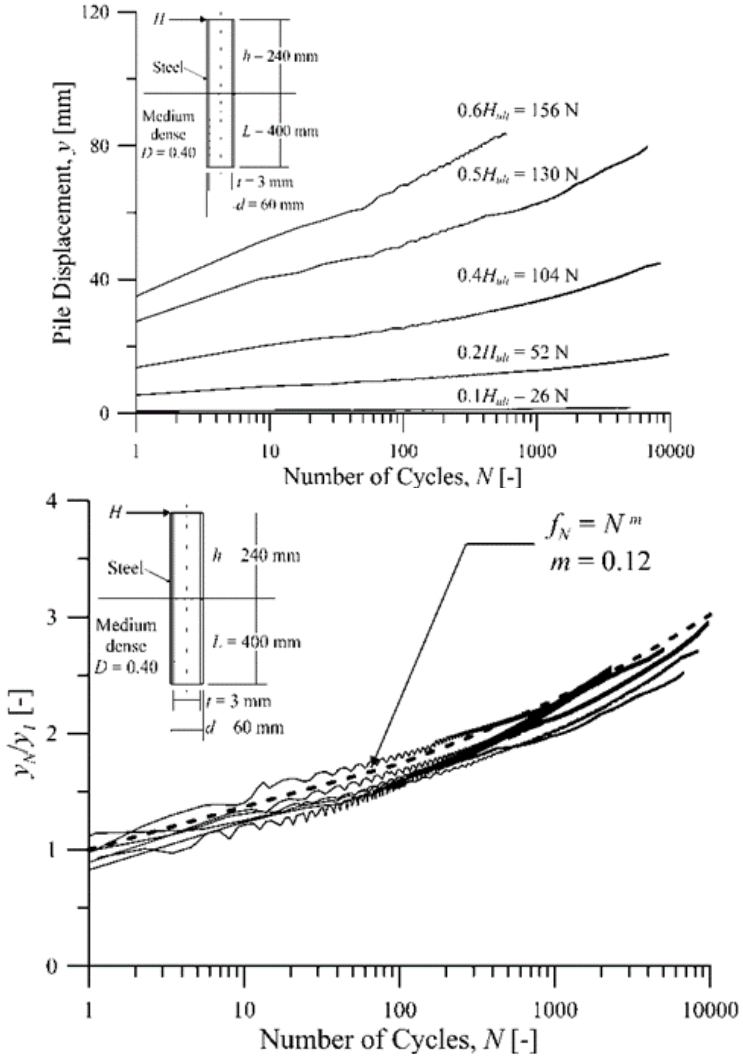

Figure 3-3 Pile deformation under lateral cyclic load (Peralta & Achmus, 2010)

(LeBlanc, 2009) carried out model tests with an almost rigid monopile and derived the following approach for the increase of the pile head rotation $\Delta\Theta(N)$:

$$\frac{\Delta\Theta(N)}{\Theta_s} = T_b T_c N^{0.31} \quad (4)$$

Here, T_b and T_c are dimensionless parameters depending on the magnitude of the cyclic load, the relative density of the sand and the type of cyclic loading. Θ_s is the pile head rotation under static load.
The development of excess pore water pressure can reduce the effective stress in the ground and therefore reduce the structural safety of a lateral loaded monopiles. The (EAP, 2011) states clearly that for the proof of the structural safety the reduction of soil resistance under cyclic loading should be considered. Moreover, a layering of the subsoil as usually present will affect the pile behaviour under cyclic loads. Thus, several questions remain open and further research is needed to develop generally applicable empirical relations.

3.3.2 Axially loaded piles

Under cyclic axial loads, degradation of ultimate skin friction, and with that a decrease of the pile capacity, is to be expected. The main reason for this is a compaction of the soil beneath the pile shaft due to cyclic shearing, which leads to a reduction of the normal contact stresses acting between pile and soil. According to Randolph, who evaluated cyclic interface tests on sand, the compaction occurs mainly within a small shear band beneath the pile. In a model proposed by Richter and Kirsch, compaction occurs up to a distance at which a threshold value of cyclic shear stress in the soil is reached.
No pile capacity reduction is to be expected if a certain magnitude of the cyclic load portion is not exceeded. The threshold value is termed the critical level of repeated loading (CLRL):

$$CLRL = \frac{E_{cycl}}{R_k} \quad (5)$$

Here E_{cycl} is the cyclic load amplitude and R_k is the static pile capacity.
(Poulos, 1988) presented a cyclic stability diagram for axially loaded piles (Figure 3-4). Based on several model and field tests, the load cycle numbers leading to pile failure are given dependent on the normalised mean load E_0 and the cyclic load amplitude. A 'stable' region is defined here with $E_{cycl}/R_k \leq 0.2$ (i.e. CLRL = 0.2) for $E_0 \leq 0.6\ R_k$.
From the diagram, critical cyclic load amplitude (leading to failure) can be obtained dependent on the mean axial load and the number of load cycles.

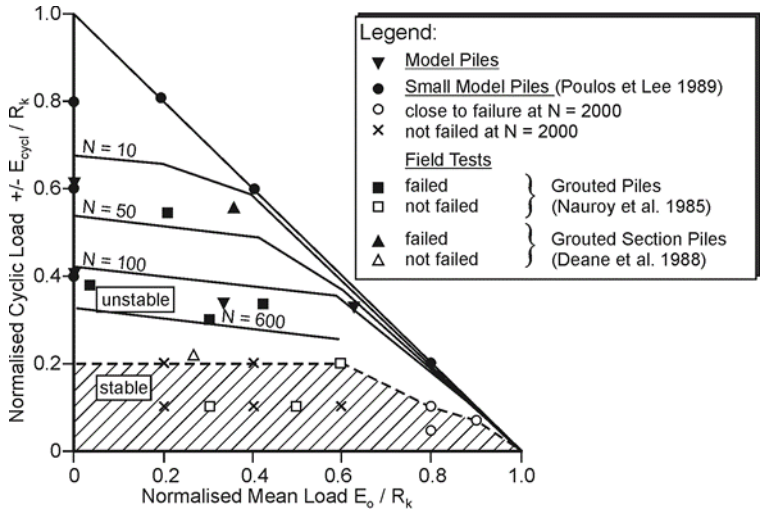

Figure 3-4 Stability diagram of Poulos (Poulos, 1988)

Usually, in offshore engineering no explicit consideration of a possible decrease of pile capacity is made in the design. It is assumed that the negative effect of cyclic loading is counterbalanced by positive effects like pile ageing

(increase of pile capacity with stand time) or loading rate (increased capacity for a short-term load due to a wave). However, in Germany the BSH regulations require explicit consideration of cyclic capacity degradation, and a 'design storm' must be taken into account.
The German 'EA Pfähle' recommendation [33] presents the following design proof for cyclic axially loaded piles:

$$\gamma_E E_k \leq \frac{R_k}{\gamma_R} - n_{cycl} \cdot \Delta R_k \qquad (6)$$

Here γ_E and γ_R are the partial safety factors, E_k is the axial load, R_k is the static pile capacity, η_{cycl} is a model factor and ΔR_k is the capacity decrease due to cyclic loading. The model factor should be greater than 1 and should consider the uncertainty of the model used to determine the capacity degradation ΔR_k. In the informative annex of the 'EA Pfähle', some methods which might be used to determine the capacity degradation are presented.

3.3.3 Liquefaction

According to actual guidelines a liquefaction of the soil must be considered. Liquefaction happens when excess pore water pressure accumulates to the point that the effective stresses become zero. Especially loose, non-cohesive saturated soils and silty sands are highly sensitive to liquefaction. In the praxis, the possibility of liquefaction (liquefaction potential) can be tested in-situ (e.g. (Youd & Idriss, 2001)). But these results are applicable only for the effect of earthquakes.

3.4 CYCLIC LABORATORY TESTS

3.4.1 General Remarks

Cyclic tests can be divided to test groups with high and low frequencies. Results from tests with high frequencies allow the determination of "dynamic" soil parameters, while such with low frequencies (e.g. <1.0 Hz) give results about the behaviour of the soil under quasi-static cyclic loads. Technically speaking, the dynamic soil parameters have nothing to do with dynamic, but they are soil parameters for very small strains.
Under high-frequency dynamic loads soil behaves like a perfectly elastic material. The main reason for this is that under such loads only very small shear strains occur due to inertia effects. In fact, the secant soil stiffness of soil under two-way loading is dependent on the shear strain amplitude (Figure 3-5, left). In case of very small shear strains ($\gamma < 10^{-5}$), as induced under high-frequency loading, the soil stiffness is equivalent to the dynamic shear modulus G_0. If larger shear strains occur, the secant stiffness G_{sec} decreases as presented in Figure 3-5 (right). The secant stiffness G_{sec} is thereby equivalent to the un- and reloading stiffness, which is needed in the dynamic analysis of the OWEC.
Under very small shear strains ($\gamma<10^{-5}$), soil acts nearly elastic and shows a comparable high stiffness. Figure 3-5 shows the loss of shear modulus (G_{sec}) according to the cyclic shear strain.

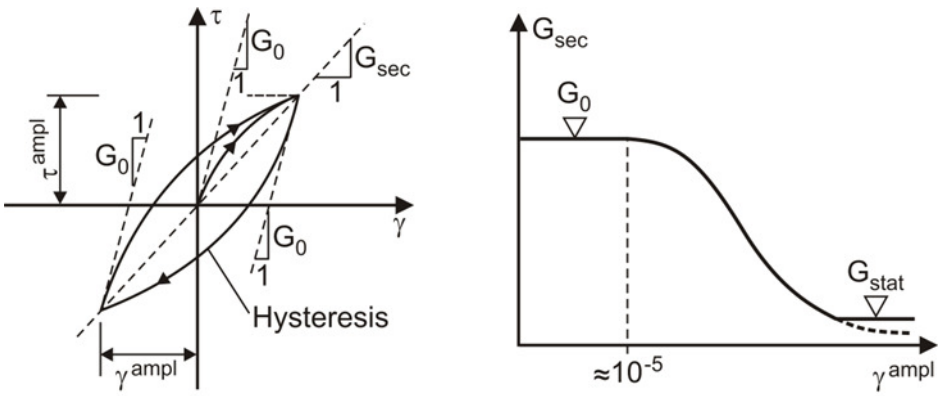

Figure 3-5: Loss of shear modulus of soil with shear distortion

In Table 3-1 (from EAP 2011) laboratory tests for cyclic and dynamic loading are listed below:

Suitability of the tests: ++ very good / + good / o conditionally / - not suitable	Object of study					
test method	development of excess pore water pressure	solidification / softening	change of volume	small strains	material damping	wave velocity
cyclic triaxial test (undrained)	++	+	-	o	o	-
cyclic triaxial test (drained)	-	+	++	o	o	-
cyclic simple shear test (volume constant)	++	+	-	o	o	-
cyclic simple shear test (drained)	-	+	++	o	o	-
cyclic direct shear test (drained)	-	+	+	o	o	-
cyclic simple shear test (drained) under CNS (constant normal stiffness) conditions	-	+	+	o	-	-
cyclic uniaxial compression test with restricted side expansion (odeometric test)	-	o	+	-	o	-
cyclic torsional shear test (undrained)	+	+	-	o	o	-
cyclic torsional shear test (drained)	-	+	+	o	o	-
resonant column test	-	+	o	++	++	++
bender element test; tension-compression element test	-	-	-	+	-	++

Table 3-1 Laboratory tests for cyclic and dynamic loaded soils (from (EAP, 2011))

3.4.2 Determination of Soil Parameters

3.4.2.1 Resonant Column Tests

The Resonant Column Test (RC) is a standard test to obtain the shear modulus and the material damping of a soil sample for small strains. Harmonic torsional vibration is applied to a prismatic soil sample; through variation of the excitation frequency the resonant frequency f_t is determined. It is dependent on the shape (height l) of the sample and the modulus of shear G. The shear modulus is defined as follows:

$$G = 16\, f_t^2\, l^2\, \rho \qquad (7)$$

where ρ is the sample density.

Some devices are able to apply vertical vibrations on a sample. From the dependent resonant frequency, the modulus of elasticity can be obtained. The damping of the material can be determined through analysis of the magnification factor for the forced vibration or through observation of the decay after deactivation of the engine.

3.4.2.2 Bender Element Test

The shear modulus for small strains (dynamic shear modulus) is given by the velocity v_s of a shear wave in the soil, the dynamic modulus of elasticity by the velocity v_L of a longitudinal wave:

$$G = v_s^2 \, \rho \quad (8)$$

$$E = v_L^2 \, \rho \quad (9)$$

Bender elements are to the sample fixed piezo-ceramic elements which can be electrically stimulated and thereby produce shear- or pressure waves. The vibrations are monitored by an opposing receiver, whereby the duration and velocity of the wave can be obtained. Bender elements can be used either in RC- or triaxial devices.

3.4.3 Cyclic triaxial Test

The triaxial test (Figure 3-6) determines the stress-strain behaviour of a cylindrical soil sample. In the conventional triaxial compression test (CTC), starting from a hydrostatic state of stress (σ_3, carried out by water pressure inside the cell), through increase of a vertical force ($\sigma_1 > \sigma_3$) a shear force is applied; and in the end, the sample is sheared. Usually the test is strain controlled and the velocity of the vertical load is kept constant. Other test procedures are possible. The pressure inside the cell can be reduced and the vertical stress can be held constant (TE, triaxial extension), or through control the mean principal stress can be hold steady throughout the shearing process. As a result, the behaviour of the soil can be tested under different loading paths.
The consolidated drained test (CD) applies a force so slow that no excess water pressure occurs. A change of volume of the sample is allowed and the mass of the escaping pore water is measured (a nearly saturated sample is required). The results are plotted with the axial strain ε_1 of the sample and the volumetric ε_v against the deviatoric stress (σ_1-σ_3).
The consolidated undrained test (CU) prevents the drainage of a saturated sample ($\varepsilon_v = 0$) and the development of the pore water pressure (excess pore water pressure Δu) is monitored. Instead of ε_v, Δu is measured against the deviatoric stress (σ_1-σ_3).

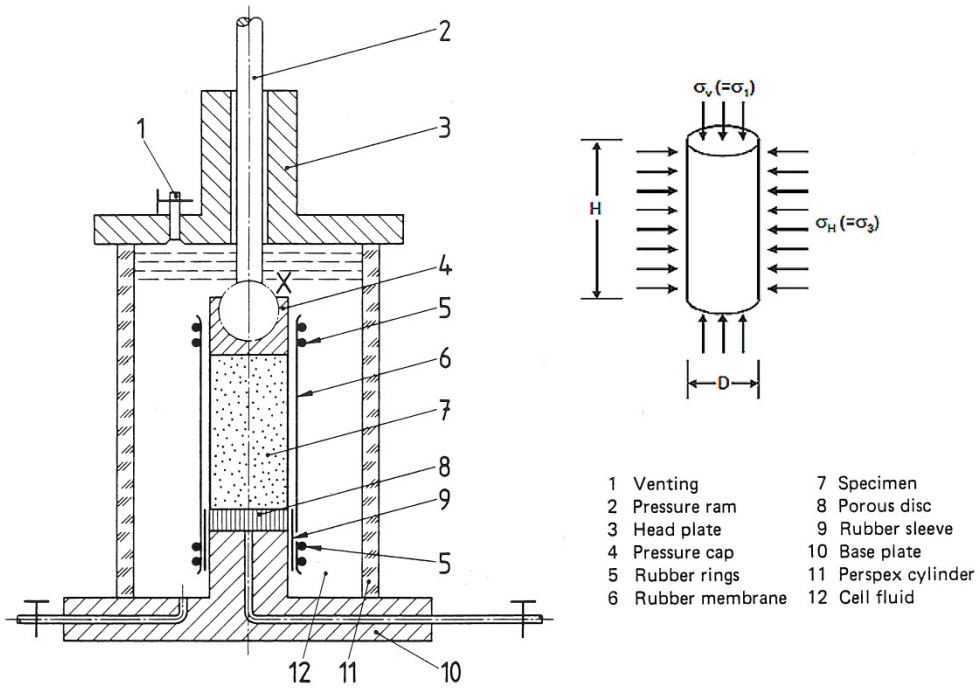

Figure 3-6 Schematic view of a triaxial device

The testing procedure allows to obtain the shear parameters of the soil; form the CD- and CU-tests the "drained" or effective shear parameters φ' and c' can be obtained and for the UU (unconsolidated undrained)-test the undrained shear parameters c_u and φ_u can be measured. The main use of the triaxial test is the examination of the (elastoplastic) stress-shear-behaviour of the soil before reaching of the state of failure.
Accordingly, the cyclic triaxial test investigates the behaviour of the soil under cyclic loading conditions. As an example, Figure 3-7 shows the results of CU-tests for sand samples under cyclic loading. In these tests, the cyclic behaviour under different side pressures and for different cyclic loading amplitudes can be investigated.
Drained cyclic triaxial tests give information about the increase of strain ε_1 and ε_v related to number of cycles N, undrained cyclic triaxial tests can be used to investigate an eventual accumulation of the excess pore water pressure Δu with the number of cycles.
Figure 3-8 shows the result of cyclic CD-tests with cyclic load under different CSR (cyclic stress ratio) values. CSR (in Figure 3-8 CLR, cyclic load ratio) describes the ratio of the cyclic stress difference to the stress difference at the peak calculated from static testing:

$$CSR = \frac{(\sigma_1 - \sigma_3)_{cyc}}{(\sigma_1 - \sigma_3)_{f,stat}} \quad (10)$$

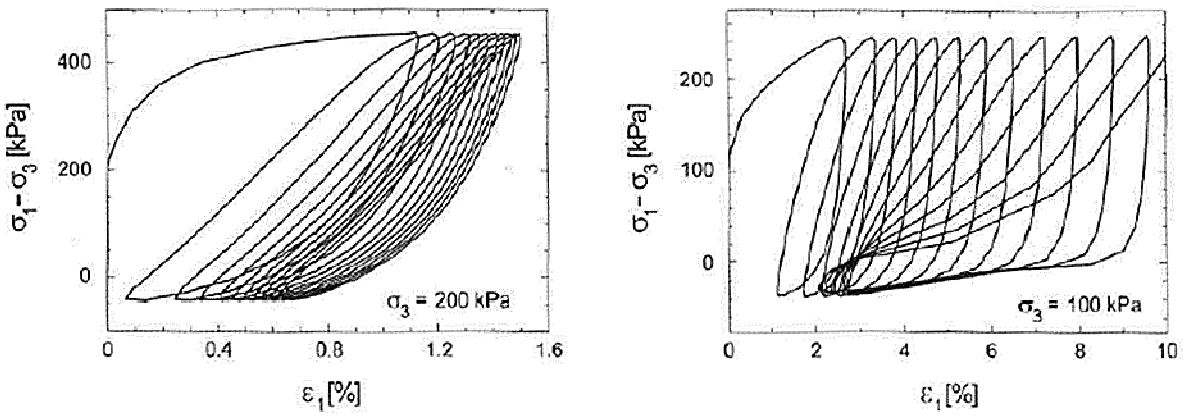

Figure 3-7 Results of cyclic CU triaxial tests in sand (Vrettos, 2008)

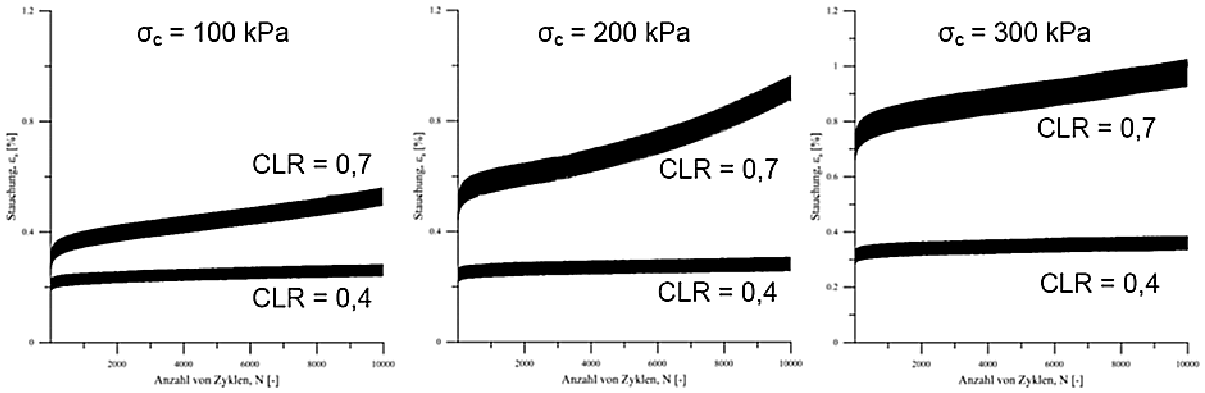

Figure 3-8 Results of cyclic CD triaxial tests in sand

3.4.4 Cyclic Direct Shear Test

The primary function of direct shear test is to determine the shear resistance of a soil sample (Figure 3-9). Basis for the test is that no excess water pressure occurs, wherefore the appropriate shearing velocity can be really slow. Various vertical forces are applied to the upper surface of the sample, monitored is the development of the shear stress in response to the horizontal movement (Figure 3-9, right) and the change of height of the sample during the shearing process (measurement of the volumetric strain).

A negative aspect of the frame shear test with reference to the triaxial test or the simple shear test is that the soil sample is exposed to a non-homogeneous deformation and stress conditions during the shearing process. Parameters which determine the stress-strain behaviour of the sample, cannot be derived directly. The shear parameters φ' and c' can be obtained from the state of failure.

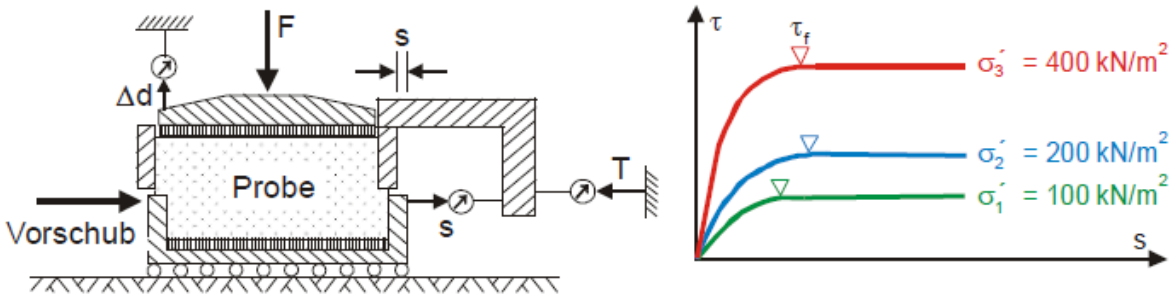

Figure 3-9 Schematic view of a frame shear test and results

Cyclic direct shear experiments on sand were done by (Malkus, 2000). Between lower and upper half a profiled steel plate was mounted to simulate the rough surface between the soil and the footing. Figure 3-10 shows the results of such an experiment in which the shear stress was applied as a cyclic load with a maximum of 80% of the maximum static shear stress. It can be seen that the maximum and the permanent shear deformation increases with the number of load cycles. This experiment was done under constant normal load (CNL-condition).

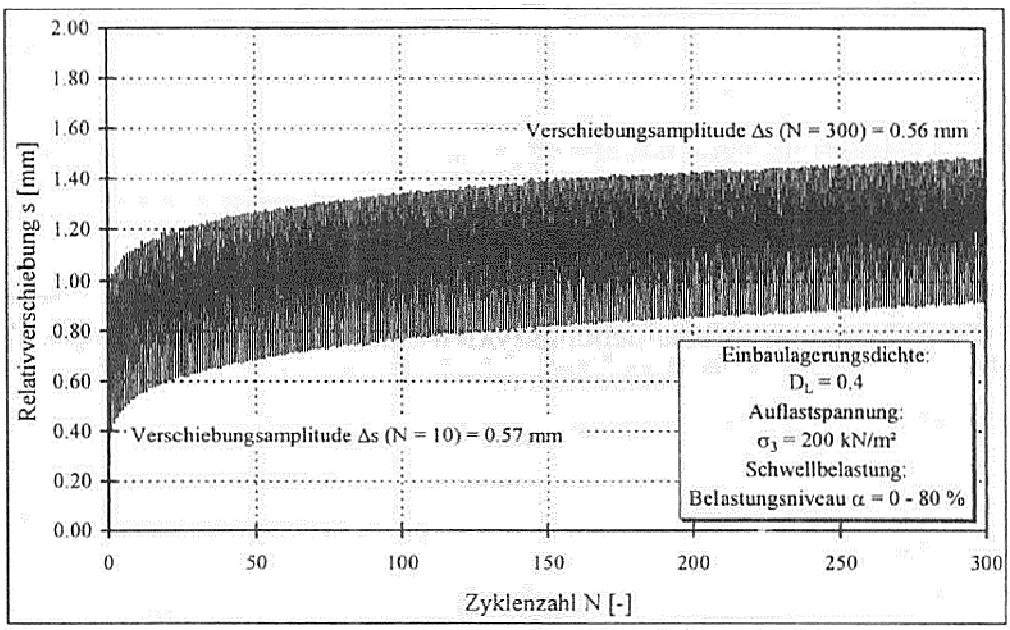

Figure 3-10 Results of a cyclic composite shear experiment by (Malkus, 2000)

A simulation of the processes around the pile shaft, which lead to degradation of the skin friction, is possible through a special laboratory test, which is the cyclic normal stiffness test (CNS) using a modified frame shear device.
In the CNS-test, the normal stress between soil and pile (represented through a steel plate) is controlled in response to the change of volume of the soil. As result of the soil compaction (caused by the cyclic shearing) the vertical stress is reduced and consequently the frictional stress between the plate and the soil. Figure 3-11 shows a schematic set-up of a CNS-test. More detailed information is available through the publications of (Boulon & Foray, 1986), (Mortara, Mangiola, & Ghionna, 2004) and (Randolph, 2009).
In cyclic CNS-tests, the governing parameters are initial vertical stress $\sigma_{n,o}$, the spring stiffness K_b, the type of cyclic loading (force- or deformation controlled, the force- or deformation amplitude) and the number of loading cycles. The initial vertical stress depends mainly on the depth of the considered point at the pile under the sea bed while the spring stiffness mostly depends on the properties of the soil (unloading modulus) and the geometry of the pile.

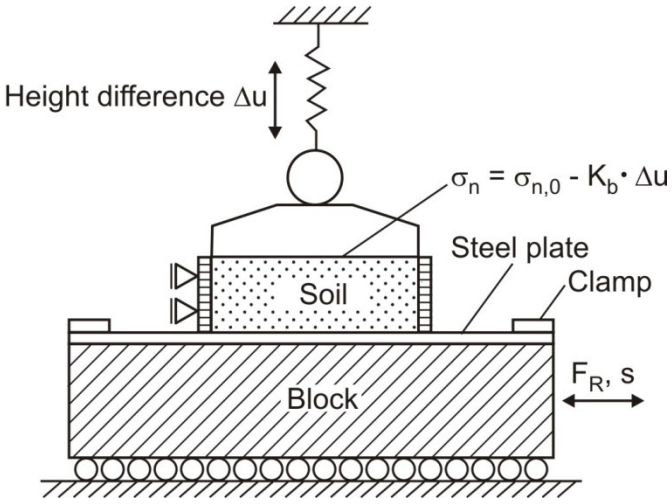

Figure 3-11 Experimental set up CNS test (test of friction between soil and steel)

Figure 3-12 shows exemplary the results of a CNS-test for very dense sand. The cyclic shear amplitude with a maximum of 5mm was adopted. This cyclic shear amplitude is noticeably higher than the displacement required to mobilize the maximum shear stress; this is the reason for the dramatic decrease of shear stress. The behaviour of the

sample is contractant, which means that the settlement grows with every cycle that means that with the chosen stiffness K_b the normal stress and also the mobilized shear stress is reduced.

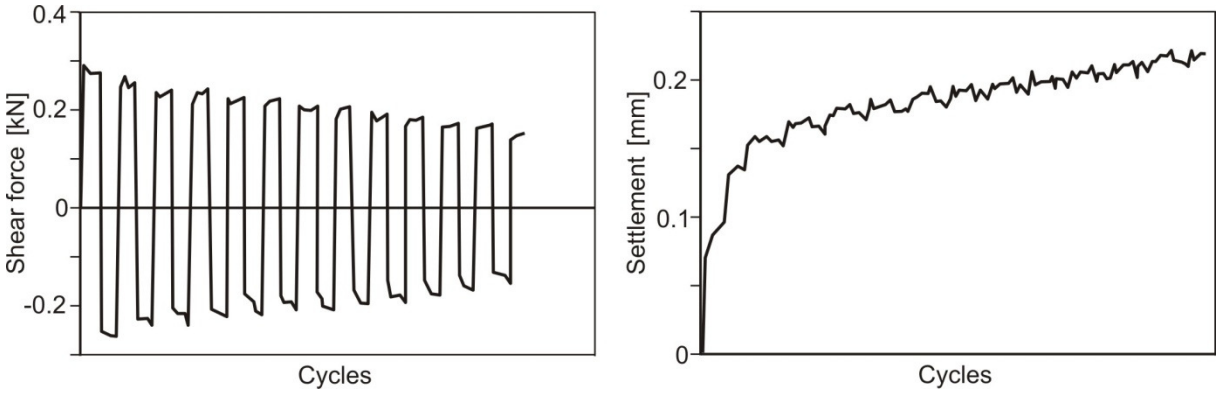

Figure 3-12 Results of a CNS-test in dense sand

3.4.5 Simple Shear Testing

The simple shear test applies a shear deformation for the full height of a soil sample (shear strain γ) (Figure 3-13). In the standard test, the normal stress remains constant throughout the experiment. Unlike in the simple shear test, the soil sample is under homogeneous stress and strain conditions.

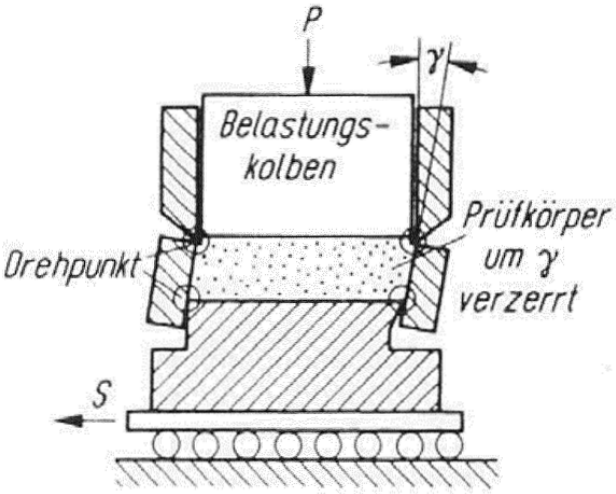

Figure 3-13 Schematic set-up of a simple shear test (von Soos & Engel, 2008)

The results of a simple shear test are shown in Figure 3-14. A relatively high cyclic shear strain was applied. Under high shear strain amplitudes, the sample behaves dilatant, whereby the swelling is reduced with the number of cycles. Under small shear amplitudes and generally in loose sand, the soil sample behaves contractant.

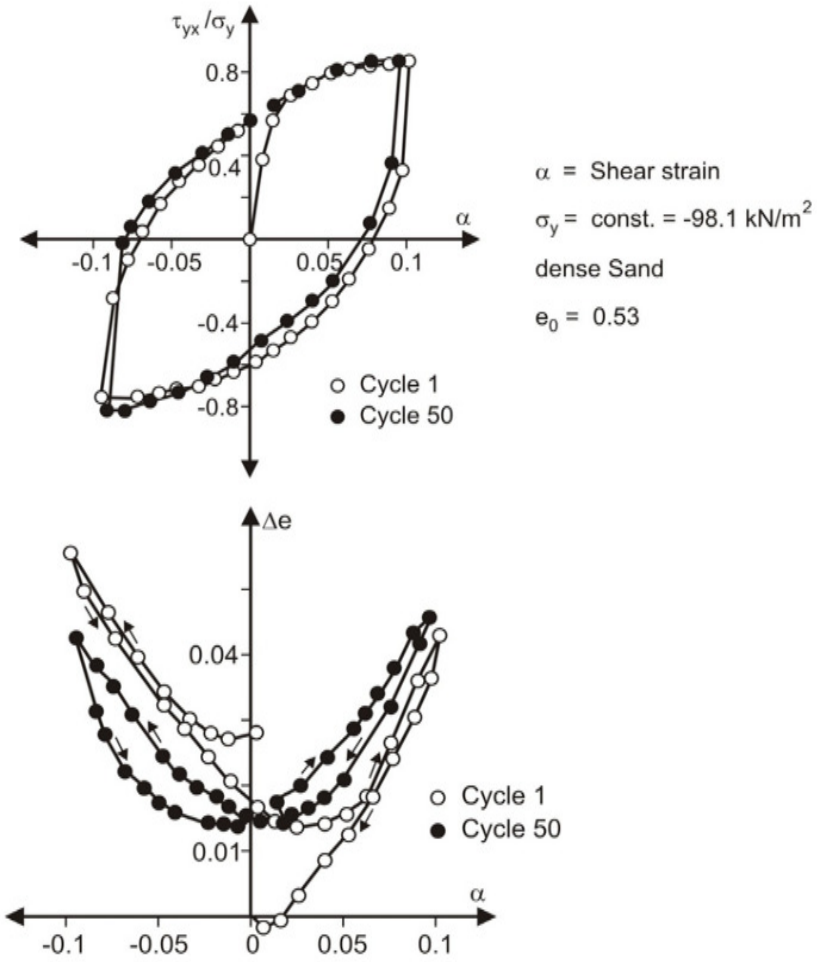

Figure 3-14 Results of a simple shear test (Winselmann, 1984)

(Silver & Seed, 1971) investigated systematically the change of volume of sand samples in cyclic simple shear tests. Figure 3-15 shows the results. The compaction of the sample grew with the growing number of cycles, which was mainly dependent on the shear strain amplitude and subsidiary from the applied vertical loading.

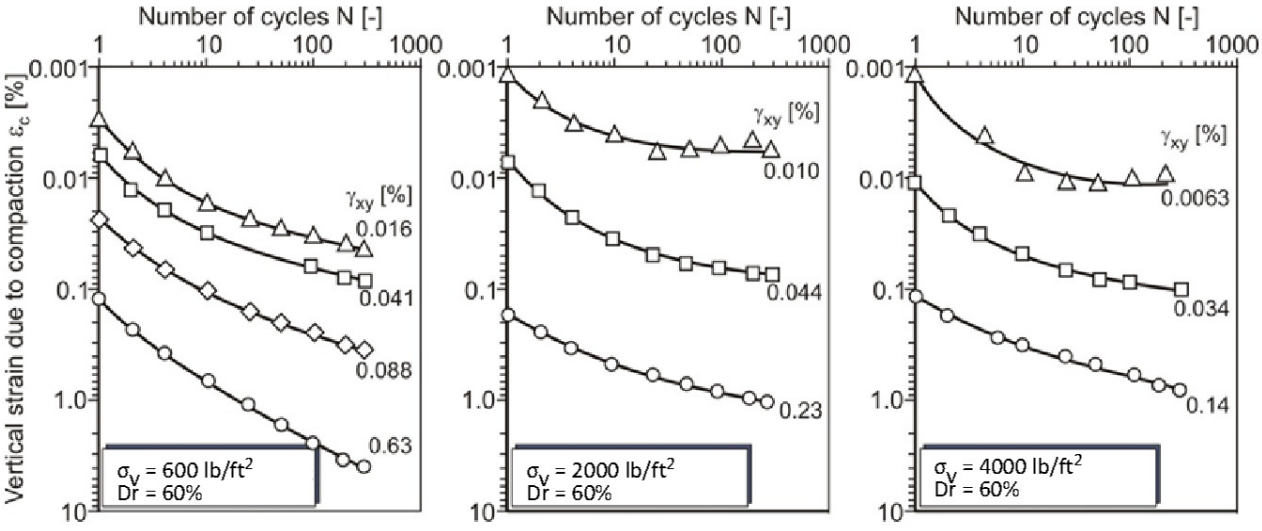

Figure 3-15 Results of simple shear tests by (Silver & Seed, 1971)

3.4.6 Cyclic Compression Testing

The compression test investigates the stiffness of the soil under restricted radial strain. The load is applied to the soil in steps – if necessary, unloaded between – and the final settlements of every load level are monitored in the load-settlement curve (Figure 3-16). The load-settlement curve is normally non-linear, which shows the dependency of the modulus of elasticity E_s on the load level.

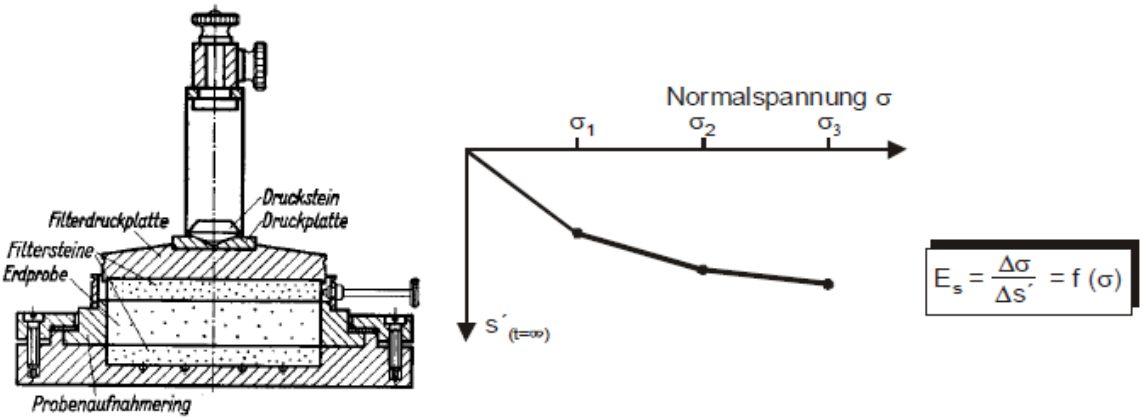

Figure 3-16 Compression test and load-settlement curve

In cyclic compression tests, the increase of the sample settlement and development of the odeometric modulus under cyclic loading can be investigated. Figure 3-17 shows the test results made by (Malkus, 2000). Malkus found that the growth of deformation depends on the size and type of cyclic loading (upper and lower load limit).

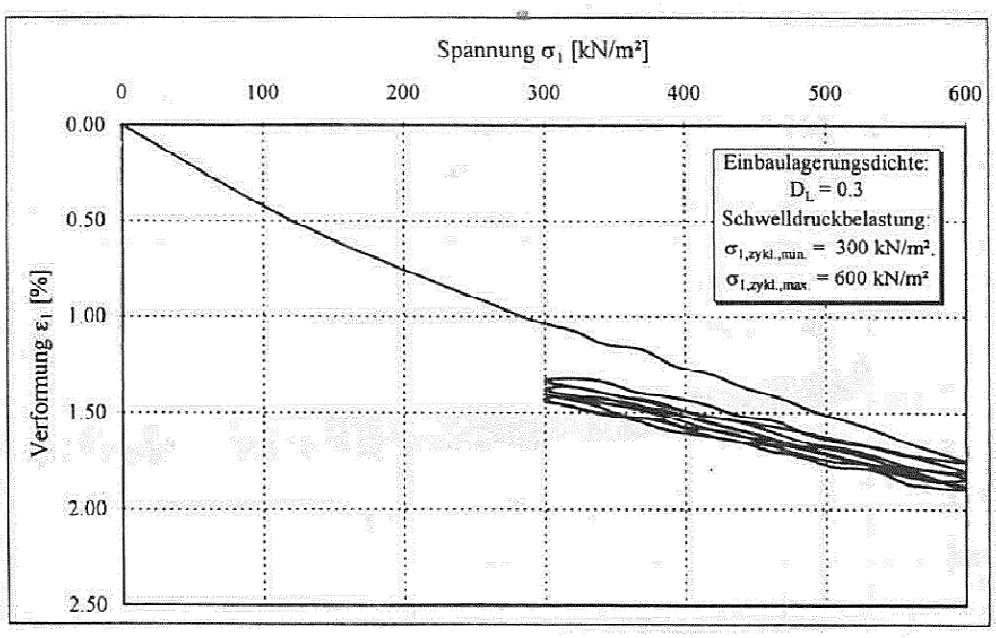

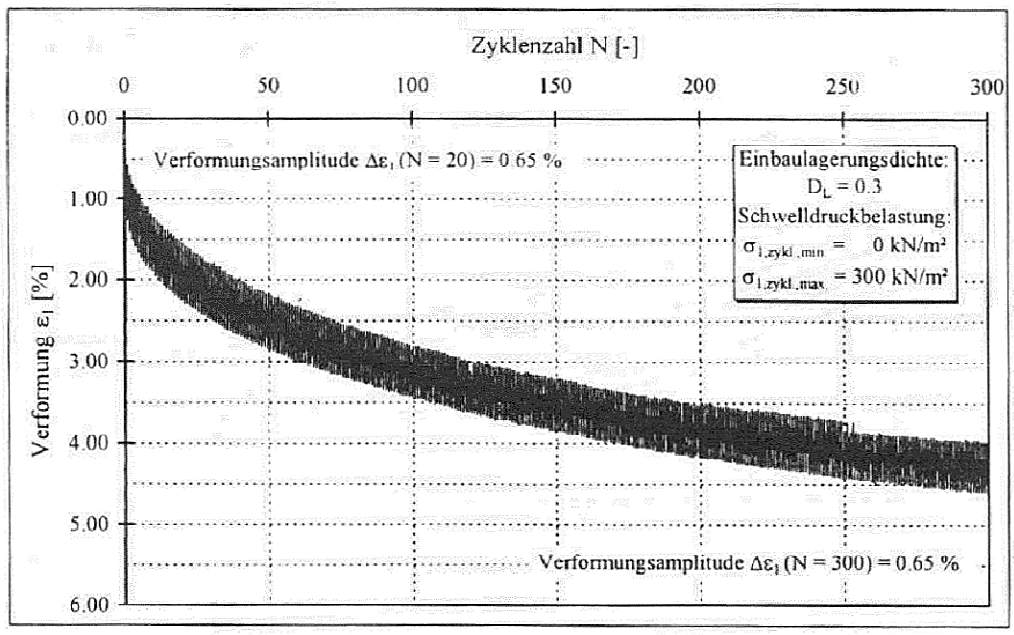

Figure 3-17 Results of cyclic compression tests by (Malkus, 2000)

3.5 ADAPTATION IN THE DESIGN

3.5.1 General remarks

The results of cyclic laboratory tests can be used for the determination of material parameters for a constitutive equation which considers the effect of cyclic loads. With this constitutive equation, the behaviour of Monopiles and axial loaded piles under any cyclic loading could be investigated. In the application process, some problems occur:

- Constitutive equations that consider the behaviour of soil under cyclic loads are very complex. One example is the hypoplastic constitutive law which is used often in research in Germany. This law has (in the version which considers “intergranular strain” to describe cyclic soil behaviour) 13 material parameters, whereby 5 describe the behaviour under cyclic loads. The necessary experimental program to determine all of the parameters is extremely costly.
- Even highly complex constitutive equations cannot describe the soil behaviour under any stress state with the same accuracy; therefore they are limited in their exactness.
- It must be added that in the implicit calculation, that means in the simulation of the cyclic load, step by step numeric errors accumulate. The change of stress and strain in the soil are very small from step to step, therefore the numeric errors can lead together with a big number of load cycles to an even big change of the result. Therefore, the implicit calculation is only for a limited number of load cycles (e.g. about 20) sufficiently accurate.

As a result, the implicit calculation with highly complex constitutive equations is not effective in praxis. Instead, calculation methods which use a monotonic load and adapt the number of load cycles through adjustment of the soil parameters must be used.
Following below, calculation methods for Monopiles, and axially loaded piles are presented and it is shown how the results of cyclic laboratory tests can be considered.

3.5.2 Design of Monopiles

It is known from different experimental investigations that the deflections of a horizontally loaded pile increase under cyclic one-way loading. As an example, model test results of (Hettler, 1981) for flexible piles in homogeneous sand are shown in Figure 3-18.

In general, the increase of head deflection can be described by the following equation:

$$y_N = y_1 f_N(N) \quad (11)$$

Here y_N and y_1 are the horizontal pile head deflections after N load cycles and after 1 load cycle (static loading), respectively. $f_N(N)$ is a function which describes the increase of deflections. As long as the cyclic load amplitude is well below the ultimate pile capacity, sedation behaviour can be expected, which means that the deflection rate decreases with increasing number of load cycles. The most common functions for piles under cyclic loading that are found in literature are of the exponential type such as (4) (e.g. Little & Briaud 1988) and of logarithmic type such as (13) (e.g.(Hettler, 1981)):

$$f_N = N^m \quad (12)$$

$$f_N = 1 + t \cdot \ln N \quad (13)$$

Here m and t are empirical degradation parameters. Assuming that these parameters (m and t) are constants, (12) and (13) imply that the function of load cycle number is independent of the load amplitude. (Peralta & Achmus, 2010) found, based on model tests, that the exponential function of displacement increase with respect to number of load cycles better fits the cyclic displacement curves of almost rigid piles while the logarithmic function better fits the displacement curves of flexible piles.

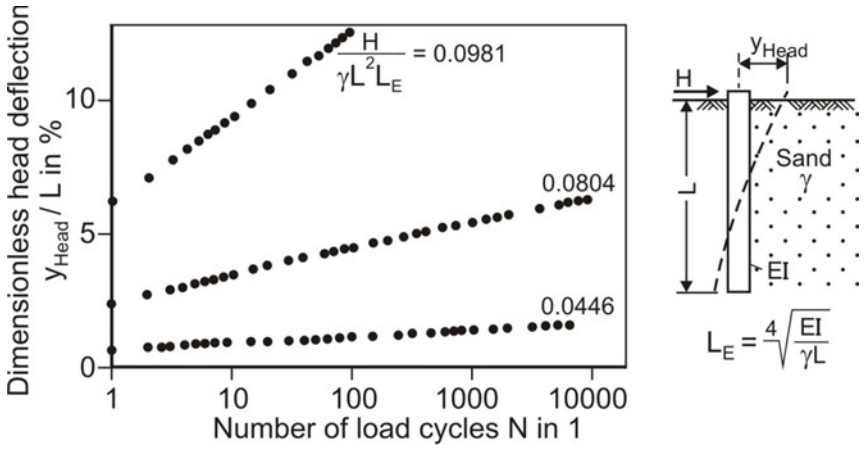

Figure 3-18 Model test results of (Hettler, 1981)

These empirical equations take the number of load cycles explicitly into account. However, only one parameter governs the displacement accumulation, and it is more or less unknown how this parameter is affected by soil, geometry and loading conditions. Moreover, a layering of the subsoil as usually present will affect the pile behaviour under cyclic loads. Thus, several questions remain open and further research is needed to develop generally applicable empirical relations.

3.5.2.1 Stiffness Degradation Method

The stiffness degradation method (SDM) developed by the authors and co-workers is a method based on a combination of a finite element simulation of the pile-soil interaction and an evaluation of drained cyclic triaxial tests. In cyclic drained triaxial tests, the accumulation of plastic strains with the number of cycles under different loading conditions can be observed. This increase of plastic strain can be interpreted as a decrease in soil secant stiffness. Assessing the stress conditions in the distinct elements and introducing the stiffness degradation obtained by comparison with the cyclic test results in the finite element model yields the accumulated deformations of the pile-soil system. This is the basic concept of this model.

In the numerical simulation, an elastoplastic material law with Mohr-Coulomb failure criterion and a stress-dependent stiffness approach is applied. This simulation model forms the basis for the cyclic analysis. The degradation stiffness approach to account for cyclic loading effects is elucidated in Figure 3-19. In a cyclic triaxial test, an increase of the plastic axial strain can be observed. Assuming the elastic strain to be negligible, the degradation rate of secant stiffness after first cycle E_{s1} and Nth cycle E_{sN} can be presented by the plastic axial strains after first cycle $\varepsilon^a_{cp,N=1}$ and after Nth cycle $\varepsilon^a_{cp,N}$ according to the following equation:

$$\frac{E_{sN}}{E_{s1}} \approx \frac{\varepsilon^a_{cp,N=1}}{\varepsilon^a_{cp,N}} \quad (14)$$

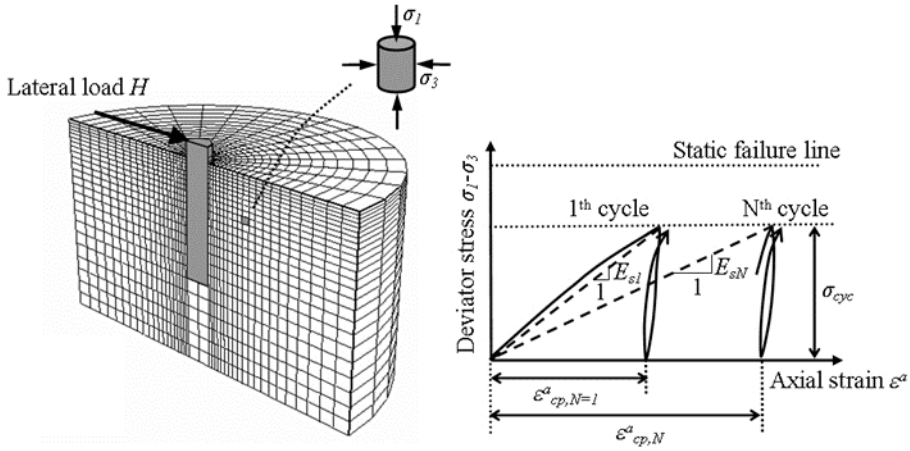

Figure 3-19 Degradation of secant modulus under cyclic loading in the pile-soil model (schematic)

The accumulation of plastic strains in a cyclic triaxial test can be estimated from a semi-empirical approach of Huurman (1996). With that, the degradation of stiffness can be de-scribed using two material parameters b_1 and b_2 as follows:

$$\frac{E_{sN}}{E_{s1}} = \frac{\varepsilon^a_{cp,N=1}}{\varepsilon^a_{cp,N}} = N^{-b_1(x)^{b_2}} \quad (15)$$

Here N is the number of load cycles and X is the cyclic stress ratio defined by Huurman (1996) for cohesionless material as follows:

$$X = \frac{\sigma_{1,cyc}}{\sigma_{1,sf}} \quad (16)$$

where $\sigma_{1,sf}$ is the major principal stress at static failure state and $\sigma_{1,cyc}$ is the major principal stress for the cyclic stress state under consideration. The cyclic stress ratio is thus dependent on the confining pressure and on the cyclic stress level. From cyclic triaxial test results documented in the literature, typical regression parameters b_1 and b_2 were found for dense sand to be $b_1 = 0.20$, $b_2 = 5.76$ and for medium dense sand $b_1 = 0.16$, $b_2 = 0.38$ (Kuo, 2008).
A problem to be dealt with is that the Equations 11 and 12 are valid for triaxial test conditions with isotropic initial stress conditions and a constant confining pressure σ_3 during cyclic loading. In the pile-soil system, the initial stress conditions (before application of the horizontal load) are anisotropic and the minor principal stress in the elements as well as the direction of the principal stress axes in general change with the application of the load. To overcome this problem, a characteristic cyclic stress ratio X_c is defined here as

$$X_c = \frac{X^{(1)} - X^{(0)}}{1 - X^{(0)}} \quad (17)$$

Here the index (1) means the cyclic stress ratio at loading phase and the index (0) means at unloading phase (Figure 3-20). At the initial (and unloading) phase, only the vertical load V due to the tower weight is considered, and the lateral load H is applied subsequently in the loading phase. The characteristic cyclic stress ratio is derived from the difference between the stress ratios in the loading and the unloading phase. Due to the denominator in (16) this value varies from 0 to 1. The accumulation of plastic strain and the degradation of stiffness of the soil element can be obtained from (15) by replacing X by X_c.
In the last step of the simulation (model C in Figure 3-20), the deformation response of the system is analysed using the degradation stiffnesses obtained from evaluation of models A and B.

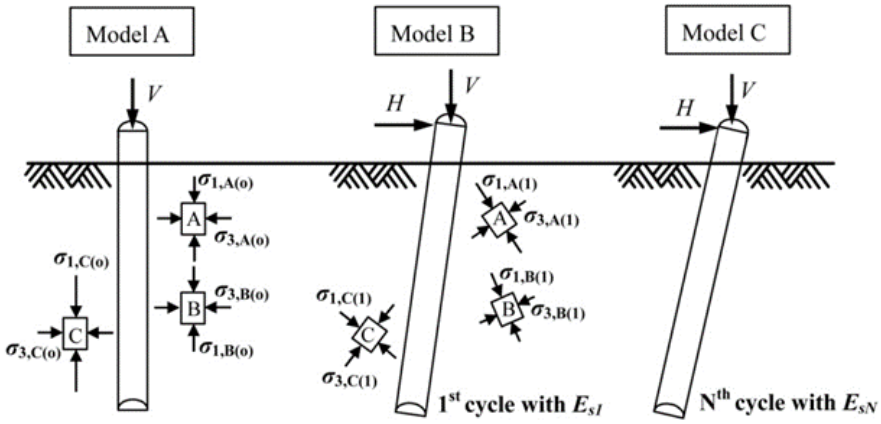

Figure 3-20 Schematic sketch of the determination of degradation stiffness in the pile-soil system

By back-calculation of model tests it was shown that the method can well capture permanent deformation responses of a soil element and of a pile-soil system ((Achmus M. , 2011),(Kuo, 2008)). In Figure 3-21, calculation results are depicted for a monopile with a diameter of 4m embedded in dense sand. A steel pipe pile with a wall thickness of 46mm was considered. A horizontal load was applied with a moment arm of 37.9m. The load magnitude was chosen to 40% of the ultimate load.
The deflection lines depicted in Figure 3-21 top show that the monopile with an embedded length of 15m behaves almost rigid, whereas the pile with an embedded length of 21m behaves more flexible. The stiffness degradation method was applied, using the typical parameters b_1 and b_2 for dense sand stated above. In Figure 3-21 bottom the relative increases (with regard to the static deflection) of pile head displacement are shown. These curves can be interpreted as a measure of the cyclic performance of a pile. The longer flexible pile (L=21m) has a greater deflection under cyclic load, but it performs better than the shorter and almost rigid pile (L=15m) under cyclic loading. Thus, the function $f_N(N)$ (cf. Equations 8 and 9) is obviously also dependent on the pile-soil system, i.e. the relative stiffness of the pile.
The calculated performance curves can be well described by the exponential equation type given in (11).
The parameter m is m=0.145 for the shorter pile and m=0.123 for the longer pile. These values are plausible. (Little, 1988) reported measured m-values for long and flexible piles between 0.04 and 0.09, whereas from results of (Long, 1994) m-values for rigid piles between 0.10 and 0.25 can be derived. For a driven pile in dense sand, the Long & Vanneste-approach yields m=0.136.

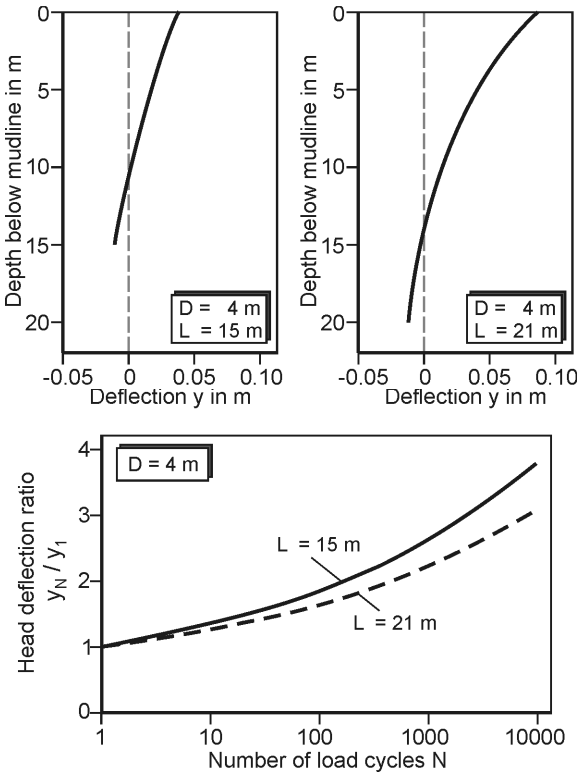

Figure 3-21 Deflection lines of monopiles D=4m in dense sand (top) and results of the stiffness degradation method (bottom)

3.5.2.2 Accounting for different loading types

The previous method (SDM) can be used to determine the accumulation parameter for a certain system under one-way loading with constant amplitude. Actually, under offshore conditions the maximum load occurs only once, and all the other loads occurring over the lifetime have different amplitudes and also different eccentricities.
(LeBlanc, 2009) carried out model tests with monopiles under general loading conditions. They proposed the following approach to calculate the increase of pile head rotation after N cycles with the number of load cycles:

$$\Delta\Theta_N = \Theta_1 T_c T_b N^{\alpha} \quad (18)$$

Here α is an accumulation parameter, θ_1 is the static pile head rotation, T_b is a function dependent on the load magnitude and T_c is a function dependent on the type of loading, which is described by a parameter ζ_c:

$$\zeta_c = \frac{M_{min}}{M_{max}} \quad (19)$$

Here M_{max} is the maximum and M_{min} is the minimum load applied. For one way loading with full unloading $\zeta_c = 0$ ($M_{min} = 0$), and for two-way loading $\zeta_c = -1$ ($M_{min} = -M_{max}$) applies.
LeBlanc et al. found that the T_c-function shown in Figure 3-22, was identical for the same pile once in loose and once in medium dense sand. It can thus be supposed that this function is generally valid at least for very rigid piles in sand soils.
Based on this, the accumulated rotation of a monopile can be determined for arbitrary cyclic load packages. The accumulation parameter α and the function T_b can be derived from simulations with the stiffness degradation method, assuming one-way loading conditions ($\zeta_c = 0$). With these results and the function T_c given in Figure 3-22, the effect of loads of different types and magnitudes can be calculated. If a reference load is chosen with $\theta_{1,ref}$, $T_{b,ref}$ and $T_{c,ref}$, then the equivalent load cycle number $\Delta N_{ref,equ}$ for another load package with N cycles can be determined as follows:

$$\Delta N_{ref,equ} = \left(\frac{\Theta_1 T_b T_c N^{\alpha}}{\Theta_{1,ref} T_{b,ref} T_{c,ref}} \right)^{1/\alpha} \quad (20)$$

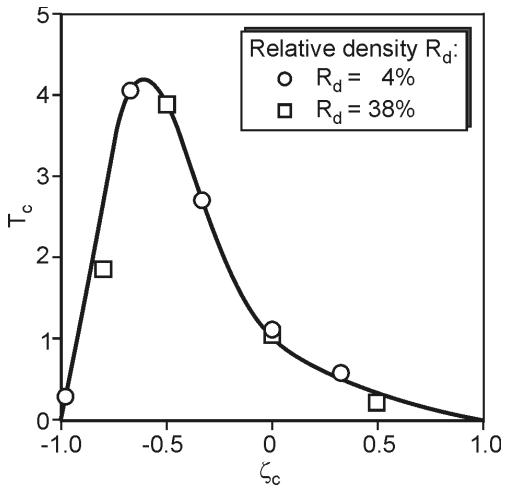

Figure 3-22 Function T_c found by (LeBlanc, 2009)

3.5.3 Design of cyclic axially loaded piles

For axially loaded piles, it is necessary to determine the reduction of the bearing capacity due to cyclic loading. According to BSH (2011), a defined 35h-storm has to be considered for the design of axially loaded piles. Right now there are no confirmed methods for the calculation of the reduction of bearing capacity. In (EAP, 2011), the calculation methods for estimation are provided in the appendix. Those are the interaction diagram method, the method according to (Kirsch & Richter, 2010) and the method according to (Thomas, 2011).

The 'interaction diagram method' uses stability diagrams, similar to the Poulos diagram shown in Figure 3-4, to calculate the capacity degradation. In Figure 3-23 a stability diagram proposed by Kirsch et al. (Kirsch & Richter, 2010) and also mentioned in 'EA Pfähle' (EAP, 2011) is shown. This diagram was derived from cyclic pile load tests reported in the literature.

The input data needed are the static pile capacity R_k, the cyclic load amplitude E_{cycl}, the average load E_0 and the number of load cycles N. The parameters X_{cycl} and X_{mean} are the dimensionless cyclic and average loads, normalised with respect to the static capacity:

$$X_{cyc} = \frac{E_{cyc}}{Rk}; \; X_{mean} = \frac{E_0}{R_k} \quad (21)$$

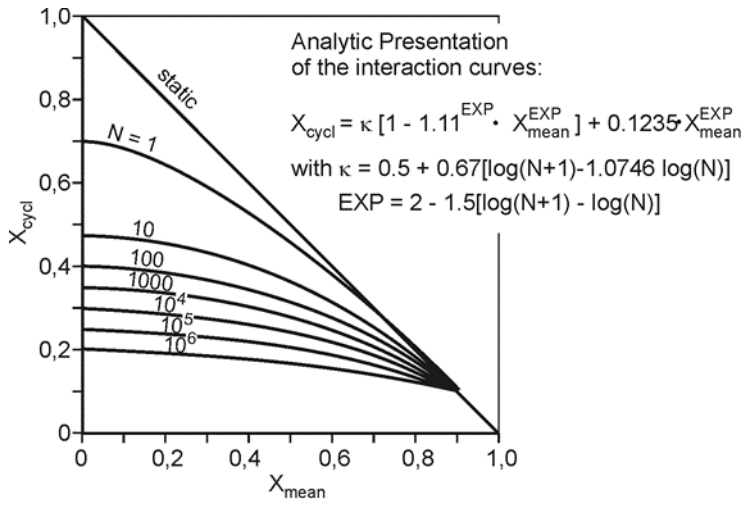

Figure 3-23 Interaction diagram of Kirsch et al. (Kirsch & Richter, 2010)

If the point (X_{cycl}; X_{mean}) in the interaction diagram lies below the interaction curve for the considered number of load cycles (μ<1, see Figure 3-24), then no failure occurs. The capacity reduction would be $f_R \cdot R_k$, if the point lies on the interaction curve. The reduction factor f_R is also defined in Figure 3-24. The 'EA Pfähle' proposes to calculate ΔR_k belonging to the actual point as follows:

$$\Delta R_k = \mu f_R R_k \qquad (22)$$

This 'EA Pfähle' procedure is just a proposal which lacks experimental evidence. Another possible procedure is to consider the number of load cycles N_f for the interaction curve intersecting the actual point (X_{cycl}; X_{mean}) and to use N/N_f instead of μ as the "damage variable":

$$\Delta R_k = \frac{N}{N_f} f_R R_k \qquad (23)$$

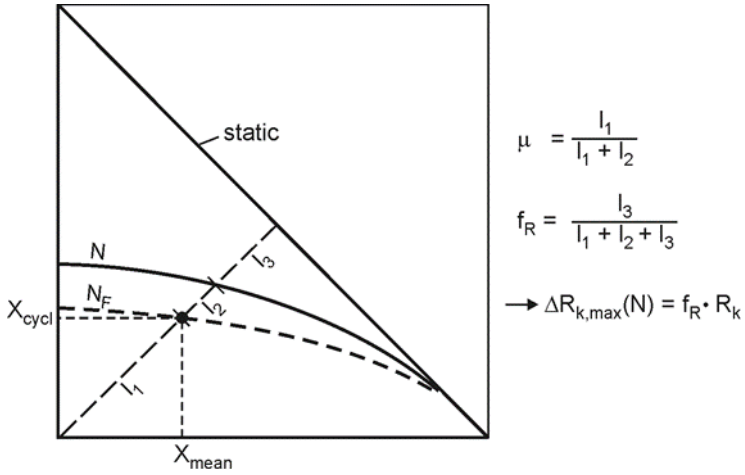

Figure 3-24 Evaluation of an interaction diagram

Figure 3-25 elucidates by an example that the two damage laws lead to totally different degraded pile capacities. Equation 19 results in a constant capacity degradation ΔR_k independent of the pile length, i.e. independent of the absolute value of the static pile capacity, whereas Equ. 20 predicts a strong decrease of ΔR_k with an elongation of the pile. There is obviously urgent need for further research to clarify which damage law is realistic and should thus be used in the design of cyclic axially loaded piles.

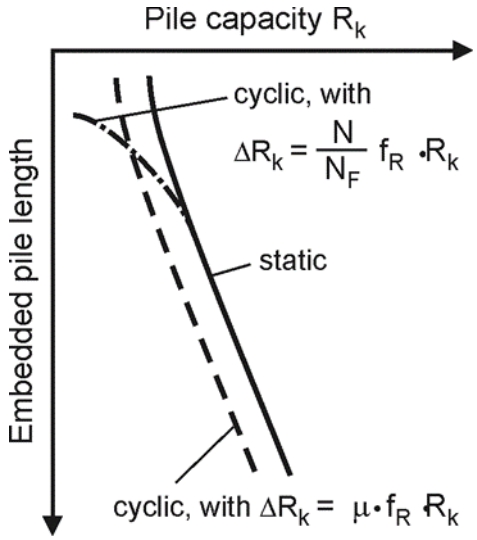

Figure 3-25 Pile capacity degradation dependent on pile length

The approximation procedure by Kirsch & Richter (2010) takes into account that under cyclic shearing the soil is compacted in the area around of the pile, which leads to a loss of radial stress between pile and soil and consequently the skin friction is reduced. The compaction effect due to application of 10 cycles of shear strain was investigated previously by Silver & Seed (1971) by performing cyclic simple shear tests on sand. Their results can be presented as a relationship between the volume reduction due to compaction (ε_{ii}) and the cyclic shear strain $\tilde{\gamma}$ (see Figure 3-26). Richter & Kirsch assumed a logarithmic dependence of volume compaction and number of cycles and thus extended the equation by introducing $\log_{10}N$.

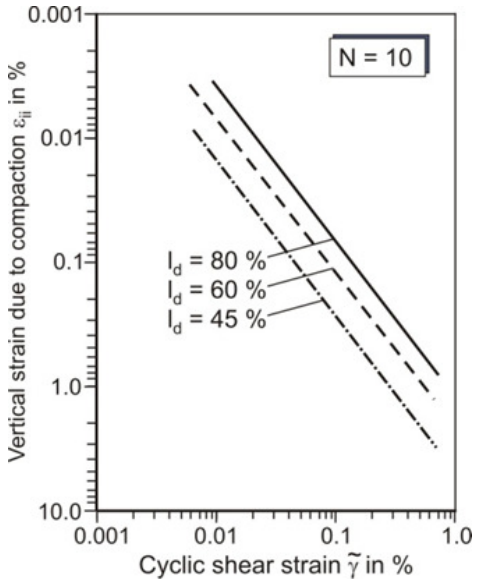

$$\varepsilon_{ii} = 0.5 \cdot (\tilde{\gamma} - 5 \cdot 10^{-5}) \cdot I_d^{-2.32}$$

Figure 3-26 Results of cyclic simple shear tests by Silver & Seed (quoted in(Kirsch & Richter, 2010))

Thomas (2011) developed a new method based mainly on modelling the pile supported by two kinds of springs (t-z) and (q-z) (see Figure 3-27). The t –z springs describe the behaviour of skin friction along the pile while q-z describes the base resistance of the pile. The required parameters can be obtained from static and cyclic model tests. For more details refer to Thomas (2011).

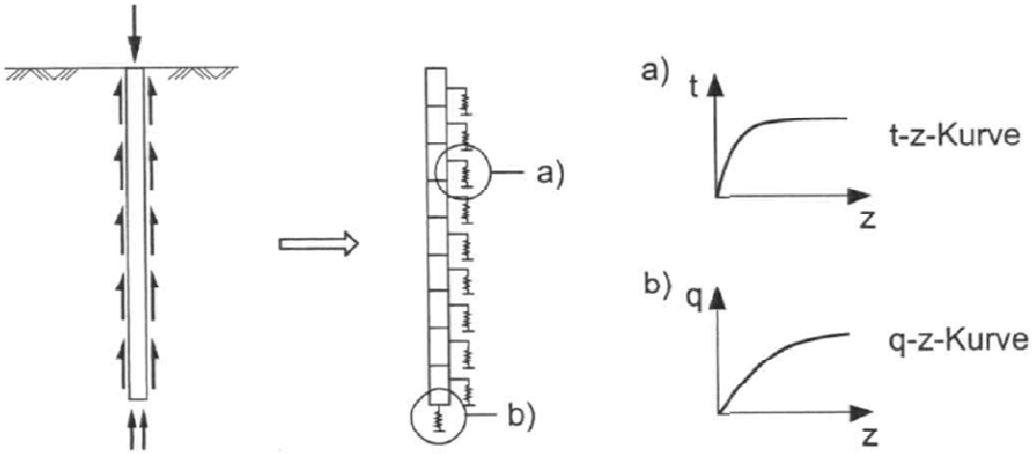

Figure 3-27 Pile behaviour using t-z and q-z approach

Last but not least, a calculation model by Randolph, named Cyclops (Randolph 2003), should be mentioned (Figure 3-28). In this, the interaction between soil and pile is simulated through non-linear springs (in case of skin friction by so-called t-z – curves). The calculation model considers a change of the t-z – curves under cyclic loading and unload-

ing through “flow functions”. If all parameters that have influence on the form of the t-z – curve are known, the behaviour of the pile under any cyclic load path and also the loss of bearing capacity can be calculated.

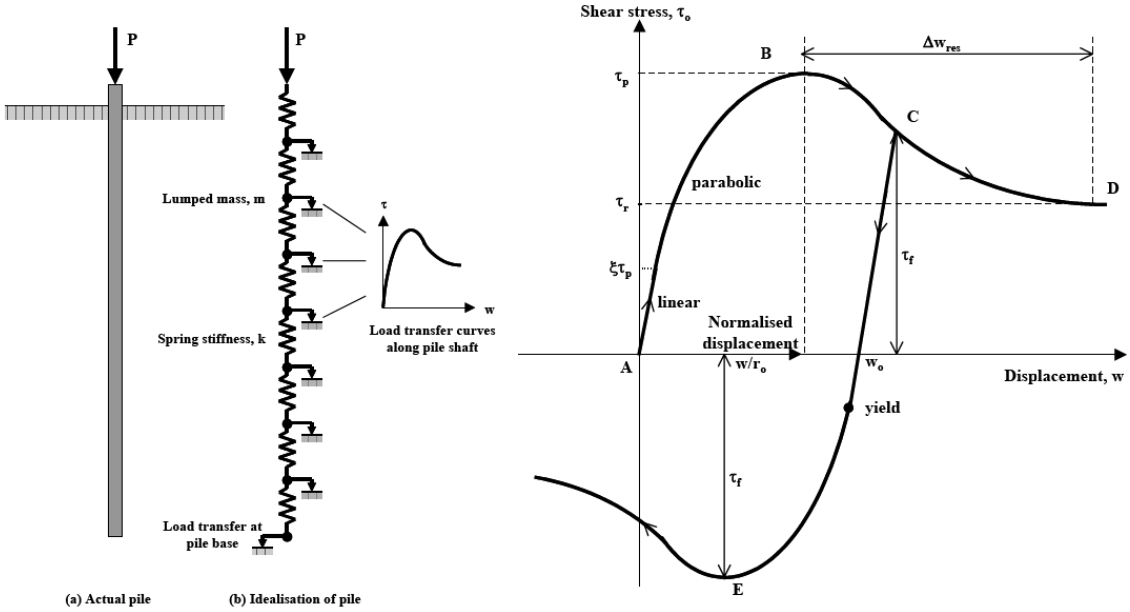

Figure 3-28 Calculation of the cyclic behaviour with Cyclops (Randolph, 2003)

3.6 DESIGN CONCEPT FOR STRUCTURE-SOIL-INTERACTION

The design of foundation elements for offshore wind energy structures is a challenging task for geotechnical engineers. No standard calculation methods exist for many sub problems, particularly regarding the consideration of cyclic load effects in ULS and SLS design proofs.

3.6.1 Monopile

In view of the deficient knowledge the question comes up which methods or concepts shall currently be used in the design of horizontally loaded piles for offshore wind energy foundations. Possibilities to carry out the practical design are presented in the following. Essentially, the following geotechnical design proofs have to be carried out:

- Proof of sufficient bearing capacity with respect to horizontal loading under extreme load (ULS, ultimate limit state),
- Proof of serviceability (SLS, serviceability limit state), in particular determination or at least conservative estimation of the permanent accumulated deflection or rotation at pile head, and
- Determination of the stiffness of the pile-soil system under operational loads. This is necessary for the calculation of the natural frequency of the whole structure, which significantly affects the fatigue loads.

The following recommendations are thus focused on the consideration of effects due to cyclic loading.

ULS design proof

According to German regulations for offshore wind energy foundations a potential pile capacity degradation induced by a design storm has to be taken into account. The problem in that is that for horizontally loaded piles no such calculation method exists. However, in the view of the authors the explicit consideration of loads induced by a design storm is obsolete. Instead, the p-y method with p-y curves for cyclic loading can be used for the analysis of the pile behaviour under extreme load. These curves are valid for about 100 load cycles of the extreme load. If the actual load spectrum of the design storm would be transferred to an equivalent number of load cycles of the extreme load,

probably a load cycle number much smaller than 100 would result. Thus, it can be assumed that the strength and stiffness reduction due to a design storm are considered by the cyclic p-y approach.
In that context it should be noted that for the monopile foundations realized so far no problems regarding lateral capacity under storms have been reported. The required soil parameters for p-y method can be obtained from CPT-measurements based on the correlation between CPT and the soil frictional angle.
Additional soil laboratory testing e.g. direct shear test triaxial drained test (CD) on artificial soil samples can be done to determine the required soil parameters (internal friction angle and soil cohesion). In case of cohesive soil, undrained soil testing should be performed like uniaxial compression test or undrained triaxial testing (UU) to find out the required undrained soil parameters.
An at least qualitative assessment of a possible accumulation of excess pore pressure which leads to a reduction of strength can be done by carrying out cyclic undrained triaxial tests. By a series of tests or alternatively by a multi-stage test a critical cyclic stress ratio (CSR) can be determined. The principle procedure is elucidated in Figure 3-29. A load-controlled cyclic test is executed, in which the confining stress σ_3 is adapted to the stress state at the depth under consideration in situ. The critical cyclic stress ratio CSR_{crit} is reached when the excess pore pressure progressively increases with increasing time or load cycle number, respectively. In the design of the pile it has then to be ensured that the actual cyclic stress ratio remains well below the critical value.

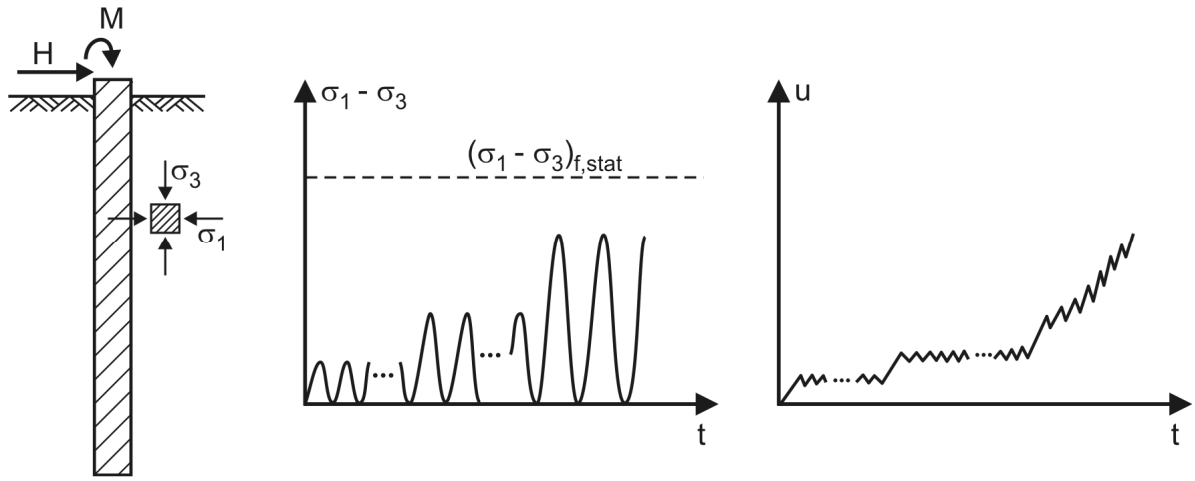

Figure 3-29 Results of a cyclic triaxial CU test (multi-stage test, schematically)

The problem with the assessment of such tests is that the boundary conditions in the tests do not coincide with the actual boundary conditions in situ. At the pile, in particular the drainage conditions are different to the test conditions. At the pile high excess pore pressures occur only locally and drainage can occur upwards, downwards or horizontally around the pile, which was shown in numerical simulations from (Grabe, 2004). Moreover, the magnitude of excess pore pressures in cyclic tests is frequency dependent.
Thus, the behaviour of a soil element cannot be directly transferred to the system behaviour. Generally, by the element tests in the laboratory a complex material law for the soil must be calibrated, and then by means of a numerical simulation model the behaviour of the pile-soil system can be analysed. This was done by (Grabe, 2004) and recently also by Cuellar et al. (2010). However, this effort cannot be done in a practical design. Besides, material laws capable of realistically modelling the soil behaviour for arbitrary stress paths are still a matter of research. Thus, cyclic undrained triaxial tests or other element tests can only enable a qualitative assessment of a possible pile capacity reduction.

SLS design proof

A critical value for monopile foundations is the permanent rotation of the pile head induced by the accumulated permanent pile deflections. In recent projects usually a maximum permanent rotation of 0.5° had to be ensured over the whole lifetime of the structure. The authors recommend using a design criterion stated in DNV (2007) and elucidated in Figure 3-30 to find a preliminary value for the required embedded pile length. The pile length should be

chosen such that a further elongation has only minor effect on the pile head displacement under characteristic extreme load. Of course, for the length chosen also sufficient pile capacity has to be proved.

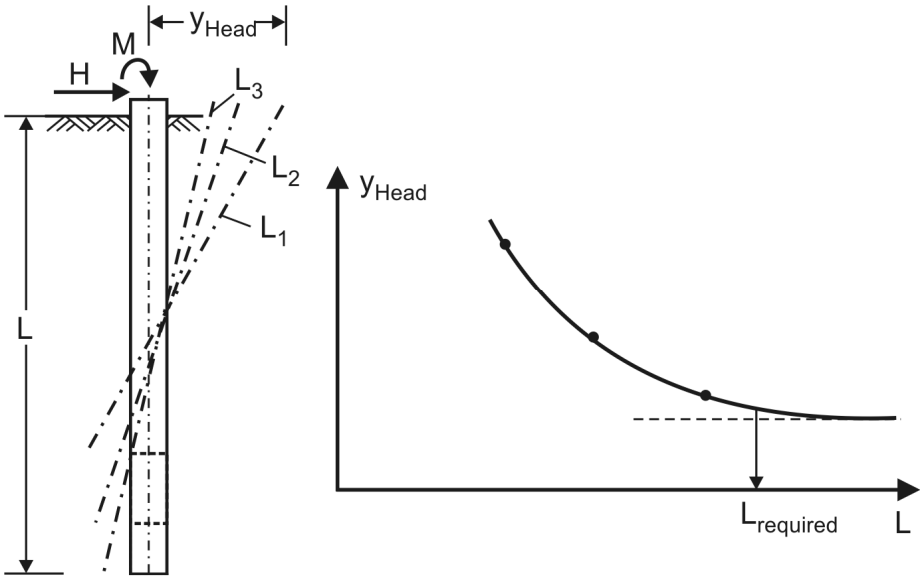

Figure 3-30 Design criterion for monopile lengths according to (DNV, 2007)

For stiffness degradation method (SDM) developed by the authors and co-workers, drained cyclic triaxial tests can be performed to obtain the required soil parameters (pl. refer to 5.2.1). In cyclic drained triaxial tests, the accumulation of plastic strains with the number of cycles under different loading conditions can be observed, which can be interpreted as a decrease in soil secant stiffness.
For the estimation of the permanent rotation at mud line a calculation with the SDM method described above can be carried out. Alternatively, the strain wedge method might be used. This method (see e.g.(Lesny, 2008)) also enables the consideration of results of cyclic drained triaxial tests. It should be noted that the calculation methods give the pile head deflection and rotation after N load cycles under load. Thus, the elastic portion has to be subtracted to obtain the (plastic) permanent deflection. As an approximation, the elastic pile deflection line can be determined by calculating the pile behaviour using linear springs having the initial stiffnesses of the p-y curves.

Stiffness under operational loads

For load calculations due to wind and waves usually dynamic calculations of the system consisting of blades, tower, foundation structure and piles have to be carried out. Time series of wind and wave loads are applied in such calculations. In order to limit the numerical effort, the behaviour of the foundation structure with the piles has to be linearized. Thus, by calculations with the p-y method linear spring stiffnesses representative for operational loading conditions have to be derived. From the p-y results, a linear (secant) spring stiffness k=p/y can be calculated and used in the dynamic calculations.
In the view of the authors, static p-y curves can be used in these calculations. This is due to the fact that the stiffnesses sought for are un- and reloading stiffnesses. Model tests of (LeBlanc, 2009) showed that un- and reloading stiffnesses of a monopile-sand system do not decrease, but even increase with the number of load cycles. Moreover, the secant stiffnesses derived from the p-y method are first loading and not un- or reloading stiffnesses. Thus, the use of secant stiffnesses might even give a conservative estimation of the operational pile stiffness.
Considering this stiffness in a dynamic analysis of the whole OWEC structure, it must be ensured that the eigen frequency of the wind turbine has a sufficient distance to the main excitation frequencies of the dynamic loading. In that, neither an overestimation nor an underestimation of the foundation stiffness is conservative. An incorrect estimation of soil stiffness results in an increase of uncertainties, leading to additional but unnecessary costs and decreasing the feasibility of the monopile foundation.

3.6.2 Axially loaded piles

Under cyclic axial loads, degradation of ultimate skin friction, and with that a decrease of the pile capacity, is to be expected. The main reason for this is a compaction of the soil beneath the pile shaft due to cyclic shearing, which leads to a reduction of the normal contact stresses acting between pile and soil and consequently to increase of the accumulated vertical pile displacement.

Usually, in offshore engineering no explicit consideration of a possible decrease of pile capacity is made in the design. It is assumed that the negative effect of cyclic loading is counterbalanced by positive effects like pile ageing (increase of pile capacity with stand time) or loading rate (increased capacity for a short-term load due to a wave). However, in Germany the BSH regulations require explicit consideration of cyclic capacity degradation, and a 'design storm' which must be taken into account is defined in BSH-guide lines.

If the pile capacity under cyclic loading will be determined using the interaction diagrams (refer to 3.2), no need for any cyclic load testing. In a model proposed by(Kirsch & Richter, 2010), compaction occurs up to a distance at which a threshold value of cyclic shear stress in the soil is reached. The cyclic strain depends on the shear modulus of the soil, which must be chosen according to the shear strain. For this, the strain dependent stiffness of the soil must be determined, e.g. with a Resonant Column Test. The volume contraction due to cyclic shearing can be determined using cyclic simple shear testing. For using this approximation procedure, the execution of Resonant-Column Tests and cyclic simple shear tests would basically be very useful.

The method developed by (Thomas, 2011) is based on cyclic model test parameters, which should be derived from static and cyclic pile load tests. It can be expected that with growing experience in this field, the necessary parameters can be obtained from cyclic shear tests, see also (EAP, 2011).

According to (Randolph, 2009), who evaluated cyclic interface tests on sand, the compaction occurs mainly within a small shear band beneath the pile. The current challenge to use his method (refer to 4.5.3) is to determine parameters which describe the interaction between the soil and the pile. This could e.g. be done through adjustment of the results from cyclic test loadings on piles. In the future, the acquisition of the needed parameters could be done through cyclic contact normal stiffness (CNS) shear tests, which is currently a subject of research.

3.7 CONCLUSION

The behaviour of soil under cyclic loading can be investigated in cyclic laboratory tests. The problem with the obtained results is to convert these from "unit level" (single soils samples under defined stress- and strain conditions) to "system level" (pile-soil or fundament-soil). Basically, for the characterization of soil behaviour under cyclic load conditions, a suitable material law should be calibrated. With such a law, the properties of the system could be simulated numerically. However, this approach is, while limited in its accuracy, very costly and limited to a small number of load cycles.

Therefore, the results from cyclic tests must be converted in another way to the system level. For this, smaller or greater idealisations are necessary. Especially undrained tests to monitor the accumulation of excess pore water pressure can lead, due to different draining conditions on system level, only to qualitative results.

In this report, different ways for the interpretation of cyclic laboratory tests are presented. It is shown that cyclic tests are helpful and also necessary for the evaluation of the systems behaviour. But it is also obvious that these tests can give only qualitative design values. The design of Monopiles and axially loaded piles is up to this point done without direct recognition of results from cyclic tests. The test results can only ensure the assumptions made in the deign process. Regarding the further development of design processes of offshore wind converters under cyclic loading, more research is highly needed.

4 EXEMPLARY TESTING PROCEDURES FOR INVESTIGATIONS ON SCOUR DEVELOPMENT AND SCOUR PROTECTION AT FOUNDATIONS FOR OFFSHORE WIND TURBINES

4.1 GENERAL

The progressive development of the construction and operation of offshore wind turbines (OWT) in the North and Baltic Sea puts more emphasis on long-term usability and stability of the foundations. Complex foundation structures in water depths of up to 40m are a significant cost factor compared to systems that are constructed and operated on land. Foundation structures of OWTs affect the local, natural environmental conditions, especially the dynamic balance between external hydrodynamic effects and the seabed, which in the North Sea consists primarily of more or less densely packed sands and fine sands. Current and wave induced interactions between the foundation structure, the modified flow field and the seabed cause more or less distinct erosion, transport and accumulation process of sediment in the near field of the foundation. This may affect operation and usability, as well as the stability of the OWT.

4.2 SCOUR DEVELOPMENT AND SCOUR PROTECTION

In rivers and oceans, the interaction between structure, water and soil can cause a local amplification of turbulence and structure-induced flow, which leads to a mobilization and consequently to a rearrangement of soil material, and can thus compromise the stability of the structure. There are two kinds of scour (Whitehouse, 1998):

- Global scour
- Local scour

Global scour is the general lowering of the river or seabed, and is a lengthy, large-scale process. Local scour, however, occurs immediately in the vicinity of structures and results from the disturbance of the primary flow conditions caused by the structure. Scour shape, depth and width are directly dependent on the geometry of the structure, whereby the maximum scour depth is mainly the parameter of main interest for scour problems. The development of local scour is relatively short compared to global scour and only takes a few days or weeks. A distinction of local scour types is made by the installed structural types, such as vertical cylinders, piers, pipelines, complex foundation structures etc.. In addition, the local scour can be divided into two classes, which depend on the local shear stress τ_0 and the critical shear stress threshold value for sediment motion τ_{cr} (Whitehouse, 1998):

- clear-water scour with $\tau_{cr}/M < \tau_0 < \tau_{cr}$
- live-bed scour with $\tau_0 > \tau_{cr}$

Clear-water scour means that the shear stress in the vicinity of the structure (without structural influence) is less than the critical threshold for initiation of sediment motion, but larger than the ratio τ_{cr}/M, wherein the reduction factor M considers the geometry of the structure. In this case, the flow can only mobilize sediment directly around the structure, but not in the far field.

Live-bed scour means that the shear stress is everywhere larger than the critical threshold for sediment motion. Thus, there is sediment transport directly around the structure as well as in the far field. For further reading, see e.g. Whitehouse (1998), Annandale (2005), Shields (1936), Hjulström (1935).

As scour can compromise the stability of the marine structure, a scour protection system may be necessary. The typical scour protection system consists of a filter and armour layer of stone-material (rip-rap revetment), which is heavy enough to provide the required stability against the hydrodynamic forces and to protect the soil against scouring. As the estimation/determination of scour is difficult, there are only guidelines, but no exact solutions, for the design of scour protection systems. For further reading, see e.g. Heibaum (2002), Heerten and Peters (2010), MAG (1993), RPG (1994).

4.3 INVESTIGATIONS ON SCOUR DEVELOPMENT AND SCOUR PROTECTION (STATE-OF-THE-ART)

The scour at foundations for OWTs depends on many factors and influences. The following parameters and processes have a decisive influence:

- Geometry of marine structure: dimension and shape of the structure, spacing of foundation piles, number and arrangement of bracing struts (framework) and sharp edges, etc.
- Local, near-bed flow conditions in dependence of direction and strength of current and sea state.
- Conventional soil parameters: grain size distribution, deformity, bulk density and specific mass.

Due to the variety and complexity of the significant variables, the design of foundations and scour protection systems is more or less based exclusively on practical experience.

Generally, the cylindrical structure represents the typical and most studied structural component for offshore platforms as well as for OWTs. The flow around a cylinder with stationary uniform flow has been analyzed extensively in laboratory and prototype scale. Especially for the analysis of flow characteristics around cylindrical bridge piers and the resulting formation of scour, numerous studies can be found in literature. In contrast, near-bed flow processes at stationary offshore structures under waves and currents are insufficiently studied. Due to the complex structure of the superimposition of wind, wave and tide, structure-induced flow processes are only partly possible to investigate in the laboratory, if at all with strong restrictions and numerous assumptions. With regard to the specific physical phenomenon of structure-induced scour, there are few studies, see e.g. compilations in Hoffmanns and Verheij (1997), Zanke (1982), Melvile and Coleman (2000) and Sumer and Fredsøe (2001).

Knowledge about the altered flow phenomena around a cylindrical pile cannot be applied directly to marine foundations with innovative, complex designs, as the flow phenomena strongly depend on the geometrical shape of the structure. Furthermore, an exact analytical formulation of the flow processes and the flow velocities in the immediate vicinity of the structures is currently not possible. Also, numerical models have their limitations due to the complexity of the flow. Complicated three-dimensional numerical flow models require a precise calculation of these complex flows involving a meaningful illustration of the locally prevailing turbulence. Moreover, the information provided by such numerical flow models have been severely limited because the necessary data base for calibration or validation, respectively, are largely absent. In order to obtain knowledge of the hydrodynamic situation around offshore structures, hydraulic model studies are essential and thus form an engineering tool for obtaining reliable design bases for scour protection systems. For further reading see e.g. Ungruh and Zielke (2003), Maidl et al. (1978), Breuers et al. (1991), Rance (1980), Melville et al. (1977), Richardson et al. (1998), Hamill (1999), Unger (2006), Zielke (1999), Sumer and Fredsøe (2002), Whitehouse et al. (2011a) and Whitehouse et al. (2011b).

Because of the complex scour phenomena, the adequate, but also economical design of scour protection systems is an import issue. In areas with strong current and wave actions, it is infeasible to install scour protection with the regular approach of filter layers. Therefore, different innovations with geotextile sand containers, rubber mats and coarse-grained sands were developed, see e.g. Werth et al. (2012), Wilms et al. (2012) and Schendel (2012). The application of geotextile sand containers will be discussed in the following presented testing procedures.

Besides the difficulties to model the natural sea state with combined wave and current load in laboratory experiments or numerical models, there is the difficulty to model the natural bed material of the sea bed. Applying the approach to a direct Froude scaling typically results in extremely small grain sizes and thus large influences of cohesion, which should be avoided as it leads to a different scour development. As an alternative, sediment scaling based on the Shields parameter can be applied. In this approach there are two scaling parameters: the grain size and the material density. Thus, natural lightweight or artificial material can be used, e.g. Polystyrene, Bakelite, PVC or coal, see e.g. Bettess (1990) and Ettmer (2007) for further details. When using cohesionless sediments with grain sizes larger than theoretically given, possible scaling effects should be kept in mind, but general knowledge on scour development can be gained.

4.4 SCOUR AND SCOUR PROTECTION TEST PROCEDURES

Over the past years the Franzius-Institute investigated various offshore structures, including monopile, tripod (Stahlmann and Schlurmann (2012), RAVE (2010), Stahlmann (2013)), tripile (Goseberg et al., 2012) and two different gravity based foundations (Wilms, 2012). The investigations had a resembling, basic test procedure. The overall objective of investigations was to gain general knowledge on physical processes, the local and global scour development as well as local flow patterns leading to scour.

Based on the experiments with the gravity based foundation developed by the company STRABAG Offshore Wind, the test procedure is shown here. It should be noted, that the test procedure presented exemplary here is based on an industry project, and thus is subject to different requirements than basic research projects.

In order to study the scour phenomena around a gravity based foundation and scour protection system, physical model tests have been carried out in wave flumes on model scales of $\lambda = 50$ and $\lambda = 17$ by applying the Froude model law (see Table 4-1).

	Froude Model
Length	$L_p = L_m \lambda$
Area	$A_p = A_m \lambda^2$
Volume	$V_p = V_m \lambda^3$
Force	$F_p = F_m \lambda^3$
Time	$t_p = t_m \sqrt{\lambda}$
Velocity	$U_p = U_m \sqrt{\lambda}$
Discharge	$Q_p = Q_m \sqrt{\lambda}$
Acceleration	$a_p = a_m$

Table 4-1: Parameter scaling by Froude model law with λ as length scale parameter.

The small-scale model tests furthermore served as a kind of feasibility study for the later following large scale experiments, which further analyze scour phenomena around the foundation in detail and under minimized laboratory modeling effects, especially with regard to the scaling of the model sediment.

The small-scale model tests intended to phenomenologically analyze the flow and the wave-induced scour development around the structure considering different values for the load parameters “water depth”, “wave height” and “wave period” as well as the orientation and embedding of the gravity foundation. As design basis for the wave parameters a typical storm event in the North Sea (in the sample wind park Global Tech I) with a recurrence interval of 50 years was chosen. The sample wind park is located in the Exclusive Economic Zone (EEZ) in the German North Sea, approximately 111km northwest of Cuxhaven and about 50km north the research platform FINO 1, in about 40m water depth.

The subsequent large-scale model tests in the Large Wave Flume (GWK) of the Coastal Research Center (Hannover, Germany) intended to quantitatively analyze the flow and the wave-induced scour development around the foundation with and without scour protection systems using geotextile containers as well as the hydraulic stability of single geotextile containers on a scale of 1:10. As boundary conditions for the large-scale test series, the former determined load parameters from the small-scale tests leading to maximum scours were used.

Tests using geotextile containers were carried out without the presence of the foundation in order to investigate the hydraulic stability of the single geotextile container against displacement subject to the parameters “size”, “weight” and “filling rate” of the containers and to finally determine the smallest and optimal geometrical dimensions of the geotextile containers necessary to withstand the given load parameters.

Furthermore, investigations of the wave-induced scour development around the structure without scour protection are carried out in order to validate the results from the former small-scale experiments. Afterwards, investigations of the scour development around the foundation using three different variations of a scour protection system are conducted in order to verify the effectiveness of the protection system. Figure 4-1 gives an overview of the physical model tests and their outputs.

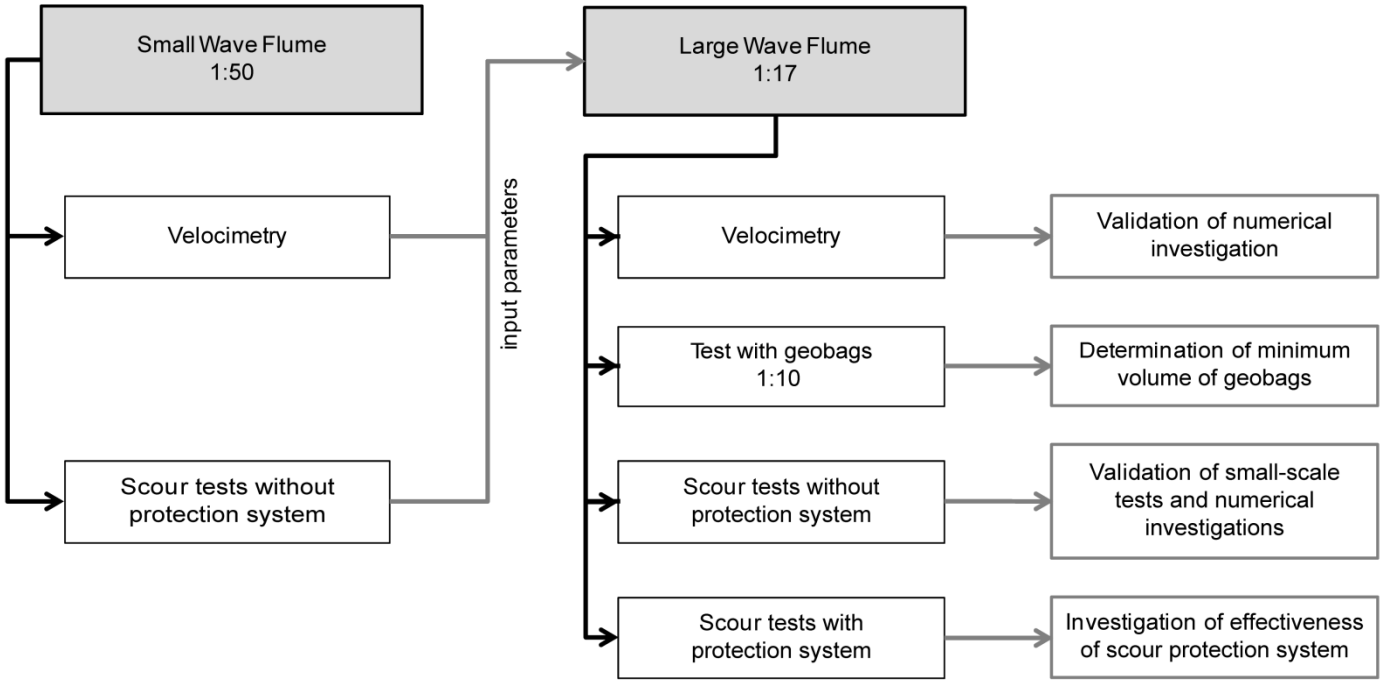

Figure 4-1: Overview of the physical model tests.

The choice of model scales relied on the scaled boundary condition parameters in combination with the limitations in laboratory facilities, i.e. water depths, possibilities of wave generation and general blockage effects. It again has to be noticed that only the effect of wave load on scour development by means of physical model tests in wave flumes was investigated here.

4.4.1 Instrumentation

4.4.1.1 Test facilities (small scale tests)

The small-scale model tests were carried out in the wave flume of the Franzius-Institute (WKS), which has overall dimensions of 100m length, 2.2m width and 2.0m height. The piston type wave maker is hydraulically driven and capable of generating regular and irregular waves with wave heights up to 0.35m while using a stroke of up to ±0.30m by a water depth of up to 1.2m. In the rear part of the flume, a beach is installed as a passive wave absorber in order to minimize reflections.

4.4.1.2 Test facilities (large scale tests)

The large-scale model tests were carried out in the Large Wave Flume (GWK) of the Coastal Research Center in Hannover. The GWK wave flume has a length of 307m, a width of 5.0m and a height of overall 7.0m. The piston type wave maker installed in the front section of the flume is capable of generating regular and irregular waves with wave heights up to 2.0m while using a stroke of up to ±2.1m.

4.4.1.3 Test set-up (small scale tests)

For the tests on scour development around structures, a false bottom was installed in the wave flume as originally no deep section holding the model sediment was available. The sand bed had a length of about 4.5m, resulting in an overall bed area of about 9.9m^2, with a bed depth of 0.25m. As bed material, fine sand was used, i.e. having a grain size of d_{50} = 0.148mm. The bed was installed in combination with sand traps and a covered pump well in the front of the test section as well as concrete ramps on both sides. A sketch of the model setup is given in Figure 4-2. A drainage system connecting the test section with the pump well as given in Figure 4-3 (left) was used to drain the water in the sand bed when the model was dried up for flattening the bed after a test series. The movable bed section was bordered with solid walls in order to prevent it from horizontal flow during flume filling. Parts of the test section where no scour formation was expected, were filled with lime sand bricks. Stahlmann (2013)

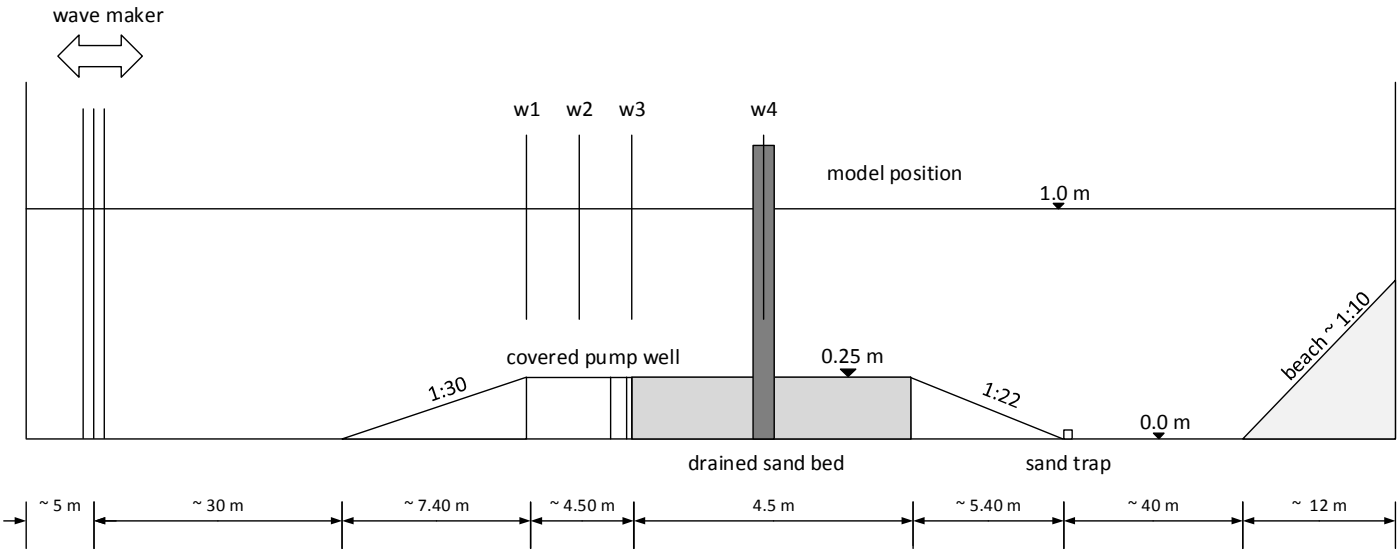

Figure 4-2: Sketch of the experimental setup in the WKS wave flume. Foundation structure is given symbolically.

For the experiments, a model on a length scale of 1:50 was manufactured from aluminum elements. The STRABAG gravity based foundation is a further development of the classical, simple type of gravity foundation, consisting mainly of a cross shaped base forming the foundation of the wind turbine.
For the flume installation, a turnable bottom mounting system was installed, which allowed to modify the rotating direction of the model in relation to the incoming wave direction. In the model, main dimensions of the structure are as follows: The main column has a diameter of D_{mc} = 17cm, while the cross shaped base has a height of h_{cross} = 16cm and an overall length of l_{cross} = 80cm.

Figure 4-3: Left: Foundation installation in the WKS wave flume with drainage system and lime sand bricks. Right: Foundation during water filling.

It should be taken care of that the overall blockage ratio of the tested structure does not exceed the threshold of $r_b = 1/6 \approx 0.167$, after Whitehouse (1998), to avoid influences on the result due to high blockage effects. In case of the gravity based foundation the vertically projected area is $A_t \approx 0.20\text{m}^2$ and thus its blockage ratio $r_t \approx 0.12 < r_b$.

4.4.1.4 Test set-up (large scale tests)

For the large-scale model tests in the Large Wave Flume, fine sand (d_{50} = 0.148mm) as used in the WKS tests was installed as bottom material (movable bed) with a thickness of 1.20m on a length of approx. 34m. The front and back areas of the sand bed were profiled with an inclination of 1:20. The fine sand was also used as filling material for the geotextile sand containers. A 1:17 model of the STRABAG gravity foundation was manufactured and installed in the sand bed by a fixed, rotatable connection to the bottom of the wave flume. Figure 4-4 schematically shows the profile and cross-section of the test setup in the Large Wave Flume. The applied model scale of 1:17 was given as a compromise between grain scaling and possible wave generation.

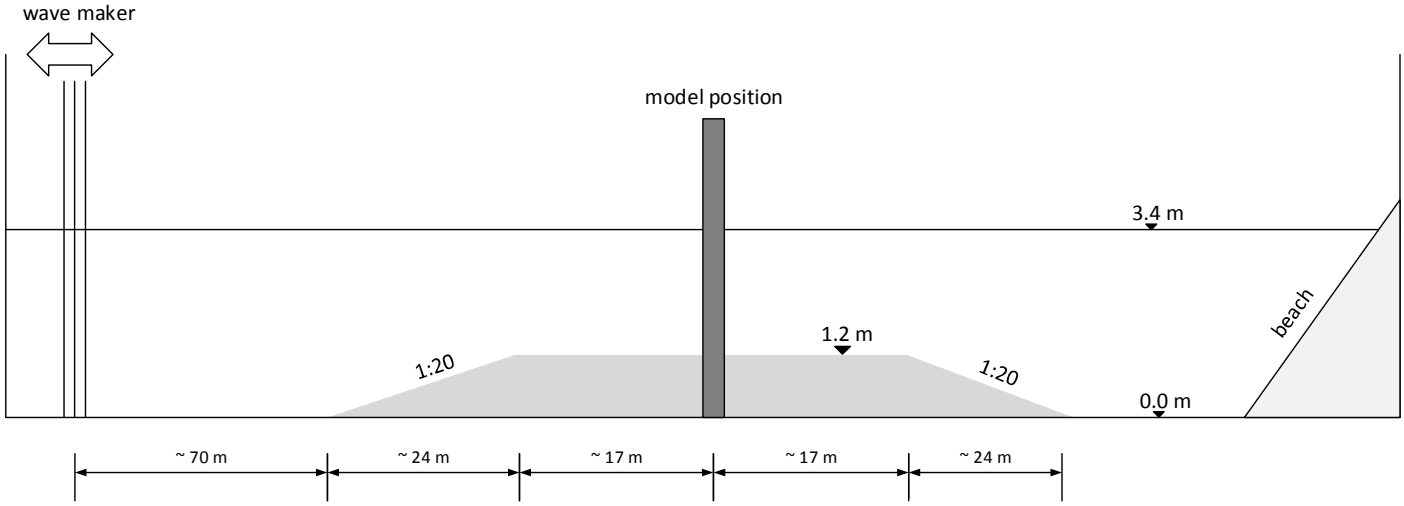

Figure 4-4: Sketch of the experimental setup in the GWK wave flume. Foundation is given symbolically. Positions of wave gauges are not marked.

Figure 4-5: Gravity based foundation installation in the GWK wave flume for scour experiments.

Geotextile containers

As filling material for the geotextile containers, fine sand as it was already used in the sand beds was used again, i.e. having a grain size of d_{50} = 0.148mm. The hydraulic stability investigations were conducted without the presence of the foundation in order to maximize the scale factor up to 1:10 and to minimize scaling effects.

Different types of sand-filled geotextile containers made from needle-punched nonwovens (NP NW) as well as a composite made from needle-punched nonwoven combined with a woven (W-NW) were investigated simultaneously relating to their hydraulic stability either singularly installed or in groups, see Table 4-2.

Container type	width/length ratio	fill rate [%]	dimension [m]	mass [kg]
N1 (NP NW)	1:1	100	0.205 x 0.205	2.7
N2 (NP NW)	1:1.5	100	1.79 x 2.69	2.7
N3 (NP NW)	1:1.33	100	0.4 x 0.3 x 0.05	10.8
H1 (W-NW)	1:1.33	80	0.4 x 0.3	9.0
H2 (W-NW)	1:1	80	0.205 x 0.205	1.8

Table 4-2: Investigated types of sand filled containers.

Beside the material of geotextile, a variation of fill rate and therefore weight was included. The ratio of width and length of the model containers were varied from 1:1, 1:1.33 und 1:1.5. Investigations on the group arrangement were carried out to determine the interlocking effects between the sand-filled containers. According to the wave direction, the arrangement of the rectangular containers was done longitudinally as well as perpendicularly. The quadratic sand-filled containers (W/L = 1:1) were arranged in wave propagation direction as well as in an angle of 45°. The test arrangement is shown in Figure 4-6.

Figure 4-6: Arrangement of sand-filled geotextile containers (before test).

For the scour tests with scour protection system, the container type N1 is used as scour protection because the investigation on the hydraulic stability of the single sand containers against displacement showed that the sand container type N1 was hydraulically stable and represented the minimum dimensions to withstand the given hydraulic wave boundary conditions (Wilms et al. (2011), Werth et al. (2012)). The amount of sand containers used for the scour protection system was determined by calculating the required volume of sand containers. The calculation was based on a random, two-layer installation of the sand containers on the given area of the scour protection system with a diameter of 52.5m (prototype scale). A total number of 1104 sand containers were used in the model tests.

4.4.1.5 Measurement equipment (small scale tests)

The water surface elevation were measured using four capacitive type wave gauges.
The flow field around the model structure was measured point-wise by use of a Nortek AS Vectrino+ ADV probe in tests with a non-moving bed (see Figure 4-7 (right)). The ADV probe was mounted at a positioning platform, which moved the probe automatically on predefined paths.

The evolution of the sand bed at the structure and in the near-field was measured by use of an underwater laser distance sensor (LDS, Baumer OADR20), which was mounted at the same positioning platform that was used for the ADV probe (see Figure 4-7 (left)).

Figure 4-7: Pictures giving LDS Laser distance sensor for surface profile collection (left) and ADV flow measuring probe in velocimetry setup (right).

4.4.1.6 Measurement equipment (large scale tests)

The water surface elevation was measured using 24 capacitive type wave gauges installed along the flume walls and concentrated around the model. Similar to the WKS flume tests, the flow field around the model structure was measured point-wise by use of four Nortek AS Vectrino+ ADV probes in separate test runs.

Evolution of the sand bed at the structure and in the near-field were measured by use of a multi-beam echo sounder (Reson SeaBat) and several single-beam echo sounders as well as underwater cameras, which allowed a highly-resolved three-dimensional and contact-free continuous monitoring of bottom profiles, i.e. scour depths or accumulation areas. The multi-beam echo sounder was mounted on a movable positioning platform and was driven automatically on predefined paths (see Figure 4-8). For continuously recorded bed depths, two single-beam echo sounders and one set of three acoustic backscatter probes (Aquatec AQUAScat 1000) were installed at one foundation hollow box (see Figure 4-9). Although the acoustic backscatter probes were originally designed as backscatter sensors, the probes were used as single-beam echo sounders here.

At locations directly in front of the four foundation hollow boxes, a total of four underwater cameras were used for the determination of local bed levels. The cameras were installed in outward-looking position (see Figure 4-9) so that they could continuously record bed level changes through Plexiglas windows during the experiments.

In the experiments of the hydraulic stability of geotextile sand containers, the measurement of container displacement and sand bed level was carried out by the multi-beam echo sounder in submerged condition and by camera after the water was drained slowly from the flume.

Figure 4-8: Multi-beam echo sounder and positioning platform installation for collection of bed surface profiles during GWK wave flume scour experiments.

Figure 4-9: Echo sounder and underwater camera installation for point-wise, continuous scour recording in the GWK wave flume experiments.

4.4.2 Test procedure (small scale tests)

4.4.2.1 Local Flow Measurment

The point-wise measurement of flow velocities around the structure by use of the ADV probe was carried out independently from the scour development tests. Locations of special interest with structural influence on the flow field where regarded here, e.g. near and between the foundation hollow boxes. Test conditions see Table 4-3. The parameter “angle” describes the wave direction regarding the foundation, whereby an angle of 0° means that one

foundation hollow box points to the same direction as the wave and an angle of 45° means that the foundation is rotated by 45° (in Figure 4-9 the foundation has an angle of 45°).

#	wave type	wave height H_m/H_s [cm]	wave per. T_m/T_p [s]	angle [°]	water depth [m]	max. # waves
1	regular	15.3	1.640	0	0.750	10
2	regular	15.3	2.135	0	0.750	10
3	regular	15.3	1.640	0	0.856	10
4	regular	15.3	2.135	0	0.856	10
5	regular	15.3	1.640	45	0.750	10
6	regular	15.3	2.135	45	0.750	10
7	regular	15.3	1.640	45	0.856	10
8	regular	15.3	2.135	45	0.856	10
9	regular	15.3	2.135	no foundation	0.750	10

Table 4-3: Compilation of conducted experimental local flow measurements in the WKS wave flume.

The structure was installed approx. 15m in front of the test section, as tests were conducted in non-moving bed conditions. A total of 88 locations around the structure were defined, resulting from 8 locations in horizontal plane and 11 points per vertical at each location, out of which vertical velocity profiles could be created later. The measurement position coordinates in vertical direction lay within 10 and 600mm over ground. The interim values had distances of 20-100mm. The flume was filled to still water level and the wave maker was started. At each measuring location, the velocity components were measured for a time span of ten wave cycles. In post-processing, ADV data were first filtered using a Butterworth filter approach to reduce noise in the signals. Data for each measuring location were then averaged over the recorded wave cycles in order to generate a kind of mean velocity profile.

4.4.2.2 Investigations on Scour Development

After installation of the model in the test section, sand was filled into the bed area and finally flattened by hand. Sand was filled in completely wet form, so that a saturation of the bed was guaranteed. The flume was then slowly filled with fresh water from the storage system. The wave maker was started and ran for time spans of multiples of 250 wave cycles per period for regular waves and 450 wave cycles per period for the spectrum in order to measure the scour development around the foundation after defined wave periods between 250 and 1000 wave cycles in still water conditions. A more detailed measurement was chosen near the structure compared to free bed areas with less structural influence. Distances between single measuring tracks were 10mm (close to foundation) to 15mm-25mm (free area). Therefore, the wave maker was stopped during scour measurements in between the wave load periods. Afterwards, the wave maker was started again for the next load intervals. This procedure was repeated until the end of the tests. Due to a more rapid scour development in the beginning, the measuring interval was higher at the start of the tests, while longer measuring intervals were chosen when approaching an end condition. The evolution of the sand bed was measured after 0, 250, 500, 1000, 2000, 3000, 4000 and 5000 wave cycles in the tests with regular waves and after 0, 450, 900, 1800, 2700, 3600, 4500 and 5400 wave cycles in the tests with a spectrum. After a test series was terminated and had reached an almost equilibrium stage, the wave flume was drained and the bed was prepared for the next test series (Stahlmann (2013)).
Surface elevations and orbital motions were continuously measured during the test runs. Several tests using different experimental configurations of wave heights H_m/H_s, wave periods T_m/T_p and turning angles of the structure were carried out for regular waves and JONSWAP wave spectra; test parameters are given in Table 4-4. Test numbers SF6 and SF7 were repeated three times and after those tests showed reproducibility, test numbers SF8 to SF11 were repeated two times. Furthermore, test numbers SF6 and SF7 were carried out to investigate on the blockage effect by the flume walls and to compare the resulting scour depths. The tests showed that the foundation could be installed in the flume center and the scour development was not affected by the flume walls.

Name	wave type	wave height H_m/H_s [cm]	wave per. T_m/T_p [s]	angle [°]	water depth [m]	position of foundation	max. # waves
SF6	regular	15.3	2.135	0	0.75	close to wall	5000
SF7	regular	15.3	2.135	0	0.75	flume center	5000
SF8	spectrum	21.6	1.952	0	0.75	flume center	5400
SF9	spectrum	21.6	1.952	0	0.856	flume center	5400
SF10	spectrum	21.6	1.952	45	0.75	flume center	5400
SF11	spectrum	21.6	1.952	45	0.75	flume center	5400

Table 4-4: Compilation of conducted experimental scour tests in the WKS wave flume.

4.4.3 Test procedure (large scale tests)

After installing the sand bed, the model including sub-structure and measuring instrumentation was installed in a building pit of the test section and sand was finally filled into the pit around the structure. Before starting the first test series, the flume was filled and a short test series with high regular waves was run in order to compact the soil material. The water level in the flume was lowered, the bed was flattened by hand and the flume was finally filled again slowly. For the tests, the wave maker was started and ran for time spans between 500 and 1000 wave cycles. Reflections during the tests where minimized by active absorption control of the wave maker. All instruments given above were continuously collecting data during the test runs, with exception of the multi-beam echo sounder. The multi-beam echo sounder measured the areal scour development after defined wave periods in intervals of 500, 1000 and 2000 wave cycles each in still water conditions, i.e. the wave maker was stopped. While moving over ground along the flume axis, the echo sounder collected overlapping stripes of bed profiles, out of which surface plots of bed elevation were calculated in post-processing. This procedure was repeated until the end of each test. A series was terminated after 5000 wave cycles, achieving an almost equilibrium state. Afterwards, the water level in the flume was slowly lowered and the bed was flattened for the next run (Stahlmann (2013)).
Selected load conditions derived from the 1:50 experiments in the WKS flume tests were chosen as boundary conditions for the tests. Resulting test parameters for scour tests without scour protection system are given in Table 4-5. The water level above sand bed was kept constant at 2.21m for all tests.

#	wave type	wave height H_m/H_s [m]	wave per. T_m/T_p [s]	angle [°]	max. # waves
1	regular	0.45	3.66	0	5000
2	spectrum	0.64	3.35	0	5000
3	spectrum	0.64	3.35	45	5000

Table 4-5: Compilation of conducted experimental scour tests without scour protection system in the GWK wave flume.

The effectiveness and design of the scour protection system was tested with a total of three different variants of the protection system. Parameters of the test series are given in Table 4-6. The installation of the sand containers was carried out under water with a water depth of 0.45m. The sand containers were installed randomly by being immersed in water and released afterwards in order to reach their final positions in free-fall. To achieve an even distribution of the sand containers around the gravity foundation, the circular area of the given scour protection area was divided into four sections. In each section 276 sand containers were distributed in a defined pattern. In the scour protection system variant 2 (see Table 4-6) a fleece was used in addition to the sand containers. At one half of the foundation, the fleece was attached between the cross-shaped hollow boxes and at the contact areas. The sand containers were then installed consecutively on top of the fleece. The pit was subsequently filled, so that the foundation was embedded 0.18m (model scale) in the sand bed. In Figure 4-10 (left) the fleece is shown after its installation. Figure 4-10 (right) shows the foundation with a completed section of the scour protection system. As hydraulic parameters, the parameters of test number 3 were taken, see Table 4-5.

Variant	sand container type	fixing-in depth [m]	scour protection system
1	N1	0.0	sand container
2	N1	0.18	sand container + fleece
3	N1	0.18	sand container

Table 4-6: Compilation of conducted experimental scour tests with scour protection system in the GWK wave flume.

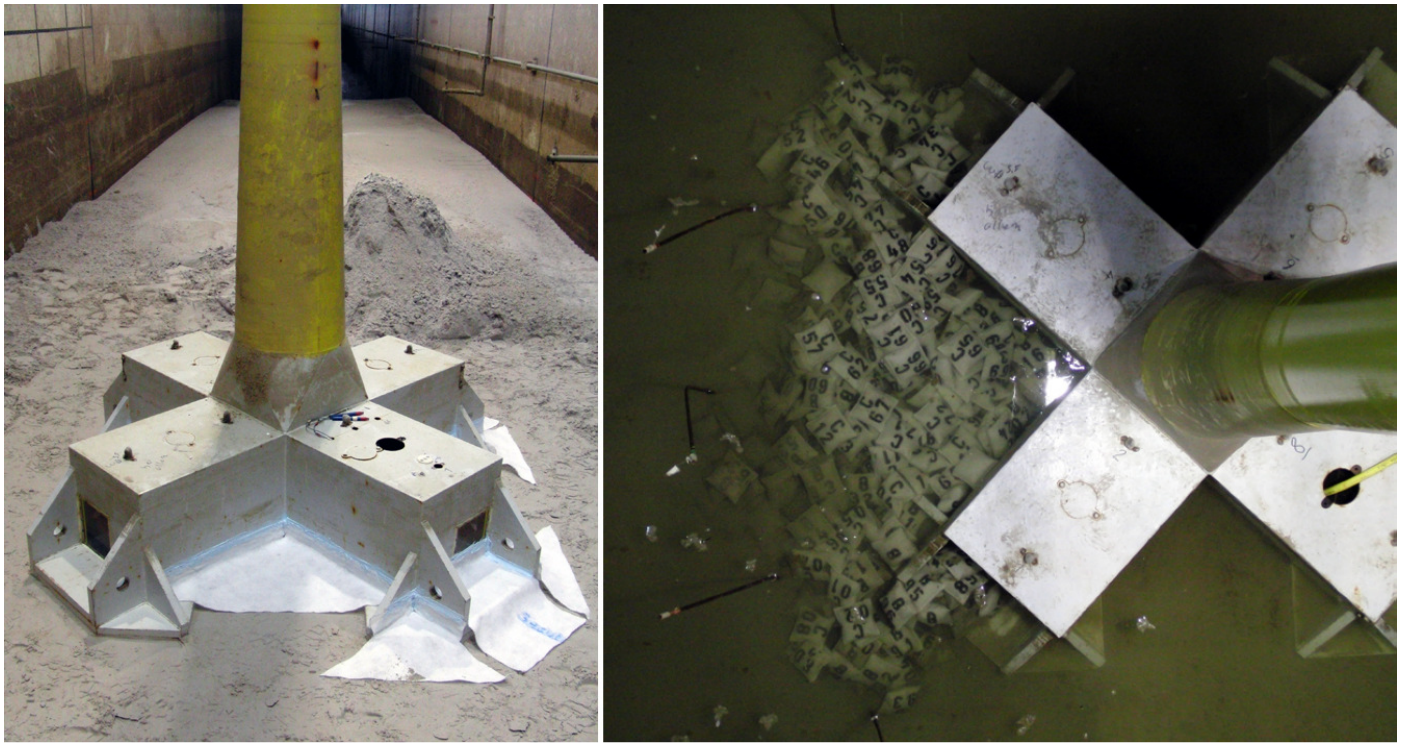

Figure 4-10: Foundation with installed fleece for Variant 2 (left) and foundation during installation phase of the scour protection system (right).

4.4.4 Data analysis and presentation formats

For all measuring devices in the WKS wave flume tests, an analog output system (voltage outputs) were used. A National Instruments NI-DAQ NI USB-6259 analog-digital converter sampled the data in digital form. For data storage, the National Instruments DIADEM sampling and control software was used and Mathworks Matlab was used for post-processing. For the tests in the GWK wave flume the individual probes were connected to an in-house analog-digital converter array, while data were stored in digital form on the measuring system. A sampling rate of 100Hz was used for all probes in order to get consistent data sets and time lines, which has proven to give accurate results for the present investigations.

In post-processing, ADV data were first filtered using a Butterworth filter approach to reduce noise in the signals.

The multi-beam echo sounder of type Reson SeaBat collected overlapping stripes of bed profiles while moved over ground along the flume axis, out of which surface plots of bed elevation were calculated in post-processing by means of the Reson SeaBat's software and the software package ArcGIS of ESRI.

In Table 4-7 an exemplary overview over the commonly used measurement devices for scour phenomena measurements, their measured data and the subsequently derived output diagrams is given. This combination of visual documentation with pictures and decidedly analyses with areal plots and cross-sections, lead to a good estimation and evaluation of the scour development.

Measurement device	Measured data
Camera / Video	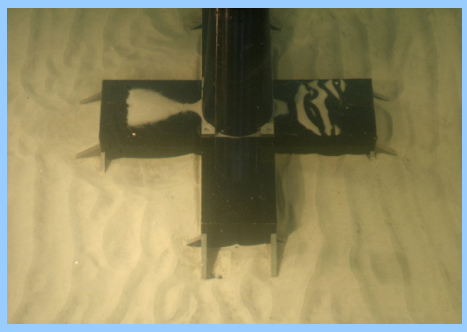     
LDS Laser distance sensor (Matlab plot)	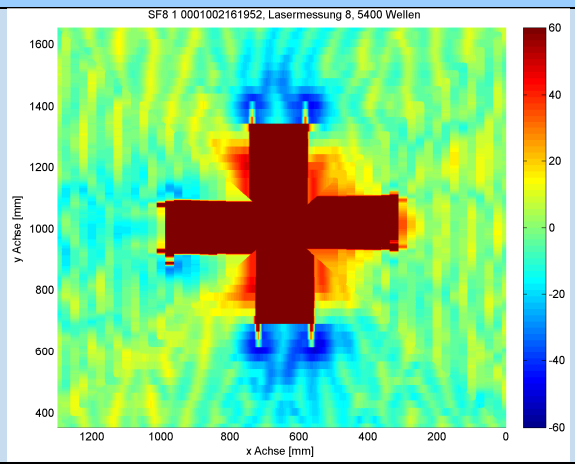

Multibeam echo sounder (ArcGIS plot)	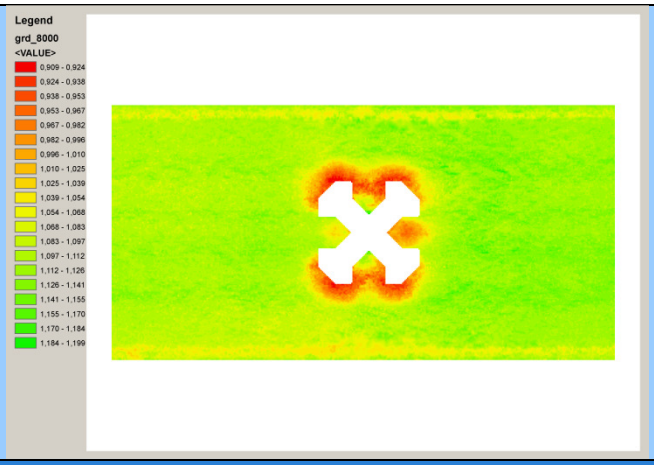
OUTPUT	
Cross section with bed level profiles after every measurement	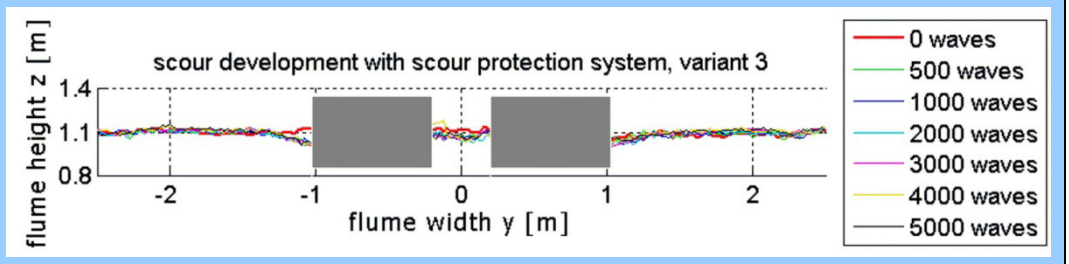
Diagram with relative scour depth S/D against number of waves with S as absolut scour depth and D as foundation diameter	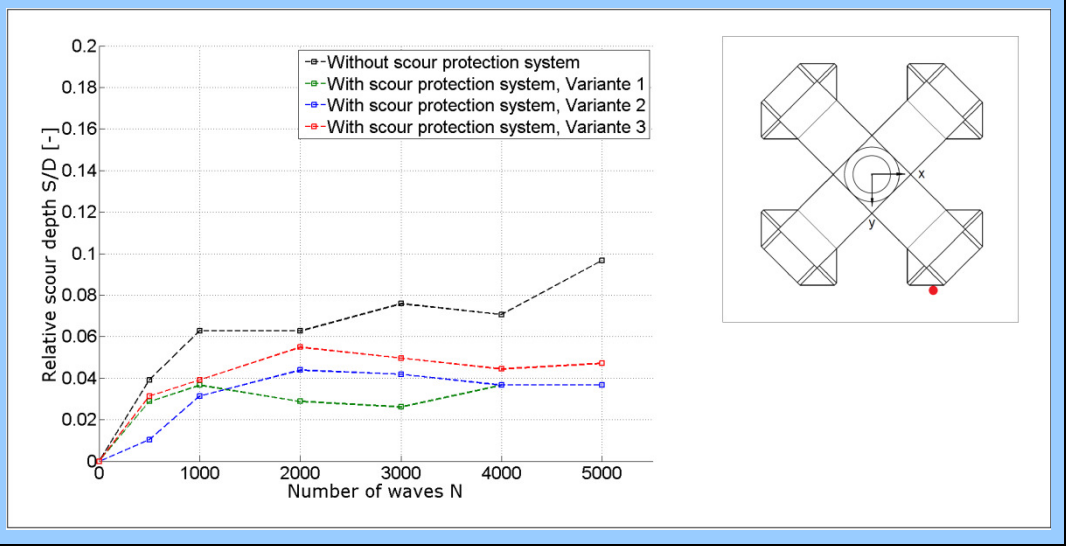

Table 4-7: Compilation of presentation formats.

4.5 CONCLUSION

Experiences from the recently installed wind turbines in the German Exclusive Economic Zone (EEZ) in the North Sea show that scour is a very serious phenomenon concerning the stability of the OWT. So far, the existing calculation methods cannot describe any particular mechanism of action especially for geometrically complex foundation structures. Furthermore, for complex foundation structures there is no practical experience with scouring so far, which could be used as a basis for an appropriate design method for the scour protection system. Laboratory experiments are therefore essential to achieve a sufficient degree of planning certainty. Nonetheless, certain scaling effects in the scaled model must be expected because the compliance of an exact physical similarity between model and prototype is not achievable. Thus, gained results of scaled model tests give only a guidance on physical processes in prototype scale.

Over the past years the Franzius-Institute investigated various offshore structures, including monopile, tripod, tripile and two different gravity based foundations. The overall objective of investigations was to gain general knowledge on physical processes, the local and global scour development as well as local flow patterns leading to scour.

The following two-step test procedure resulted:

1. Small-scale tests to determine the general scour phenomena and local flow pattern. The scale parameter was between $\lambda \sim 40$ to 50. Small-scale tests provide the possibility of carrying out more parameter combinations in less time and with less effort in the test set-up (compared to large-scale tests), but with the limitation of higher scaling effects.
2. Large-scale tests to repeat selected parameter combinations, that resulted in the small-scale tests in the largest scour depth, but with minimized scaling effects, especially regarding the sediment. The scale parameter was between $\lambda \sim 4$ to 17. Moreover, studies on scour protection systems should be done in large-scale because not only is the sediment material, but also the material of the scour protection system itself, e.g. geotextiles, very sensitive to scaling effects.

The primary hydraulic boundary condition was the extreme wave event with a recurrence interval of 50 years, because the design wave height for offshore sturctures is derived from its significant wave height $H_{s,50}$, Germanischer Lloyd (2005). It has to be noted that due to the set-up of the facilities, the models were solely loaded with wave or current boundary conditions. A combined wave-current load was solely investigated in numerical model tests (Stahlmann and Schlurmann (2012), Stahlmann (2013)) so far, due to the absence of such combined test facilities during the test periods. It is however generally recommended to investigate the scour phenomena and the scour protection system in laboratory tests in combined wave-current load to avoid neglecting the interaction of naturally given multi-directional sea states and tidal currents. Therefore, Franzius-Institute is currently upgrading its present large 3D wave basin in Hannover-Marienwerder, which has a multi-directional wave maker, by adding a current generation system.

5 MARINET OFFSHORE WIND RESEARCH AND TESTING ACTIVITIES

5.1 GENERAL

Besides testing activities regarding support structures and foundation systems of offshore wind turbines, MARINET research facilities are performing high class research on various fields of offshore wind turbine energy conversion systems and components. Some of the main research activities and testing practices are described in the chapter. This testing practices can be regarded as state-of-the-art for experimental investigations in the respective fields.

5.2 WIND FIELD ANALYSIS FROM WIND TURBINE NACELLE BASED ON LIDAR MEASURMENT

5.2.1 Research objectives

The possibility of gathering wind field information from the nacelle of a wind turbine is manifold. There are four different applications at the Stuttgart Chair of Wind Energy (SWE), University of Stuttgart (USTUTT), developed and further investigated:

1. Power performance testing
2. Load estimation
3. Wind turbine control
4. Wake wind field analysis

Besides SWE other research facilities are working on nacelle-based lidar measurements, e.g. DTU Wind Energy, ECNeth or NREL. In all four points mentioned above the main research objective is how to scan the wind field in the most accurate way, how many measurement points give the best time and space resolution and which scan figure is useful for which application.

The first two points can be used in the certification process of a wind turbine prototype which is installed either onshore or offshore (Figure 5-1), on fixed or floating platforms. That means that site independent measurement techniques are developed. The third point is a very promising approach to use wind field information from the “future”. To know the wind speed the next seconds has the advantage to react to the disturbance wind in advance. The wind turbine loads and rotation speed can be influenced by so-called feed forward control. By the use of predictive control strategies turbine loading can be lowered, life time can be increased or wind turbines can be designed more lightweight. In the fourth application different existing wake models are validated with wake wind field measurements from the nacelle (Figure 5-2).

Figure 5-1: Lidar scanner operating at the German offshore test site “Alpha Ventus” (left) [GL-GH],

Figure 5-2: Lidar scanner measuring the wake at DTU Risø Campus, Denmark (right) [SWE]

5.2.2 Instrumentation

The SWE owns a measurement system for large scale wind turbines. Since 2004 one has been performing the measurement of loads and inflow and wake conditions of a 5MW offshore prototype wind turbine. The system has two main components suitable for offshore applications namely

- a nacelle-based lidar scanner and
- a data acquisition system

which specifications are as follows.

Nacelle lidar (scanner)

The lidar scanner system is an extended commercial system of the type Windcube™ LS-7 Figure 5-3. A self-developed scanner enables nacelle-based wind measurements (Rettenmeier et al. (2010)). This flexible system can be setup for inflow and wake-flow measurement with different scanning strategies tailored for different applications:

- Pulsed lidar with wave length of 1.5 µm
- Multiple focus lengths from 40m up to 200m
- Spatial resolution in the line-of-sight of 20m
- Scanner with flexible trajectories for wind shear profiling and slicing
- Scanning rate between 5-10 seconds (depending on scanning strategy)
- LAN and UMTS remote access for control and data acquisition

Figure 5-3: SWE lidar scanner based on a commercial pulsed lidar (right hand side) and a self-developed scanner (left hand side)

As an update of the current measurement equipment regarding the nacelle lidar scanner the extension of the maximum range from currently 200m up to approximately 400m is aspired. For the lidar measurements from the nacelle of a wind turbine a faster scanning system with a so-called all-sky scan head and a high measurement range would offer new possibilities for novel research ideas. For the development of such a system still research is required.

Data Acquisition System (DAS)

The system (Figure 5-4) contains of following components

- Various temperature, strain gauges, pressure, voltage and current measurements
- Adaptable measurement and control system for mixed signal testing (imc CRONOS PL 13)
- CAN measurement modules for applications in industrial environments, for the decentralized capture of physical measurement data (imc CANSAS modules)
- CAN-Bus support for digital data transport
- Ethernet interface for system communication and data transport
- Measurement computer for data storage, management and remote control

As update of the current measurement equipment regarding the data acquisition system another I/O card for additional monitoring turbine signals, e.g. as ProfiBus, is aspired.

Figure 5-4: SWE Data acquisition system

At ECNneth several research projects are ongoing about the application of lidars, both ground-based and mounted on the nacelle. For the ground-based case the WindCube V2 and WinCube V2FCR are applied. A non-scanning WindIris lidar is mounted on the nacelle of turbine N6 in the ECN Wind turbine Test site Wieringermeer. More specifically it is mounted on the cooler with a tripod also part of the system. The optical head on top of the tripod is connected via a cable to the processing unit in the back of the nacelle. This processing unit is connected to a CompactRIO measurement system using the CANBus protocol.

5.2.3 Data presentation

Measuring the wind field from the nacelle of a turbine makes it possible to gather wind field information (wind speed, wind direction) in a high temporal and spatial resolution. To scan a wind field in any vertical and horizontal direction, the laser beam runs along a predetermined path and executes the measurement at predefined points. For designing a scan pattern the wind turbine simulator WITLIS was developed (Schlipf et al (2009)). This software supports the development of trajectories considering the motor speed and acceleration.
One of the basic trajectories used in different measurement campaigns of the SWE was a Lissajous figure with a ratio of 3:4. If a lidar scans the figure in such a way, it becomes more difficult to evaluate and recalculate a wind field from the measured points (Figure 5-5). Therefore, specific measurement points have to be defined, and the figure was adapted to 7x7 measurement grid points (Figure 5-6). The time needed to scan the 49 measurement points was 8.4 sec. which led to a good temporal and spatial resolution. Based on the pulsed lidar technology, each trajectory point is measured at 5 focus planes simultaneously which even allows an interpolation between the different focus planes (see Figure 5-7, Figure 5-8).

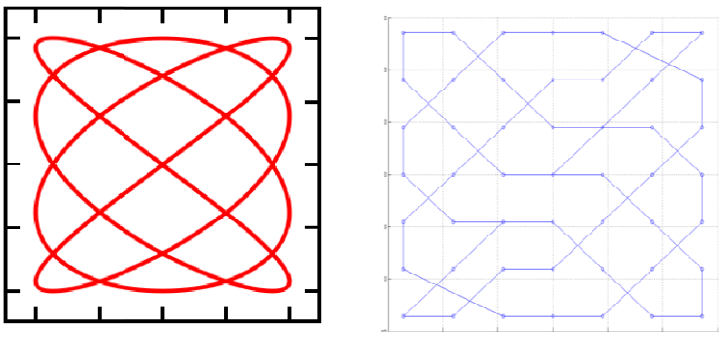

Figure 5-5: Left: Lissajous figure with a frequency ratio of 3:4 (left),

Figure 5-6: Lissajous figure adapted to 7x7 measurement grid (right)

Power performance testing of a wind turbine as an example

The advantage of measuring from the nacelle of a turbine is that the whole swept rotor area is covered and that horizontal and vertical wind shear can be taken into account. According to the standard for power performance testing (IEC 61400-12-1), fewer sectors have to be excluded because there is no met mast in the wake of the turbine or of other obstacles. Thus measurement campaigns can be carried out in a shorter time.

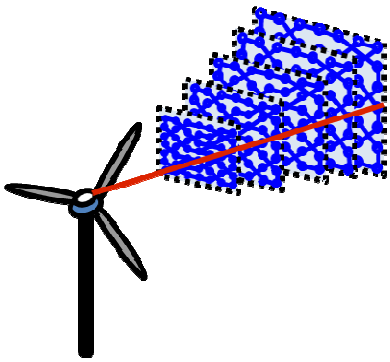

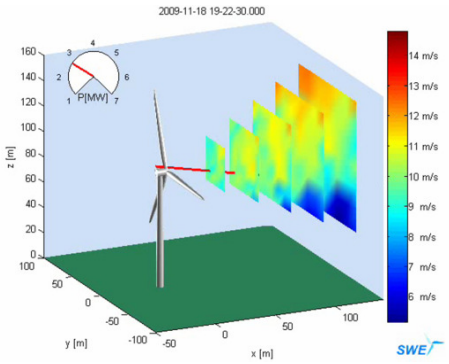

Figure 5-7: Sketch of simultaneous measurements at different distances (left)

Figure 5-8: Real measured data with an interpolation within one focus plane (right)

To determine a power curve, the mean values as well as the standard deviation of the electric power and the average wind speed over 10 minutes are necessary. The main goal is to get a power curve including all wind field information, as well as to get a smaller standard deviation. A second goal consists in the definition of relevant trajectory points.

As an example five single points were picked out of the 49 measurement points (Big-Cross, Figure 5-9). The five points contain somehow vertical and horizontal shear information. In Figure 5-10 the curve (blue) is relatively similar to the power curve measured with a met mast and a cup anemometer according to the IEC standard (red). One can see that the bars of the standard deviation are significantly smaller. That means that the uncertainties in the measurements are lower and the accuracy is higher.

$$u_{BigCross} = \frac{1}{5}\sum_{i=1}^{5}\overline{u_i} \qquad (24)$$

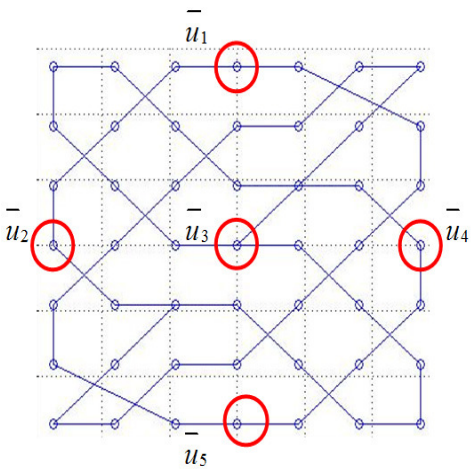

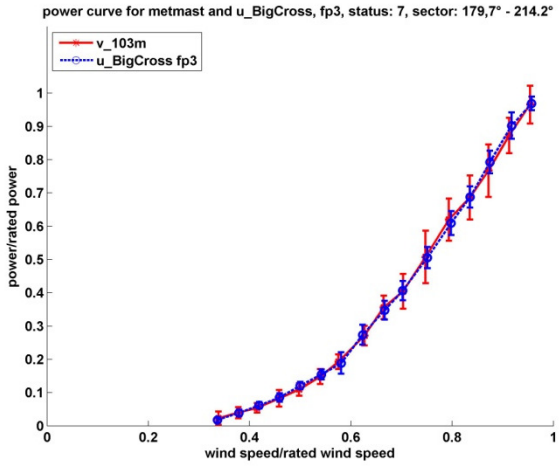

Figure 5-9: Five points out of 49 for the Big cross method (left)

Figure 5-10: Calculated power curve, electrical power and wind speed are normalized (right)

Just as a simple example the "Big Cross" method shows the big potential, measuring the wind field from nacelle and determining a power curve. But there are still some investigations that have to be done concerning turbulence, vertical and horizontal shear, comparison criteria and equivalent wind speed.

In general the use of a lidar system from the nacelle offers various applications in wake wind field analysis, wind turbine control, power curve determination and load estimation. The whole swept rotor area can be taken into account, but assumptions have to be made. Nacelle-based measurement methods show a great potential on- and offshore and even in complex terrain.

5.3 CALIBRATION OF GROUND-BASED LIDARS

5.3.1 Research objectives

Ground-based lidars are used extensively in the wind industry for measurements of the available wind resource. In flat terrain, the performance of wind lidars can be quite impressive, with an uncertainty approaching that of a boom-mounted cup anemometer. Since the sea surface is very flat, wind lidars can perform very well for marine wind energy as long as there is somewhere to deploy them. Various possibilities exist and have been extensively discussed in Marinet D4.16 (Courtney M. et al. D4.16 Report on options for full scale wind resource surveying). The main options are deploying wind lidars on existing platforms and mounting them on buoys.

In all cases, if the uncertainty of the wind resource is to be estimated, it is essential that the lidar has a traceable calibration. Apart from measuring the relative performance (in terms of a transfer function) to an established wind speed reference (usually a cup anemometer), the traceability to international standards conferred by the calibration permits an uncertainty budget to be calculated. Without this traceability, the uncertainty concept is meaningless. Lidar calibration is thus an important step towards any form for standardisation that requires the lidar as a reference wind speed. An important example here is the current revision of the IEC 61400-12-1 power curve standard in which the use of lidar, including a calibration and uncertainty scheme, are now included.

Wind lidars have been calibrated at the DTU Høvsøre Test Station for Large Wind Turbines for 6 years. DTU Wind Energy Department who manage the test station, have an accreditation for calibrating ground-based, pulsed lidars. The basic concept is to place the lidars at the foot of a meteorological mast and to perform the calibration using calibrated cup anemometers mounted on the mast as the reference wind speeds. This is shown in Figure 5-11 although here the actual wind speed comparisons are made with cup anemometers mounted at between 40 and 116m on the mast. The test setup and instrumentation will be described in more detail in the following section.

New forms for lidar deployments often require either new forms for calibrations or adaptions of existing techniques. For example at Høvsøre nacelle-mounted lidar calibrations (Figure 5-12) have recently been developed (Courtney M. Calibrating Nacelle Lidars. DTU Wind Energy Report E-0020, 2012). Another example is the testing of floating lidars on a motion platform (Figure 5-13).

Figure 5-11 Lidars under calibration at the Høvsøre Test Station.

Figure 5-12 A nacelle lidar being calibrated at the Høvsøre test station.

Figure 5-13 A lidar for a floating buoy being tested on a motion platform at Høvsøre.

5.3.2 Test site and instrumentation

5.3.2.1 The Høvsøre Test Site

Lidar calibrations are carried out at the Danish National Test Station for Large Wind Turbines, located at Høvsøre in Western Jutland, Denmark, about 30 km west-northwest of Holstebro.

The facility comprises a line of five test stands for MW-class wind turbines, oriented north-south parallel to the coast (slightly, about 3°, tilted to the east), and each stand has its dedicated upstream measuring mast for power performance tests to the west. The lidar tests are performed at the southern end of the turbine row and 200 m from the closest wind turbine, next to an intensively instrumented meteorological mast (met. mast) – see Figure 5-14 and Figure 5-15.

Figure 5-14 Outline of Høvsøre test site (picture from Google Earth).

Figure 5-15 The row of wind turbines at the Høvsøre test site with the tall met. mast in the front.

The Høvsøre Test Station is a flat site, mainly consisting of cultivated fields and grasslands, with maximum height variations less than 5 m. To the south is a lagoon, at the closest point 900 m from the met. mast. The site is about 1.8 km to the west the North Sea, separated from the land by a strip of sand dunes about 10 m high – see Figure 5-16. The land behind the dike lies about 1-5 m above sea level.

Figure 5-16 Høvsøre test site seen from the coastline in the west.

5.3.2.2 Instrumentation of reference mast

The lidar measurements are compared with reference wind speeds and wind directions that are measured at the met. mast. The purpose of this mast has been to supplement the wind measurements at the turbine test stands, providing additional information about the climatology at Høvsøre as well as meteorological data for boundary layer research. Due to the high quality of the instrumentation, maintenance and quality control, the data from this mast are well suited for the calibration of lidars.

Sensors used as references are the five cup anemometers, placed at 40 m, 60 m, 80 m, 100 m and 116.5 m height, and three wind vanes at 60 m, 80 m and 100 m. The cup anemometer at 116.5 m is top-mounted, all other reference sensors are mounted on booms pointing towards the south.

The wind speed and direction measurements are complemented by temperature sensors at 2 m and 100 m used for a filtering of the data. A sketch of the mast and its associated instrumentation is shown in Figure 5-17.

For the reference wind speed measurements, WindSensor P2546a cup anemometers are used. They are all classified as class 1A instruments and calibrated according to the respective MEASNET standard (see http://www.cupanemometer.com/products.htm for more details).

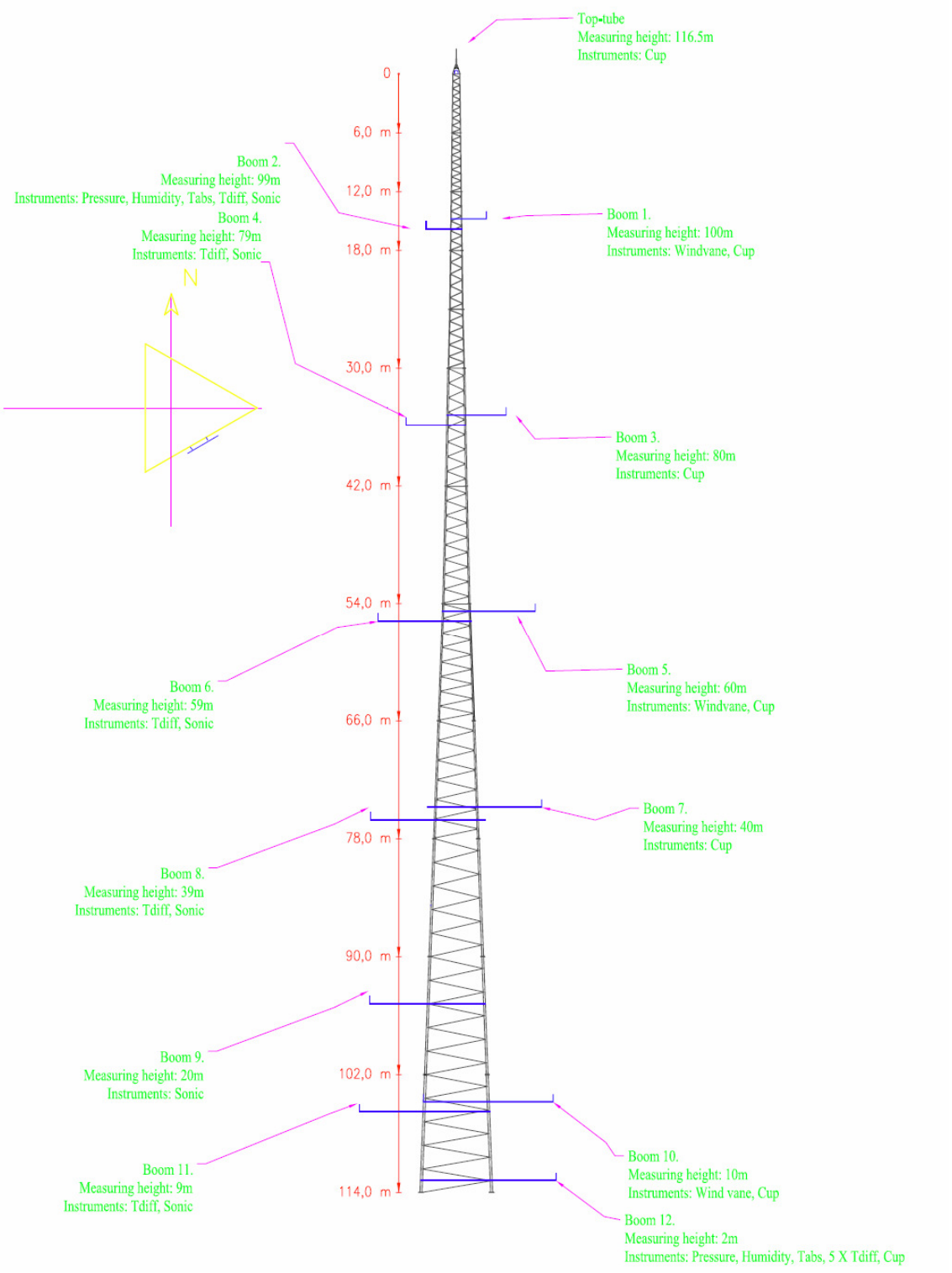

Figure 5-17: Sketch specifying the instrumentation of the met. mast

5.3.3 Data presentation

The fundamental result of a lidar calibration is a scatter plot of the lidar reported wind speed versus the reference wind speed from the cup anemometer. An example is shown in Figure 5-18 with the results from a constrained (black) and free (red) linear regression. These regression results form the basis of the transfer function between the lidar and the reference instrument.

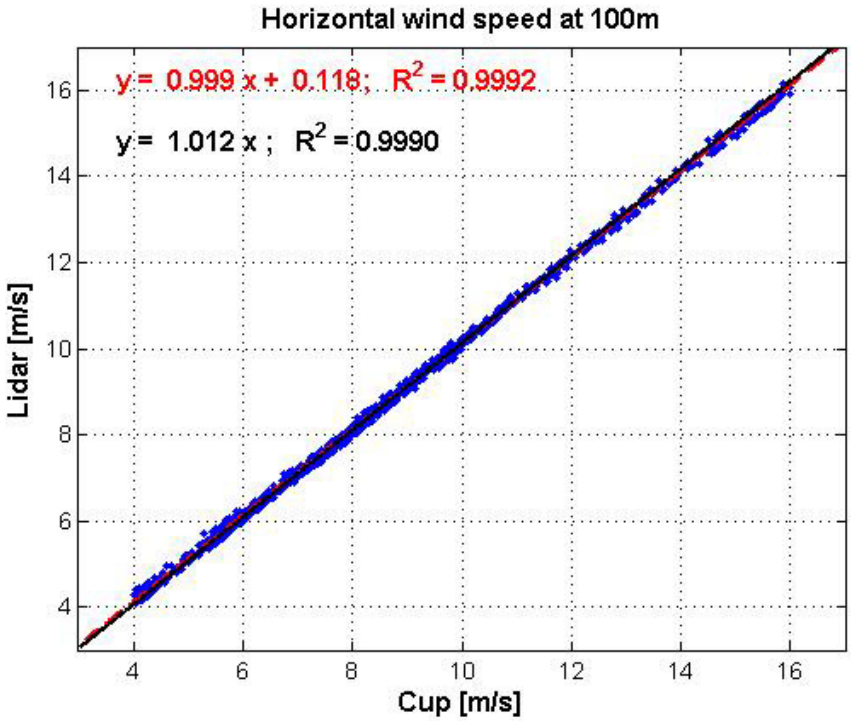

Figure 5-18 Scatter plot of lidar wind speeds versus reference cup wind speeds at 100m.

The second major results of the calibration are the estimates for the lidar uncertainty. These are shown in graphical form in Figure 5-19 which plots the deviation (difference between lidar and reference cup anemometer) as a function of wind speed. The blue squares show the k=2 uncertainty bounds for the lidar.

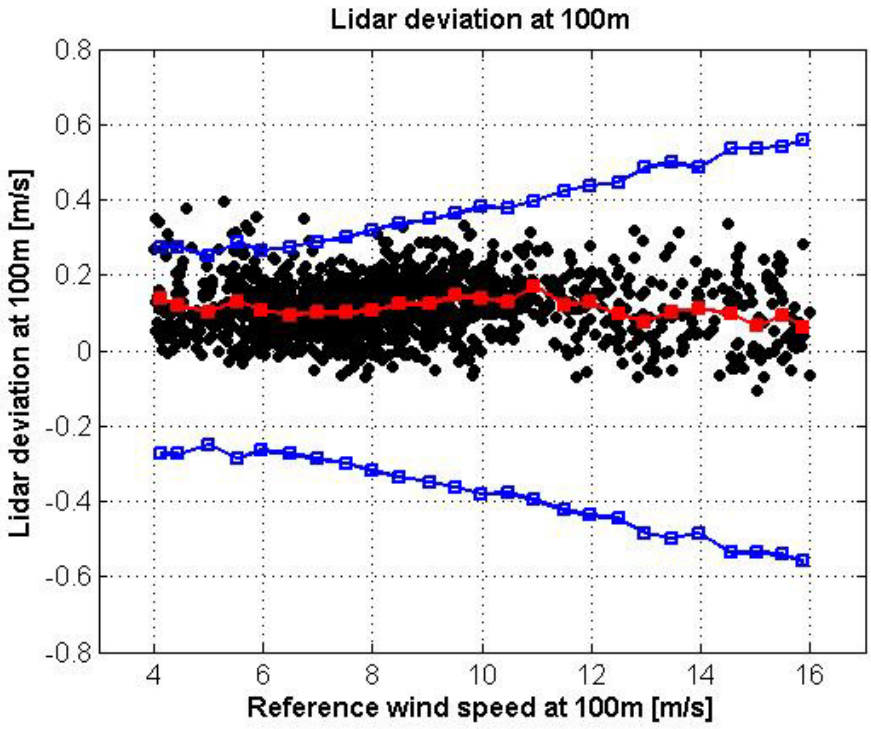

Figure 5-19 Deviation at 100m versus wind speed. Each black dot represents a 10 min value; the red dots are the wind speed bin averages and the blue squares show the (k=2) uncertainty bounds for the lidar.

5.4 DESIGN OF AIRFOILS FOR WIND TURBINE ROTOR BLADE

5.4.1 Research objectives

The rotor blades for onshore wind turbine are designed and optimized regarding high performance, less noise and rotor diameter up to 120 m (average). The design of rotor blades of offshore wind turbines are optimized for power production, too, but noise issues are not relevant at all so that rotational speed and tip speed ratio can be much higher. The design of the airfoils of offshore blades has to deal with structural issues as well. Within the "Offwindtech" research project (KIC Inno Energy) the Institute of Aerodynamics and Gas Dynamics (IAG) and the SWE of USTUTT worked on the design of blades for floating turbines as an example. Here the movement of the floating structure, the turbine and the blades itself have influence on the airfoil design as well. To validate the airfoil design, coming from simulation codes, the testing of an airfoil section is mandatory in terms of measuring the lift and drag coefficient. In this context, ECNeth and IAG are developing and wind tunnel testing new families of airfoils capable of high performance, helping to decrease the cost of energy of the wind turbines by reducing the loads on and the weight of the blade. This is achieved by adopting an advanced design methodology where requirements coming from different disciplines (i.e. aerodynamics, structures) are all taken into account to find the best compromise.

5.4.2 Testing facilities and instrumentation

5.4.2.1 Testing facility

The Laminar Wind Tunnel (LWT) of the IAG is an open return tunnel with a closed test section (Figure 5-20, Figure 5-21). The rectangular test section measures 0.73x2.73m^2 and is 3.15m long. A 2D airfoil model spans the short distance of the test section, gaps between model and tunnel walls are sealed. The effective contraction ratio of 20:1 as well as five screens and filters result in a very low turbulence level of less than Tu =2x10^{-4} for a frequency range of 10-5000Hz and a flow velocity of 30m/s. The diffusor section is covered with acoustic absorbing materials. This significantly reduces the upstream propagating sound from the fan of the wind tunnel and enables high quality acoustic measurements. The aerodynamic properties of the tunnel flow remained unchanged.

Beside standard measurements such as lift, drag and moment as well as airfoil pressure distributions, dedicated boundary-layer experiments can be performed by means of hot-wire probes. Experiments in a wind tunnel enable highly accurate drag measurements of airfoils for tidal current turbines. As a unique feature important for wind turbine blade developers the LWT enables to measure the emitted airfoil trailing-edge noise.

Flow speed and unit Reynolds number

The maximum flow speed of the LWT is around 90m/s under the assumption of a small blockage of the test section. Depending on the environmental conditions this results in a unit Reynolds number of approximately $Re_{unit} = 5.5 \times 10^6$ [Re/m]. From practical considerations a certain margin should be introduced, which leads to a reduction to $Re_{unit} = 5.0 \times 10^6$ [Re/m]. Tests at this Reynolds number are possible with standard wind tunnel models covering a standard range of angles of attack ($-20° \leq \alpha \leq +20°$).
Due to the design of the wind tunnel also a margin exist for the lowest flow velocity, which is around 15m/s. For those conditions, the tunnel gets sensitive to changes of outside wind speed and direction, which results in drifts in the mean tunnel speed.

Figure 5-20: Laminar Wind Tunnel (LWT) in the front, Gust Wind Tunnel in the back (IAG)

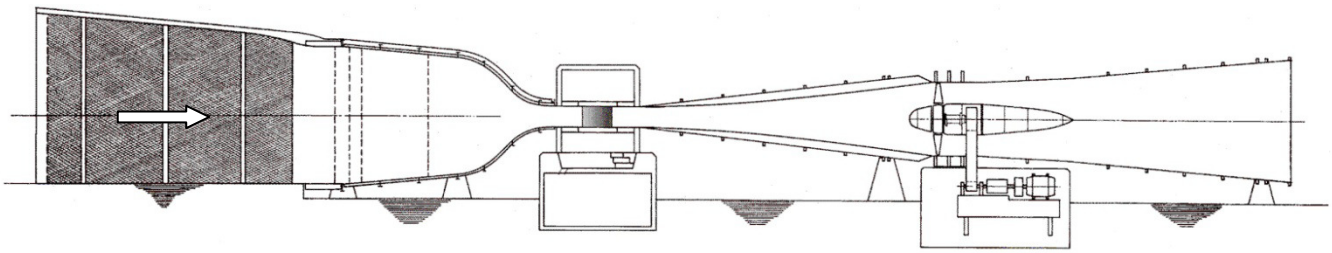

Figure 5-21: Cross section of the LWT [IAG]

5.4.2.2 Instrumentation

Lift measurement

The lift is determined by experimental integration of the pressure distribution along the opposite two tunnel walls (in general for wind tunnel models without pressure taps). The difference of both averaged pressures is proportional to the lift. In comparison to measurements with a balance it is possible to avoid any gap between model and wind tunnel wall. This is very important especially for high lift systems.

Drag measurement

The drag is determined by an integrating wake rake which is positioned approximately 0.4 chord length behind the model trailing edge. The rake automatically moves into the middle of the wake and adjusts itself parallel to the local flow direction. The width of the wake rake is selected according to the expected drag. For the typical tests a standard wake rake with a width of 120 mm is used.
During measurements the wake rake is traversed in spanwise direction and a mean value for the drag is calculated.

To obtain lift and drag coefficients, the undisturbed dynamic head, the static pressure and the maximum pressure loss in the wake are measured as well. The data acquisition system is controlled by a PC and carefully calibrated before each set of measurements. Standard wind tunnel corrections are applied and the aerodynamic coefficients are disposed on-line on a plotter. During the traverse of the wake rake the actual values are monitored in the pen-up position. This provides a good check for the variation of drag in spanwise direction.

Pitching moment

The pitching moment is measured by a balance. The wind tunnel model is mounted between two self-aligning ball bearings placed at the quarter pivot point. One side of the model is connected to a high precision load cell. The sealing of the gaps between model and tunnel wall is replaced for those measurements by special tapes to insure a minimum gap size.

Boundary layer control, blowing system

Blowing air tangential in the corners between the model and the mounting plates is used as a boundary layer control to ensure two-dimensional conditions. The nozzles were placed on the tunnel wall at 0.6 x/c of the upper and lower surface of the airfoil, which is the standard position.
Due to the radiated sound of the nozzles, the acoustic measurements are performed without blowing system.

Transition detection

The measurement of the transition position as function of the angle of attack (AOA) is performed with the help of a stethoscope. A small microphone inside the stethoscope reads the pressure fluctuations in the boundary layer. The signal is amplified and transmitted to an earphone. The turbulent boundary layer can be clearly distinguished from the laminar one by a typical loud broadband noise. In the laminar boundary layer nearly nothing can be heard. The 'onset' of transition is characterized by a strong increase in loudness. Comparison to other transition detection methods show that the determined transition 'position' is similar to the position where the skin friction starts to increase. Therefore, the detected positions are equivalent to those obtained from visualizations with surface oil-film methods.
A thermal camera system can be used to check the transition position during the speed-up of the wind tunnel. This method takes advantage from the fact that the heat transfer from the surface is different in a laminar boundary layer in comparison to a turbulent one. Therefore, only a small temperature difference (approximately 2° C) between model and free stream is sufficient to provide a picture of the boundary layer state without any disturbances to the flow field.

Pressure distributions

The pressure distributions are obtained by a PSI pressure scanning system. Up to four different 64 channel pressure scanners can used: full scale reading of 25mbar, 50mbar, 150mbar and 350mbar. The transducers are calibrated before every set of measurements against a MKS-Baratron reference pressure transducer.

5.4.3 Model construction

Chord length

The selection of an appropriate chord length for a wind tunnel model is always a more or less difficult compromise (Figure 5-22). It depends not only on the intended Reynolds number range, but also on possible Mach number effects and blockage effects which increase with the size and thickness of the model.

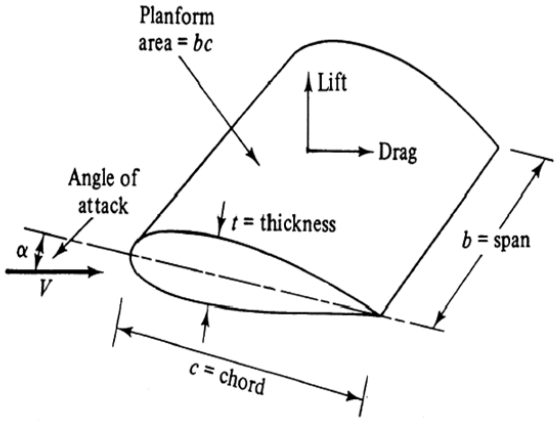

Figure 5-22: Geometric and dynamic parameters of airfoils [College of Engineering, University of IOWA]

Chord length aerodynamic testing

From the viewpoint of wind tunnel wall influence and necessary corrections the model should be small. The measurement technique of the LWT is streamlined for a chord length range of c = 0.3m – 0.8m. Usually, a chord length of c = 0.6m is preferable as long as the thickness of the model stays below t/c = 30%. This results in a Reynolds number of $Re = 3.0 \times 10^6$.

If the airfoil is designed for a much higher Reynolds number, it may be necessary to increase the chord length up to c = 0.8m to avoid to early boundary layer separation. The increasing wind tunnel wall influence (which is taken into account by standard wind tunnel corrections, with certain limitations) can be partly compensated if the results are compared with CFD analyses which take into account the tunnel walls. This extended method is up to the customer.

Often, the influence of the Mach number is neglected in low speed wind tunnel testing. Nevertheless, there are cases where the local cp-distribution can reach quite significant values. Sometimes even $cp_{\_crit}$ can be acceded leading to abrupt stall of high lift configurations.

At certain combinations of flow speed and physical dimensions flat-back airfoil sections can produce a regular vortex street which can led to a feed-back loop with a standing acoustic wave in transversal direction. This can produce sound levels beyond 150dB and makes measurements impossible.

Chord length acoustic testing

Typical chord lengths for acoustic testing are in the order of c = 0.3m – 0.6m and the corresponding flow speeds between $60 \leq U_4 \leq 75$m/s. T

Airfoil data

Regarding the modelling besides the chord length c the shape of the profile is necessary. For this purpose, each airfoil needs to have information about the thickness at a certain point of the chord length.

As an example the NACA 6-418 (Figure 5-23) airfoil profile has following relative distribution of height y/c along the normed chord length x/c.

x/c	y/c		x/c	y/c		x/c	y/c		x/c	y/c
1	0		0,34823	0,11037		0,00737	-0,01308		0,45055	-0,0644
0,95037	0,0103		0,29763	0,1073		0,01014	-0,0156		0,5	-0,05908
0,90077	0,02132		0,24707	0,10176		0,0155	-0,01942		0,54953	-0,05255
0,85108	0,03294		0,19657	0,09366		0,02848	-0,02613		0,59914	-0,04515
0,80127	0,04477		0,14617	0,08277		0,05391	-0,03536		0,64886	-0,03721
0,75135	0,05654		0,09595	0,06823		0,07905	-0,04212		0,69869	-0,02896
0,70131	0,06784		0,07095	0,05908		0,10405	-0,04755		0,74865	-0,02074
0,65114	0,07841		0,04609	0,048		0,15383	-0,05585		0,79873	-0,01293
0,60086	0,08799		0,02152	0,03357		0,20343	-0,06182		0,84892	-0,00602
0,55047	0,09635		0,0095	0,0237		0,25293	-0,06596		0,94963	0,00234
0,5	0,1032		0,00486	0,0184		0,30237	-0,06842		1	0
0,44945	0,1082		0,00263	0,01508		0,35177	-0,06917			
0,39885	0,11093		0	0		0,40115	-0,06809			

Figure 5-23: NACA 64-418 airfoil

When the data is known the model can be built by using NC-milled negative molds (Figure 5-24). The instrumentation can be done quite easily. The complete positive shaped airfoil can be mounted in a last step (Figure 5-25).

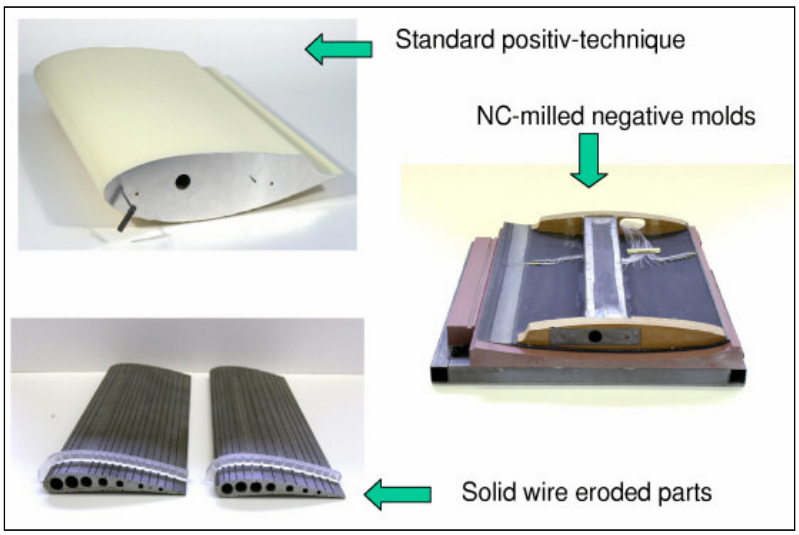

Figure 5-24: Model construction at the IAG (left) [IAG]

Figure 5-25: Airfoil mounted in test chamber of LWT [IAG]

5.4.4 Data presentation

Polar Measurements

In order to calculate the lift and drag coefficient of an airfoil, the lift L and the drag D need to be determined in a wind tunnel test first. The non-dimensional lift and drag coefficient are calculated with the following formulas.

$$c_L = \frac{2L}{v_r^2 \rho S} \quad (25)$$

$$c_D = \frac{2D}{v_r^2 \rho S} \quad (26)$$

v_r is the resulting inflow velocity, Rho is the air density, S is the overflowed area. It is calculated as S = c x sp, where c is the chord length of the airfoil and sp the span of the section. c_L and c_D are the lift and drag coefficients which depend on the shape of the airfoil, the angle of attack (AOA) of the inflow velocity and the Reynolds number. These coefficients are airfoil specific and are plotted in "Airfoil lift and drag polar diagrams" (Figure 5-26).

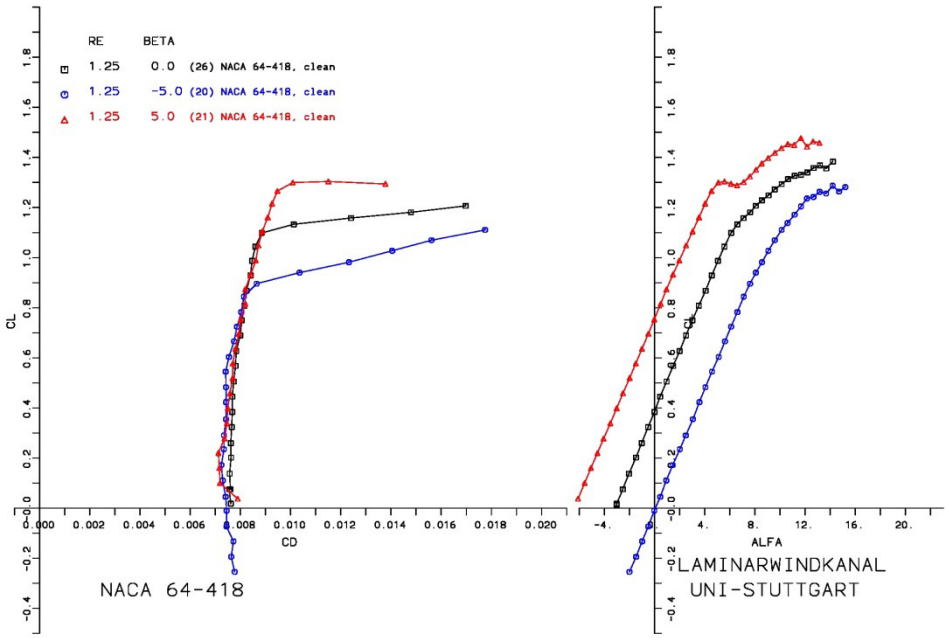

Figure 5-26: Lift coefficient is plotted on the axis of ordinate, the drag coefficient is plotted on the left axis of abscissas, the angle of attack on the right axis of abscissas

The standard procedure for polar measurements is the evaluation of lift and drag starting with the lowest angle of attack. The angle of attack is adjusted to roughly zero degree until the necessary tunnel speed is reached. Then the AOA is increased step by step and data are obtained until $c_{l\text{-}max}$ is exceeded. A few points are taken again with increasing α to show clearly the post stall behavior. Then the AOA is reduced and additional points are collected if a hysteresis of the c_l-α curve is visible. Hysteresis effects are always carefully checked. The same procedure is done in a similar way for the negative part of the c_l-α slope. Finally, the data points have to be reordered to allow plotting as one continuous curve.

Drag measurements are performed, if possible. To avoid damaging of the wake rake due to high velocity fluctuations close to $c_{l\text{-}max}$ the wake rake has to be removed for the high Reynolds numbers.

Despite the whole measurement setup for the aerodynamic testing is automated, the selection of angles of attack is done manually to cover all peculiarities of the airfoil polar. Therefore one decides about the AOA spacing depending on the shape of the polar. Usually, 50 points are collected for a full polar ($c_{l\text{-}min}$ to $c_{l\text{-}max}$).

Acoustic testing

The Coherent Particle Velocity (CPV) method can be used for quantitative measurements as long as flow separation on the model is limited ($x_{sep} \leq 5\%$) and the trailing edge is thin ($t \leq 1\%$) and forms a straight line (Figure 5-27). Sound

radiated from the trailing edge can result from different mechanisms, like turbulent boundary layer trailing edge noise (TBL-TE) or laminar vortex shedding noise (LBL-VS) or blunt trailing edge noise (BTE). Airfoils with a 'standard' trailing edge thickness often show a combination of TBL-TE and BTE noise. This can be avoided by building a wind tunnel model with extremely thin trailing edge, typically t = 0.5mm.

Flat-back airfoil sections often show pronounced BTE noise, which can be measured by CPV but not in a quantitative manner. The measurable frequency range depends on the sound pressure level radiated from the model and cannot be specified in advance.

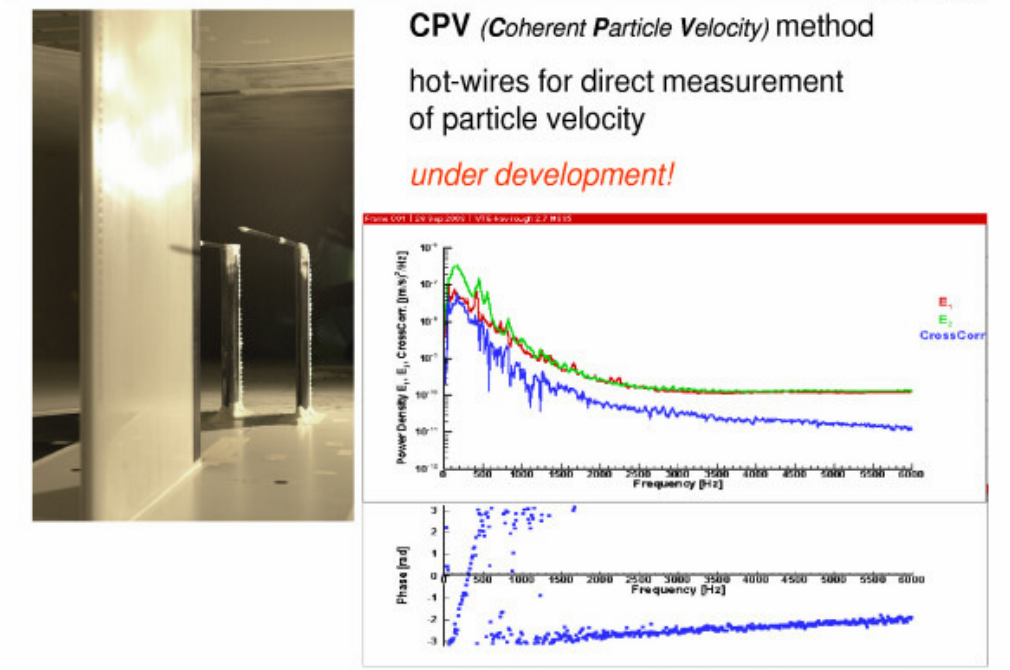

Figure 5-27: Trailing edge noise measurements using CPV method [IAG]

5.5 FULL-SCALE MODEL TESTING

5.5.1 Research objectives

At Energy Research Centre of The Netherlands (ECN) software is developed to determine the behaviour of (offshore) wind turbines, both single and in wind farms. The main objective of the measurements is to validate the models. Besides ECN performs as a service tests on prototype wind turbines and at wind farms of customers, and wind measurements.

ECN is involved in both full scale testing and model testing. Full scale tests are performed by ECN itself and include mechanical load tests, power performance measurements and noise measurements. Full scale measurements are at offshore and onshore locations. An example of ECNeth's offshore measurements is for meteomast IJmuiden (http://www.meteomastijmuiden.nl/en/home/). Here wind conditions are measured by a metmast and by lidar. Waves are measured with a wave buoy. The data is collected by ECNeth in their WDMS data base. Statistical data is public available from the website. Raw data is on request.

ECN is accredited in accordance with IEC 17025 for power curve measurements, noise measurements, and mechanical load measurements. Most of the measurements are carried out in accordance with the valid IEC wind turbine standards and technical recommendations (IEC 61400 -11, -12, and-13).

Besides ECN is involved in model tests in a wind tunnel or sea keeping basin. For wind tunnel tests, usually involving blade and rotor aerodynamics, ECN specifies the test set up and test cases and performs the analysis of the results. In case of hydrodynamic model tests on fixed and floating support structure ECN's input is its knowledge about wind turbine dynamics for instance in the design of the controller for the wind turbine model.

5.5.2 Instrumentation and test facilities

At the ECN Wind Turbine Test Site Wieringermeer (EWTW) full scale measurements are done on six prototypes, five 2.5 MW research turbines, and, until September 2013, a scaled wind farm consisting of ten 10 kW wind turbines. Signals acquired from the prototype or research turbines include data from the turbine SCADA and from dedicated sensors measuring via the DANTE system mechanical loads, electrical power, and noise.

Equipment to measure the ambient conditions at the EWTW comprise three 108 m meteo masts, six dedicated wind masts for the prototypes, plus four tall and ten small wind masts near the 10 kW turbines. Instruments include cup anemometers, wind vanes, sonic anemometers, and temperature and pressure sensors. In addition to that ECN employs a vertical-looking lidar on the ground, and an innovative forward-looking lidar on one of the nacelles.

For data acquisition ECN uses in-house developed measurement systems DANTE (Data Acquisition Network for Turbine Evaluation). A DANTE system can gather up to a maximum of 32 measuring signals at a maximum rate of 128 Hz; for example the mechanical load on the mast and turbine blades, rotation of the rotor, acceleration of the nacelle and the load upon the support structure under water.

5.5.3 Data presentation

The measured data is stored in and can be retrieved from the Wind Data Management System WDMS. This system was developed by ECN in order to fill the gap between the sheer amount of measured data and the requirements of the users of the data. On the one hand it handles and imports the data, and at the other hand serves the clients by presenting the data in various predefined ways.
In WDMS there is a clear distinction between measured signals and pseudo signals. A measured signal originates from an external source and usually after calibration coefficients have been applied. In compliance with ISO 17025, measured data is saved unaltered. A pseudo signal on the other hand is derived from one or more measured or pseudo signals by using separately stored calibration coefficients.
In addition, WDMS allows for the definition of meta data, for example the configuration data of the DANTE system.
An important aspect of WDMS is validation. In this three levels are identified: auto validation, rule-based validation, and post validation. As a result always cleaned data is available to the user.
Data is retrieved by using SQL statements. Usually a selection in the data base is based on the statistics of the time series of the signals. The statistics are exported in the form of comma-separated files; time series are best exported in binary files. For the missing values several sentinel values can be designed; the empty space being the standard.

5.6 Study of the effects of nonlinear wave loads on a monopile support structure

Offshore wind turbines are always subjected to highly varying aerodynamic and hydrodynamic loads. A correct assessment of the effects of nonlinear (breaking and steep non-breaking) wave forces on the structure have crucial implications on the design phase of the wind turbine support structures. For this reason a numerical model and an experimental small-scale (1 to 60) study in the UNIFI/DICeA wave-current flume will be carried out. The scaling is done according Froude law. The diameter of the cylinder now corresponds to a real diameter of 6 m, which is typical for offshore foundations of wind turbines.
The aim of the testing activities is to investigate the effects of wave loads on slender cylindrical substructures of offshore wind turbines. For a correct characterization of the waves-structure interaction, two different models are constructed: the first model is a stiff cylinder; the second model is an elastic cylinder to take account of the dynamic behaviour of the structure. In that case, the mass distribution and the elasticity of the model play an important role in reproducing the natural vibration frequencies of the prototype. The objective is the development of both a numerical and experimental model of cylindrical monopile foundation in intermediate-shallow water (10-30m) to evaluate the dynamic interaction waves-cylinder with particular emphasis to resonant effects, such as ringing and springing.
Experimental small-scale study to investigate waves and wave load characteristics on a slender cylindrical pile in controlled conditions are executed in the DICeA-UNIFI wave-current flume. The dimensions of the flume tank are LxBxH = 48 x 0.8 x 0.8 m. In the wave flume a current and a wave can be generated. A wave maker of the piston type generates the waves. By circulating the water in one of the directions a current can be generated. The wave flume is

made entirely of steel and glass and equipped with a wave generator (piston type) that generates waves with heights up to 0.4 m.

5.7 WIND TUNNEL MODEL FACILITY FOR OFFSHORE WIND TURBINE TESTING

5.7.1 Research objectives

The main activity in the Wind Tunnel Lab at NTNU has in recent years been centred on wind turbine wake interactions, focused on doing bench mark experiments for validation of prediction methods for wind park designs. We have successfully arranged for 3 "Blind Test" (benchmark) experiments where we have invited leading World wide groups developing numerical tools for the design of Wind Parks – where we offer the fully documented experimental results for the comparison and evaluation of the numerical models

- Blind Test #1: One wind turbine: results for performance of turbine and fully documented wake (3D mean and turbulence velocities)
- Blind Test #2: Two wind turbines inline (see picture): results for performance of both turbines at various Tip Speed Ratios and fully documented wakes (3D mean and turbulence velocities)
- Blind Test #3: Two wind turbines, the downstream turbine off-set half a rotor diameter wrt. upstream turbine: results for performance of both turbines at various Tip Speed Ratios and fully documented wakes (3D mean and turbulence velocities)

5.7.2 Instrumentation and test facilities

The NTNU wind tunnel is of the closed-return type and the fan is driven by a 220 kW DC motor. The 2 x 3 sq. meter test section is 11 m long with a maximum speed of 30 m/s. Generic equipment is a 3D traversing mechanism and balances for measuring all components of loads on structures. For the Turbine Wake Interaction studies we have 2 instrumented wind turbine models (rotor diameter ca 1 meter - see picture), such that we can measure power pro- duction, rotational speed, thrust force, torque force, and advanced instrumentation (HW, LDV, PIV, HSPIV, etc) for doing space and time resolved measurements of the turbulence characteristics in the turbine wake - important be- cause the wake from the upstream turbine will give the input flow field for the downstream turbine.

The model turbines in this study were designed in 2008, for the specific purpose to be used as test cases. This is the reason for many of the design compromises involved, as discussed in Krogstad and Eriksen (2013). Figure 5-19 shows the two turbines used in the blind tests located in the wind tunnel. **T**1 is the upstream turbine, while **T**2 is the downstream one.

Figure 5-28: Wind tunnel model tests at NTNU

5.7.3 Model construction

The model wind turbine tested has a three-bladed upwind rotor, and the overall rotor diameter is 900 mm. The rotor blade geometry was designed using a blade element momentum method developed in-house. The NREL S826 airfoil section was used throughout the span of the blade.15 This is one of the airfoils designed specifically for wind turbine applications by the National Renewable Energy Laboratory, USA, albeit for a much higher Reynolds number than could be achieved in the tests where Re was typically lower by a factor 20. The design was therefore corrected for the expected Reynolds number effects on the airfoil performance characteristics. The S826 profile was chosen for this study for two main reasons. It has a so-called separation ramp near the suction side trailing edge that, according to the originators and also verified by our own computational fluid dynamics simulations, gives a very gentle stall development. It is also designed to generate a very quick transition to turbulence due to a rather small leading edge radius. This was expected to reduce problems with Reynolds number effects and make the profile less sensitive to roughness. At model scale, the relative surface roughness is always higher than what may be achieved on a full-scale blade. Our experience from previous wind turbine model tests at similar scales has shown that the production roughness is often not enough to cause early transition at these Reynolds numbers so that the flow has to be tripped. Because of the built-in rapid transition of the S826, this was not found necessary for this model, and the power coefficient measured at the design tip speed ratio was less than 1% different from what was predicted by the design software.

Since the main purpose for this experiment was to provide data for prediction verification rather than to simulate the performance of a specific full-scale turbine, the blade chord length was made about three times wider than what is typical on commercial turbines to reduce the gap in Reynolds number. Information about the blade and airfoil characteristics may be found in Krogstad and Lund (2012).

The hub diameter is 90 mm, and its height (above the ground plane) is 820 mm. The lowest elevation when the blade rotates is therefore at 370 mm above the ground plane and thus higher than the ground plane boundary layer thickness.

The model blockage ratio, defined as the ratio between the rotor swept area and the wind tunnel cross-sectional area, was about 12.40%. This is close to the suggested upper limit of about 10% to avoid tunnel wall interference on the turbine wake expansion. As already stated, the purpose of the present tests was to provide data at controlled operating conditions to be used to check predictions by high resolution computational fluid dynamics and blade element momentum method predictions. Hence, any effects of wind tunnel walls will be included if the calculation domain is made to coincide with the tunnel area. This allows a larger model to be used compared with the case where wall interference must be avoided. During the tests, the rotor rotates in an anticlockwise direction when viewed from upstream of the turbine. The torque generated by the wind turbine was measured by a torque sensor mounted directly on the rotor shaft. The forces on the model were obtained from the six-component force balance on which the model was mounted. Both instruments were calibrated using standard weights prior to each test. To compensate for the tower and nacelle thrust, the drag force acting on the tower and nacelle system was measured without the rotor blades at the same free-stream velocity used for the performance measurements. The effective thrust acting on the rotor system during operation was then estimated by subtracting the tower and nacelle system drag from the thrust acting on the whole system (rotor blades, the tower and nacelle system). The performance characteristics of the model turbine were repeated a large number of times during the course of this study. The maximum deviation in maximum power coefficient was found to be less than 2%

5.7.4 Data presentation

Main parameters for characterizing turbines are the Power output and the Thrust on the turbine, expressed through the dimensionless coefficients C_P and C_T. Figure A-20 shows results for both the upstream turbine T1 and the downstream turbine T2, where both the experimental results and the results from 9 modelers are included – for details, see the references cited.

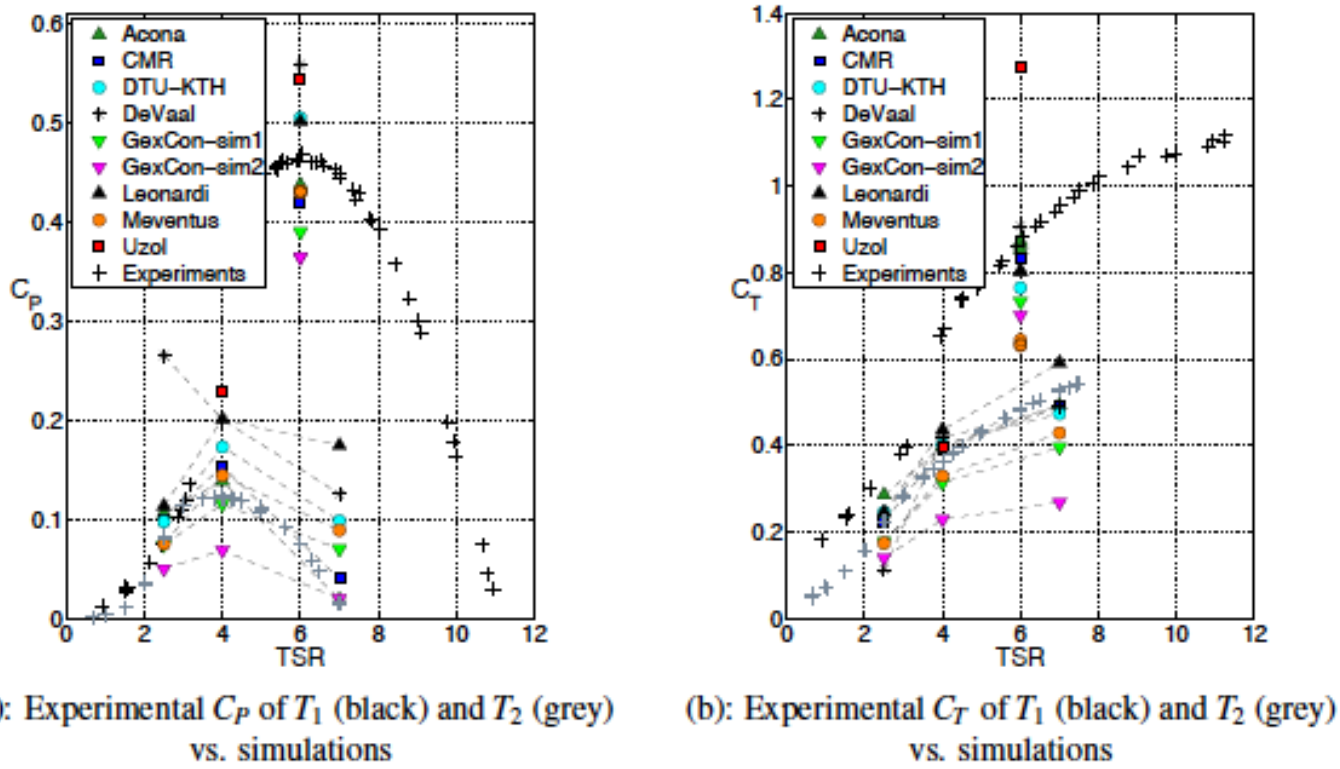

Figure 5-29: Power coefficient Cp in (a) and Thrust coefficient Ct in (b) for experiment and 9 modellers

The following references are pertinent for presenting data from the turbine wake interaction studies – as by medio 2013:

- Krogstad, Per-Åge; Adaramola, Muyiwa Samuel: Performance and near wake measurements of a model horizontal axis wind turbine. *Wind Energy* 2012 ;Volum 15.(5) s. 743-756
- Krogstad, Per-Åge; Eriksen, Pål Egil: "Blind test" calculations of the performance and wake development for a model wind turbine. *Renewable energy* 2013 ;Volum 50. s. 325-333
- Krogstad, Per-Åge; Eriksen, Pål Egil: ”Blind test” Workshop Calculations for a model wind turbine; Summary report. NOWITECH / NORCOWE Workshop; 2011-10-20 - 2011-10-21
- Krogstad, Per-Åge; Lund, JA: An experimental and numerical study of the performance of a model turbine. *Wind Energy* 2012 ;Volum 15.(3) s. 443-457
- Pierella, Fabio; Krogstad, Per-Åge; Sætran, Lars Roar:Blind Test 2 Calculations for two wind turbines in tandem arrangement. ICOWES Conference; 2013-06-17 - 2013-06-19
- Røkenes, Kjersti; Krogstad, Per-Åge: Wind Tunnel Simulation of Terrain Effects on Wind Farm Siting. *Wind Energy* 2009 ;Volum 12.(4) s. 391-410
- Pierella, Fabio; Sætran, Lars Roar: Effect of initial conditions on flow past grids of finite extension. AFMC 17; 2010-12-06 - 2010-12-10
- Pierella, Fabio; Sætran, Lars Roar: Performance and turbulence measurements on an array of two model wind turbines. AWEA Offshore WindExpo; 2011-10-11 - 2011-11-13
- Pierella, Fabio; Sætran, Lars Roar: Wake measurements on an array of two model wind turbines. EWEA Offshore 2011; 2011-11-29 - 2011-12-01
- Schümann, Heiner; Pierella, Fabio; Sætran, Lars Roar: Experimental investigation of wind turbine wakes in the wind tunnel. *Energy Procedia* 2013 ;Volum 35. s. 285-296
- Bartl, Jan Michael Simon; Pierella, Fabio; Sætran, Lars Roar: Wake measurements behind an array of two model wind turbines. *Energy Procedia* 2012 ;Volum 24. s. 305-312

6 CONCLUSIONS AND RECOMMENDATIONS

Support structures of offshore wind turbines are exposed to a combination of arbitrary wind and wave loads. Within the desired service life of 20 to 30 years the structures have to endure considerable amounts of dynamic load cycles.

Due to cyclic loading accurate fatigue assessment is crucial for design of structural components in support structures for offshore wind turbines. Experimental fatigue assessment of large components is often limited by available test facilities as well as timely and monetary expenditures. For statistical significance large numbers of tests have to be performed with high mean loads and considerable numbers of load cycles. This requirements often exceed the capabilities of test facilities. However, for certain details in support structures for offshore wind turbines common fatigue assessment approaches need to be complimented by experimental tests. In this way an economic design can be improved.
As an example for experimental fatigue assessment of characteristic structural details of offshore wind turbine support structures testing procedures for large sized bolts have been elaborated. For large sized bolts only a small number of fatigue test data exists. First investigations indicate that the thickness effect acc. to EN 1993-1-9 (2009) and GL-Guideline (2012) leads to conservative design results. Especially for application of diameters larger than M48 further investigations are necessary for an appropriate fatigue design. Especially the reduction of fatigue strength due to large dimensions, but also other influencing factors, have not yet been sufficiently investigated

The behaviour of soil under cyclic loading can be investigated in cyclic laboratory tests. The problem with the obtained results is to convert these from “unit level” (single soils samples under defined stress- and strain conditions) to “system level” (pile-soil or fundament-soil). Basically, for the characterization of soil behaviour under cyclic load conditions, a suitable material law should be calibrated. With such a law, the properties of the system could be simulated numerically. However, this approach is, while limited in its accuracy, very costly and limited to a small number of load cycles.
Therefore, the results from cyclic tests must be converted in another way to the system level. For this, smaller or greater idealisations are necessary. Especially undrained tests to monitor the accumulation of excess pore water pressure can lead, due to different draining conditions on system level, only to qualitative results.
In this report, different ways for the interpretation of cyclic laboratory tests are presented. It is shown that cyclic tests are helpful and also necessary for the evaluation of the systems behaviour. But it is also obvious that these tests can give only qualitative design values. The design of Monopiles and axially loaded piles is up to this point done without direct recognition of results from cyclic tests. The test results can only ensure the assumptions made in the deign process. Regarding the further development of design processes of offshore wind converters under cyclic loading, more research is highly needed

Experiences from the recently installed wind turbines in the German Exclusive Economic Zone (EEZ) in the North Sea show that scour is a very serious phenomenon concerning the stability of the OWT. So far, the existing calculation methods cannot describe any particular mechanism of action especially for geometrically complex foundation structures. Furthermore, for complex foundation structures there is no practical experience with scouring so far, which could be used as a basis for an appropriate design method for the scour protection system. Laboratory experiments are therefore essential to achieve a sufficient degree of planning certainty. Nonetheless, certain scaling effects in the scaled model must be expected because the compliance of an exact physical similarity between model and prototype is not achievable. Thus, gained results of scaled model tests give only a guidance on physical processes in prototype scale.
Over the past years the Franzius-Institute of the Leibniz University Hannover investigated various offshore structures, including monopile, tripod, tripile and two different gravity based foundations. The overall objective of investigations was to gain general knowledge on physical processes, the local and global scour development as well as local flow patterns leading to scour.
The following two-step test procedure resulted:

1. Small-scale tests to determine the general scour phenomena and local flow pattern. The scale parameter was between $\lambda \sim 40$ to 50. Small-scale tests provide the possibility of carrying out more parameter combinations in less time and with less effort in the test set-up (compared to large-scale tests), but with the limitation of higher scaling effects.

2. Large-scale tests to repeat selected parameter combinations, that resulted in the small-scale tests in the largest scour depth, but with minimized scaling effects, especially regarding the sediment. The scale parameter was between $\lambda \sim 4$ to 17. Moreover, studies on scour protection systems should be done in large-scale because not only is the sediment material, but also the material of the scour protection system itself, e.g. geotextiles, very sensitive to scaling effects.

The primary hydraulic boundary condition was the extreme wave event with a recurrence interval of 50 years, because the design wave height for offshore sturctures is derived from its significant wave height $H_{s,50}$, Germanischer Lloyd (2005). It has to be noted that due to the set-up of the facilities, the models were solely loaded with wave or current boundary conditions. A combined wave-current load was solely investigated in numerical model tests (Stahlmann and Schlurmann (2012), Stahlmann (2013)) so far, due to the absence of such combined test facilities during the test periods. It is however generally recommended to investigate the scour phenomena and the scour protection system in laboratory tests in combined wave-current load to avoid neglecting the interaction of naturally given multi-directional sea states and tidal currents. Therefore, Franzius-Institute is currently upgrading its present large 3D wave basin in Hannover-Marienwerder, which has a multi-directional wave maker, by adding a current generation system.

Besides testing activities regarding support structures and foundation systems of offshore wind turbines, MARINET research facilities are performing high class research on various fields of offshore wind turbine energy conversion systems and components. Some of the main research activities and testing practices have been described in the report. This testing practices can be regarded as state-of-the-art for experimental investigations in the respective fields.

7 REFERENCES

Achmus, M. (2011). Bemessung von Monopiles für die Gründung von Offshore-Windenergianlagen - Konzepte und offene Fragen. *Bautechnik, Jg. 88, Heft 9* , pp. 602-616.

Achmus, M. K.-S.-R. (2009). Behavior of monopile foundations under cyclic lateral load. *Computers and Geotechnics 36* , pp. pp. 725-735.

Alt, A. (2005): Dauerfestigkeitsprüfung und Dauerfestigkeit von Schrauben-Mutter-Verbindungen und kombinierter Zug- und Biegebeanspruchung, PhD-Thesis, Technical University Berlin, 2005.
Annandale, G. W. Scour Technology. McGraw-Hill, 2005.

API. (2000). *American Petroleum Institue (API): Recommended Practice for Planning, Designing and Constructing Fixed Offshore Platforms - Working Stress Design.* API RP2A-WSD, 21. Auflage, Dezember 2000.

Bettess, R. (1990). Survey of lightweight sediments for use in mobile-bed physical models. Movable Bed Physical Models. Kluwer Academic Publishers, Dordrecht.

Berger, C., Schaumann, P., Stolle, C., MArten, F. (2008): Fatigue strength of high strength bolts with large diameters, IGF-Report 14728 N (in German).

Boulon, M., & Foray, P. (1986). Physical and numerical simulation of lateral shaft friction along offshore piles in sand. *Third interational conference on numerical methods in offshore piling, Nantes, France, Editions Technip* , pp. 127-147.

Breuers, H. N. C.; Raudkivi, A. J. Scouring. Rotterdam, Balkema, 1991.

BSH. (2011). *Anwendungshinweise für den Standard 'Konstruktive Ausführung von Offshore-Windenergieanlagen' des BSH.* Bundesamt für Seeschifffahrt und Hydrographie (BSH).

BSH. (2008). *Standard Baugrunderkundung für Offshore-Windenergieparks.* Bundesamt für Seeschifffahrt und Hydrographie (BSH), Stand: 25. Februar 2008.

Dünkel, V. (1999): Schwingfestigkeit von Schraubenverbindungen - Optimierte Versuchsdurchführung und deren Anwendung bei der Untersuchung von Randschicht- und Oberflächenzuständen, Dissertation, Technische Universität Darmstadt, Darmstadt 1999.

DIN 969 (1997): Threaded fasteners - Axial load fatigue testing - Test methods and evaluation of results, Normenausschuss Mechansiche Verbindungselemnte (FMV) im DIN, DIN Deutsches Institut für Normung e.V., Beuth Verlag GmbH, Berlin 1997.

Dixon, W.J.; Mood, A.M. (1948): A Method for Obtaining and Analyzing Sensitivity Data, S. Am. Stat. Assoc. 43, pp. 108-126, 1948.

DNV. (1992). Det Norske Veritas (DNV). *Classification Notes No. 30.4, Foundations* .

DNV. (2007, 2009 and 2013). Det Norske Veritas (DNV): Offshore Standard DNV-OS J101. *Design of Offshore Wind Turbine Structures*.

EAP. (2011). *Tragverhalten und Nachweise für Pfähle und zyklischen, dynamischen und stoßartigen Einwirkungen.*

Efthymiou, M. (1988): Developement of SCF formulae and generalised influence functions for use in fatigue analysis, Shell International Petroleum Maatschppij B.V, 1988.

Ettmer, B. (2007). Physikalische modellierung von kolkprozessen. Mitteilungsblatt der Bundesanstalt für Wasserbau, 90:107_118.

EN 14399 (2005): High-strength structural bolting assemblies for preloading, European Committee for Standardization (CEN), 2005.

EN 1993-1-8 (2005): Design of steel structures - Part 1-8: Design of joints, European Committee for Standardization (CEN), 2005 + AC 2009.

EN 1993-1-9 (2005): Design of steel structures - Part 1-9: Fatigue, European Committee for Standardization (CEN), 2005 + AC 2009.

GL. (2005 and 2012). *Germanischer Lloyd Rules and Guidelines, IV Industrial Services, Guideline for the Certification of Offshore Wind Turbines. Germanischer Lloyd Wind Energie GmbH, Hamburg/Germany.*

Grabe, J. D.-P. (2004). Monopilegründungen von Offshore-Windenergieanlagen – Zur Bildung von Porenwasserüberdrücken aus zyklischer Belastung, . *Bauingenieur 79,* , pp. pp. 418-422 (in German).

Haibach, E. (1889, 2006): Beriebsfestigkeit - Verfahren und Daten zur Bauteilberechnung, Springer-Verlag, Berlin 2006 (in German)

Hamill (1999), L. Bridge Hydraulics. London, E & FN Spon, 1999.

Hettler, A. (1981). *Verschiebungen starrer und elastischer Gründungskörper in Sand bei monotoner und zyklischer Belastung.* TU Karlsruhe, Mitteilungen des Instituts für Boden- und Felsmechanik, Heft 90.

Heerten & Peters (2010): Kolkschutz für Offshore-Windenergieanlagen in der Nordsee, Fachorgan der DGGT e.V., Geotechnik 01/2011, Ernst & Sohn, Berlin

Heibaum, M. (2002). Geotechnische Aspekte von Kolkentwicklung und Kolkschutz. Mitteilungsblatt der Bundesanstalt für Wasserbau Nr. 85. 2002.

Hjulström, F. Studies of the Morphological Activity of Rivers as Illustrated by the River Fyris.Bulletin of the Geological Institute of the University of Uppsala, Uppsala, Almqvist & Wiksell, 1935.

Hobbacher, A (2007).: Fatigue Recommendations for Fatigue Design of Welded Joints and Components, Int. Institute of Welding, doc. XIII-2151-07/XV-1254-07, Paris 2007.

Hocine Oumeraci (2007). Untersuchung zur Kolkbildung und zum Kolkschutz bei Monopile-Gründung von Offshore-Windenergieanlagen. Abschlussbericht (BMU-Förderkennzeichen 0329973).

Hoffmanns, G. J. C. M. and Verheij, H. J. (1997). Scour Manual. Balkema, Rotterdam.

Kirsch, F., & Richter, T. (2010). Ein analytisch-empirischer Ansatz zur Bestimmung der Tragfähigkeit und der Verformungen von axial zyklisch belasteten Pfählen. *Veröffentlichungen des instituts für Bodenmechanik und Felsmechanik, KIT Süd, Workshop "Offshore-Gründungen von Windkraftanlagen", Heft 172* , pp. 151-164.

Kirsch, F., Richter, T., & Mittag, J. (2011). Zur Verwendung von Interaktionsdiagrammen beim Nachweis axial-zyklisch belasteter Pfähle. *Bautechnik 88, Band 5* .

Klausmann P., Calculation of power curves based on interpolated line-of-sight velocities of nacelle-based LiDAR-measurements, Study Thesis, SWE, 2010

Kloos, K.-H. (1976): Influence of the Surface State and the Sample Size regarding the Fatigue Strength, VDI-Berichte No. 268, pp. 63-76 (in German).

Kuo, Y. (2008). *On the behavior of large-diameter piles under cyclic lateral load, Ph.D. Thesis, Department of Civil Engineering and Geodetic Science, Institute of Soil Mechanics, Foundation Engineering and Waterpower Engineering, Leibniz University of* .

LeBlanc, C. (2009). *Design of Offshore Wind Turbine Support Structures, Ph.D. thesis, DCE Thesis No. 18.* Aalborg University, Denmark.

Lesny, K. (2008). *Gründung von Offshore-Windenergieanlagen - Werkzeuge für die Planung und Bemessung.* Hrsg. Prof. Dr.-Ing. W. Richwien, Heft 36 der Mitteilungsreihe des Instituts für Grundbau und Bodenmechanik. VGE Verlag GmbH, Essen.

Little, R. B. (1988). Full scale cyclic lateral load tests on six single piles in sand. Miscellaneous paper GL-88-27. Texas: Geotechnical Division, Texas A&M University.

Long, J. V. (1994). Effect of cyclic lateral loads on piles in sand. ; 120(1):33-42. . *Journal of the Geotechnical Engineering Division (ASCE)* .

Maening, W.-W.: Das Abgrenzungsverfahren, eine kostensparende Methode zur Ermittlung von Schwingfestigkeitswerten – Theorie, Praxis und Erfahrungen, Materialprüfung 19 , pp. 280-289, 1977.

MAG (1993): Code of Practice for geotextiles in waterways. Federal Waterways Engineering and Research Institute (BAW), Karlsruhe, Germany

Maidl, B.; Berg, J. Kolkschutzmaßnahmen für Bauwerke im Offshore-Bereich. S. 31, Bochum, 1978

Malkus, J. (2000). *Untersuchung des Bodenverhaltens im Kontaktbereich von zyklisch axial belasteten Pfählen und Ankern.* Mitteilungen aus dem Fachgebiet Grundbau und Bodenmechanik der Universität Essen, Heft 24.

Marten, F. (2009): Zur Ermüdungsfestigkeit hochfester großer Schrauben, PhD-Thesis at the Institute for Steel Construction, Leibniz Universität Hannover, Shaker Verlag, Aachen, in German.

Melville, B. W.; Raudkivi, A. J. Flow characteristics in local scour at bridg piers. Journal of Hydraulic Research, Bd. 15, 4, S. 373-380, 1977.

Melvile, B. W. and Coleman, S. E. (2000). Bridge Scour. Water Resources Publications, LLC, Colorado.

Mortara, G., Mangiola, A., & Ghionna, V. N. (2004). Cyclic behaviour of sand-structure interfaces. In *Cyclic Behaviour of Soils and Liquefaction Phenomena.* Taylor & Francis Group, London.

Peralta, P., & Achmus, M. (2010). An experimental investigation of piles in sand subjected to lateral cyclic loads. *7th International Conference on Physical Modeling in Geotechnics (ICPMG 2010).* Zurich, Switzerland, June 28 - July 1.

Poulos, H. (1988, August). Cyclic Stability Diagram for axially loaded piles. . *ASCE Journal of Geotechnical Engineering, Vol. 114 No. 8,* .

Raba, A (2011): Effects of load sequence in the fatigue performance of welded spatial tubular joints in Jackets, Diplom-Thesis at the Institute for Steel Construction, Leibniz University Hannover, 2011 (not published)

Radaj, D. et al.: Fatigue assessment of welded joints by local approaches, Cambridge: Woodhead Publishing Ltd 2006.

Radaj, D., Vormwald, M. (2007): Ermüdungsfestigkeit - Grundlagen für Ingenieure, Springer-Verlag, Berlin 2007 (in German).

Rance, P.J. The Potential for Scour Around Large Objects. Society for Underwater Technology (Hrsg), S.41-53, 1980.

Randolph, M. F. (2009). Cyclic Interface Tests on Sand and Influence of Cyclic Shearing on Axial Pile Capacity in Sand. *Lecture at the International Centre for Mechanical Sciences (CISM).* Udine, June 8-12.

Randolph, M. F. (2003). Load Transfer Analyses of Axially Loaded Piles. *RATZ Version 4.2, Programm-Manual* .

RAVE (2010). Rave - research at alpha ventus. eine forschungsinitiative des bundesministeriums

Reese, L. C. (1974). Analysis of laterally loaded piles in sand,. *6th Annual Offshore Technology Conference, Vol.2,*, (pp. pp. 473-484.).

Rettenmeier A., Bischoff O., Hofsäß M., Schlipf D., Trujillo J.J., Wind Field Analysis Using A Nacelle-Based LiDAR System, EWEC, Warsaw, Poland, April 2010.

Richardson, J. E.; Panchang, V. G.Three-Dimensional Simulation of Scour-Inducing Flow at Bridge Piers. Journal of Hydraulic Engineering, Bd. 124, 5, S. 530-540, 1998.

RPG (1994): Guidelines for testing geotextiles for navigable channels. Federal Waterways Engineering and Research Institute (BAW), Karlsruhe, Germany

Schaumann, P., Lochte-Holtgreven, S., Bechtel, A., Amezqueta Pueyo, C. (2013): Design process of WT components – Tower joints & substructures – Review on design for grouted joints and bolted connections, Version 2, EERA European Energy Research Alliance, Sub-program on structures and materials, 2013.

Schaumann, P., Marten, F. (2009): Fatigue Resistance of High Strength Bolts with Large Diameters, Proc. of the International Symposium for Steel Structures ISSS, Seoul 2009.

Schneider W. (2001): Loading and durability of highly prestressed bolted connections, PhD-Thesis,University of Darmstadt, 2001 (in German)

Schendel, A., Goseberg, N., Schlurmann, T. (2012): Experimental study on erosion potentials and nearbed transport processes of coarse grain materials, The 6th Chinese-German Joint Symposium on Hydraulic and Ocean Engineering (JOINT 2012), National Taiwan Ocean University, Keelung. Sep 23-29

Schlipf D., Trujillo J.J., Basterra V., Kühn M., Development of a Wind Turbine LiDAR Simulator, EWEC, Marseille, France, March 2009.

Seidel, M. (2001): On the design of bolted ring flange connections in wind ernergy concertes, PhD-Thesis at the Institute for Steel Construction, Leibniz University Hannover, Shaker-Verlag, 2001 (in German).

Seidel, M., Schaumann, P. (2001a): Measuring fatigue loads of bolts in ring flange connections, Proc. of the European Wind Energy Conference, Copenhagen 2001.

Seidel, M., Schaumann, P. (2001b): Fatigue resistance of bolts, in: Erneuerbare Energien 04/2001, pp. 46-50, 2001 (in German).

Shields, A. (1936). Anwendung der Ähnlichkeitsmechanik und der Turbulenzforschung auf die Geschiebebewegung. Number 26 in Mitteilungen der Preuÿischen Versuchsanstalt für Wasserbau und Schi_bau. Technische Hochschule Berlin, Germany.

Stahlmann, A. (2013). Experimental and Numerical Modeling of Scour at Offshore Wind Turbines. PhD Thesis, Pre-Defense Version, Franzius-Institute for Hydraulic, Estuarine and Coastal Engineering, Leibniz Universität Hannover.

Sumer, M. B.; Fredsoe, J., Christiansen, N. Scour around a vertical pile in waves. Journal of Waterway, Port, Coastal and Ocean Engineering. Vol. 117, Bd. No. 1, S. 15-31, 1992.

Sumer, M. B.; Christiansen, N.; Fredsoe, J. Influence of Cross Section on Wave Scour Around Piles. Journal of Waterway, Port, Coastal and Ocean Engineering, Bd. Vol. 119, Nr. 5, 1993.

Sumer, B. M., Whitehouse, R. J. S., and Torum, A. (2001). Scour around coastal structures: a summary of recent research. Coastal Engineering, 44(2):153_190.

Sumer, B. M. and Fredsøe, J. (2002). The Mechanics of Scour in the Marine Environment. World Scienti_c Pub. Co. Inc., 1 edition.

Silver, M. L., & Seed, H. B. (1971). Volume changes in sands during cyclic loading. *Journal of the Soil Mechanics and Foundations Division ASCE , Vol. 97, No. SM9*.

Thomas, S. (2011). Zum Pfahltragverhalten unter zyklisch axialer Belastung. *Schriftenreihe Geotechnik, Universität Kassel, Heft 25* .

von Soos, P., & Engel, J. (2008). Eigenschaften von Boden und Fels - ihre Ermittlung im Labor. In K. J. Witt (Ed.), *Grundbau-Taschenbuch* (7 ed., Vol. 1). Verlag Ernst und Sohn

Vrettos, C. (2008). Bodendynamik. In K. J. Witt (Ed.), *Grundbau-Taschenbuch* (7 ed., Vol. 1). Verlag Ernst und Sohn.

Werth, K., Wilms, M., Peters, K., Stahlmann, A., Schlurmann, T. (2012)**:** Offshore Wind Turbine Foundations - Hydrodynamic investigations, design, installation and durability of scour protection systems made of geotextile sand-fillled containers, 12th Baltic Sea Geotechnical Conference, Infrastructure in the Baltic Sea Region, Rostock, Deutschland, pp. 310-316, 31.05.-02.06.2012

Winselmann, D. (1984). *Stoffgesetze mit isotroper und kinematischer Verfestigung sowie deren Anwendung auf Sand.* Bericht Nr. 84-44 aus dem Institut für Statik der Technischen Universität Braunschweig.

Whitehouse, R. (1998). Scour at Marine Structures: A Manual for Practical Applications. Thomas Telford Ltd., London.

Whitehouse, R.J.S., Harris, J.M., Sutherland, J. and Rees, J. (2011a). The nature of scour development and scour protection at offshore windfarm foundations. Marine Pollution Bulletin, 62:73-88.

Whitehouse, R.J.S., Harris, J.M., Mundon, T.R. and Sutherland, J.

(2011b). Scour at Offshore Structures. Proceedings of the Fifth International Conference on Scour and Erosion, Geotechnical Special Publication No. 210, American Society of Civil Engineers, pp. 11-20.

Wilms, M., Wahrmund, H., Stahlmann, A., Heitz, C., Schlurmann, T. (2011): Kolkbildung und Dimensionierung des Kolkschutzsystems eines OWEA Schwerkraftfundaments, HTG-Kongress 2011, 07.-10.09.2011, Würzburg, Veröffentlicht in: Tagungsband HTG-Kongress 2011, Herausgeber: Hafentechnische Gesellschaft e.V., Hamburg

Wilms, M., Stahlmann, A., Schlurmann, T. (2012): Investigations on scour development around a gravity foundation for offshore wind turbines, Proceedings of the 33rd International Conference on Coastal Engineering, Santander, Spanien, 01.-06. Juli, 2012

Youd, T. L., & Idriss, I. M. (2001). Liquefaction resistance of soils: Summary Report from the 1996 NCEER and 1998 NCEER/NSF workshops on evaluation of liquefaction resistance of soils. *Journal of Geotechnical and Geoenvironmental Engineering, Vol. 127, No.4, April* .

Yotobori, T., Sato, K. (1976): The Effects of Frequency on Fatigue, in: Engineering Fracture Mechanics 8, pp. 81-88, 1976.

Zanke, U. (1982a). Grundlagen der Sedimentbewegung. Springer-Verlag, Berlin,
Heidelberg, New York.

Zielke, W. Hydro- und morphodynamische Auswirkungen von Offshore-Windkraftanlagen. Technische Eingriffe in marine Lebensräume, Insel Vilm, 27.-29. Oktober 1999.

Online

www.ieawind.org/task_32.html

http://www.iag.uni-stuttgart.de/laminarwindkanal/index_english.htm

http://www.meteomastijmuiden.nl/en/home/

http://www.ecn.nl/docs/library/report/2006/rx06055.pdf